POLITECNICO
MILANO 1863

SCUOLA DI INGEGNERIA INDUSTRIALE
E DELL'INFORMAZIONE

Characterization of Plasma Sources for Plasma-based Accelerators

Tesi di Laurea Magistrale in
Nuclear Engineering

Author: **Cristina Mariani**

Student ID: 968537
Advisor: Prof. Matteo Passoni
Co-advisors: Dr. Angelo Biagioni and Lucio Crincoli, PhD
Academic Year: 2021-22

This thesis has been carried out at INFN-LNF (Instituto Nazionale di Fisica Nucleare - Laboratori Nazionali di Frascati), in particular, inside SPARC_LAB (Sources for Plasma Accelerators and Radiation Compton with Laser And Beam) project.

Abstract

Electron plasma acceleration technology is nowadays one of the main challenges of particle accelerator physics. Novel plasma-based acceleration schemes allow a drastic reduction in size and cost of particle accelerators, offering a promising alternative to conventional RF-based accelerators.

Plasma acceleration is performed by injecting a driver beam, either a particle bunch or a laser beam, inside a plasma. The interaction between a driver beam and plasma will generate the wakefield inside the plasma. The wakefield created by the driver is able to accelerate a trailing particle bunch, called "witness", with high acceleration gradient. The density of plasma electrons inside the plasma source therefore plays an important role in the acceleration itself, since it is the medium in which the process takes place.

This thesis, carried out at INFN-LNF, inside the SPARC_LAB (Sources for Plasma Accelerators and Radiation Compton with Laser And Beam) Project, aims at offering a characterization of the plasma source, whilst analyzing many of the state-of-art methods to shape and tune the density inside the source, more specifically the capillary source, in order to obtain a high efficiency in the overall process of plasma acceleration.

The characterization of such devices, based on spectroscopic analysis of light-emitted plasma, made possible to understand the behavior of the plasma electrons inside this confined space, and how experimental conditions and capillary geometry, like pressure and current, affect the plasma formation and distribution, thus providing a deeper insight in the design of plasma sources for particle accelerators.

Furthermore the experimental analysis presented in the thesis work allowed to design novel schemes for plasma discharge capillaries, which can contribute to the compactness and cost-effectiveness of future plasma-based accelerators.

Keywords: plasma, acceleration, plasma source, plasma density

Abstract in lingua italiana

L'accelerazione di elettroni tramite plasma è una delle principali sfide della fisica degli acceleratori di particelle degli ultimi tempi. Nuovi schemi di accelerazione basati sul plasma consentono una drastica riduzione delle dimensioni e costo degli acceleratori di particelle, offrendo una promettente alternativa ai convenzionali acceleratori basati su RF.
L'accelerazione di elettroni al plasma viene eseguita iniettando un fascio di particelle o un laser all'interno di un plasma. L'interazione tra il fascio, che fa da driver, e il plasma genererà un campo d'onda all'interno del plasma stesso. Il campo d'onda creato dal driver è in grado di accelerare un secondo gruppo di particelle inviato in un secondo momento, chiamato "witness", con elevato gradiente di accelerazione. La densità di elettroni all'interno della sorgente di plasma svolge quindi un ruolo importante nella accelerazione stessa, poiché la sorgente è il mezzo in cui si svolge il processo.
Questa tesi, svolta all'INFN-LNF, all'interno del progetto SPARC_LAB (Sources for Plasma Accelerators and Radiation Compton with Laser And Beam), mira ad offrire una caratterizzazione della sorgente di plasma, analizzando molti dei metodi più avanzati per modellare e regolare la densità all'interno della sorgente, più specificamente il capillare, in per ottenere un'elevata efficienza nel processo globale di accelerazione del plasma.
La caratterizzazione di tali dispositivi, basata su analisi spettroscopica della luce emessa dal plasma, ha reso possibile capire il comportamento degli elettroni del plasma all'interno di questo spazio confinato, e come le condizioni sperimentali e la geometria capillare, ad esempio la pressione e corrente, influenzano la formazione e distribuzione del plasma, fornendo così una visione più approfondita nella progettazione di sorgenti di plasma per acceleratori di particelle.
Inoltre, l'analisi sperimentale presentata in questo lavoro di tesi, permette di progettare nuovi schemi per i capillari di scarico del plasma, che possono contribuire alla compattezza ed economicità dei futuri acceleratori al plasma.

Parole chiave: plasma, accelerazione, sorgente di plasma, densità di plasma

Contents

Introduction

Plasma acceleration technology is nowadays one of the new challenges of particle accelerator physics. Many achievements in different fields can be reached through them, like medicine, industry and physics.
Inside plasma accelerator technology, one of the most important components is the source in which the actual acceleration takes place, and where the plasma is generated.
This thesis, carried out entirely at SPARC_LAB (Sources for Plasma Accelerators and Radiation Compton with Laser And Beam), part of INFN-LNF test facility, aims at characterization of the plasma source, and analyzes many of the state of-art methods to shape and tune the density inside the source, more specifically the capillary source (fig.1), in order to obtain a high efficiency in the overall process of plasma acceleration. The research activity is also included in the European project EuPRAXIA (European Plasma Research Accelerator with Excellence in Applications) for plasma-based accelerators.
Since the plasma target represents the main component of plasma-based accelerators, a laboratory devoted to studies and characterization of plasmas for acceleration has been implemented at National laboratories of Frascati; here, the design and production of th plasma source aims to find the right parameters to optimize the acceleration gradient in the GV/m scale

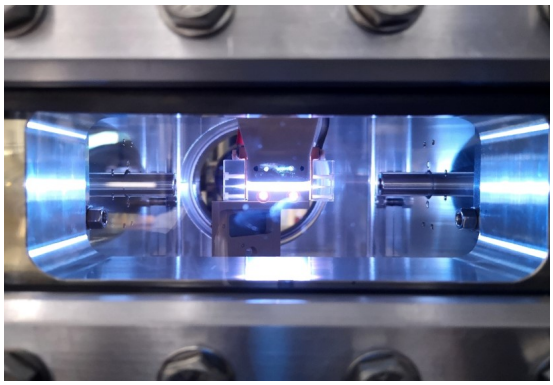

Figure 1: Plasma capillary source for acceleration placed inside the accelerator at SPARC_LAB.

Through measurements and data analysis carried on in PLASMA LAB, I was able study specific techniques to enhance the shot-to-shot stability of the acceleration and new solutions for the plasma source geometry, both to reach very large dimensions, until the m-scale, and to optimize the plasma electron distribution inside the channel. The improvements on the original scheme of the plasma accelerator source are made to achieve new challenging results related to crucial topics for plasma-based accelerators.
In this work many topics will be addressed:

- In the first chapter an overview of the theory on which the thesis is based on is given; topics as particle acceleration and Plasma physics will be addressed, in order to understand the physics behind this technology, explained subsequently. Inside the chapter, the essential relations and equations of the theory behind the work carried out will be shown, to give the reader an overview and a first knowledge of the technology and its possible applications. As last topic of this chapter, plasma acceleration physics is covered, explaining both ion driven acceleration and electron driven acceleration.

- The second chapter describes the different types of plasma sources that can be used for plasma acceleration; in particular, the last part of the chapter will show the type of source analysed later in the thesis work.

- The third chapter gives an overview of the experimental setup used for the experiments presented in the thesis. First a description of the facility and of SPARC_LAB is given. In particular, the diagnostic of the capillary source made in the plasma diagnostic lab is delineated. With this description, it is easier to explain how important the source is for all the acceleration process. The whole experimental diagnostic setup is then shown, and with it the data analysis that is done to see the measurements.

- The fourth chapter shows the measurements and results concerning the research carried out during the internship. Different graphs will be shown and explained, with the intention of finding the possible designs and parameters that can be used to improve the efficiency of the acceleration. Comparisons and comments will point out the advantages and limits of different configurations and how they can be used for different applications. A new type of capillary is then described; measurement and results also of this capillary are shown and explained.

- The last chapter is used to summarize conclusions of the research carried out at SPARC_LAB, and to outline some further perspectives of the technology presented in the thesis.

The reasons that have driven me to deepen this topic have a twofold nature: first of all, behind the choice of the topic there is a huge interest in the subjects involves. Accelerator physics always fascinated me, since I discover how useful it is for everyday life. In fact, accelerators can be found in every science field, from engineering, material science, energy and also medicine.
When the use of plasmas as an acceleration medium were addressed for the improvement of the technology, my interest grew more than before. In fact, the wide use of accelerator is known, and because of this the technology needs to be improved in every possible way and in every moment. Plasma technology can help a lot in this, since it can make accelerators both more compact and more powerful.
The second reason that drove me is the help in the society that this technology can give: this compactness achievable through plasma is very useful in many industrial fields, but specially in medicine, since many therapies for tumors are based on accelerators. Since the acceleration mostly happens in the plasma source, it is a very important matter for achieve results in the research, and I had the possibility to work on that.
Furthermore, working on the improvement of this part of the accelerator in a research facility has been a really formative experience that also introduced me to the research world around the field.

1 | Plasma based accelerators

During the last decades, particle acceleration became an essential aspect of many technologies used worldwide, such as medicine, physics, industry and energy.
Major historical discoveries leading to present day particle accelerator physics started to happen more than 150 years ago, but the major discoveries happened starting from the 1911, when Ernest Rutherford discovered the atomic nucleus in an experiment where he fired a beam of alpha particles. In 1927, Rutherford challenged the scientific community to accelerate charged particles to energies greater than that of natural radioactive decay in order to disintegrate atomic nuclei. It took many years for Rutherford's challenge to be met and one of the first major breakthroughs came from two scientists, John Cockcroft and Ernest Walton, who, using their particle accelerator to accelerate protons, were able to disintegrate a Lithium nucleus [30].
In less than the 90 years since their invention, accelerators have so propelled modern science – contributing to more than one-third of the Nobel Prizes in physics – and they have reached well beyond fundamental research towards applied science and market applications. Research leading to the discovery of elementary particles and to ideas for the acceleration of such particles is dotted with particularly important milestones, which from time to time set the directions for further experimental and theoretical research.
In the present days, particle accelerators not only have applications in the discovery of new particles, as the Higgs boson, but also in the generation of high-level radiation sources, in condensed matter physics, material science, chemistry, biology and medicine; other several fields of study are found in the industry, earth sciences, health physics, and technology.
The current applications, especially those used in healthcare and industry, tend to use rather old technology, and their performance, especially for newer applications, can be limited by this. Much research is now going into developing more efficient, better performing and more compact machines exploiting new approaches to particle acceleration: one example is the plasma based acceleration, which will be discussed below.
Looking at the list of applications above, it is possible to say how the continued development of particle accelerators is essential to further improve social and economic development in the world.

1.1. Particle Accelerators Physics

Particle accelerators are sophisticated machines which, in providing energy to subatomic particles, make them capable of interacting with other particles and delivering their energy and producing intense streams of x-rays or neutrons.
Acceleration requires the input of energy, which, for charged particles, is achieved by applying electromagnetic fields, that imparts kinetic energy to the particles such that they can reach speeds that can be a significant fraction of that of light and deflect the particles, thus offering a means to focus the particle beam – essential for the practical application of an accelerator device.
Particle accelerators can be classified according to a number of different criteria; a first criterion concerns the type of particles used, basing the classification on the q/m ratio between the charge and the mass of the accelerated particles. Three types can thus be identified: those who accelerate electron (e^-) and positrons (e^+), the protons (p) accelerators, and the heavy ions (from α particles to Uranium ions) accelerators.
A second classification criterion concerns the nature of the target. We then speak of fixed target accelerators (beam extraction) or of collision accelerators (storage ring and beam collider), characterised by two beams (circulating in opposite direction in a single ring or in two rings) that collide against each other.
From the criteria above it is possible to define some types of accelerators, as the Cockcroft-Walton and Van De Graaff accelerators - also the first types of accelerators ever built - and the LINAC (Linear Accelerator), Cyclotron, Betatron, Microtron, Synchrotron ans Storage Ring Collider - the most used ones right now.
All the types of accelerators have the same basic principles, and so the same basic components; the main chain consists on a source, an accelerating region coupled with a drift/focusing area, a target and a detector. The main components of an accelerator, present in every type of machine, are the following:

- Vacuum chamber: this is the place in which the beam moves during the acceleration process; in the chamber the vacuum is needed to reduce beam-gas interaction which is responsible for limitations in the machine performances, and to avoid electrical discharges in high voltage RF cavities.

- Dipole magnet (Fig.1.1a): it is used to bend the beam, applying a magnetic field on the transversal plane, perpendicular to the plane in which it aims to curve the beam.

- Quadrupole magnet (Fig.1.1b): it is used to focus the bunch; it focuses on one of the two transversal axes and defocus on the other one. While the dipole, with just

two poles, can curve the trajectory, the quadrupole can reduce the size of the bunch.

- Sextupole magnet (Fig.1.1c): it is used to correct the chromaticity and non-linear effects of the bunch.
- RF cavity: metallic tubes used to allow the electromagnetic field propagation, which interacts with the particle beams to increase its energy or to make beam diagnostics.
- Gun: source of electrons for electron beam accelerators; it consists of a cathode emitter of electrons, an anode with an aperture through which the beam of electrons can pass, and one or more focusing and control electrodes.

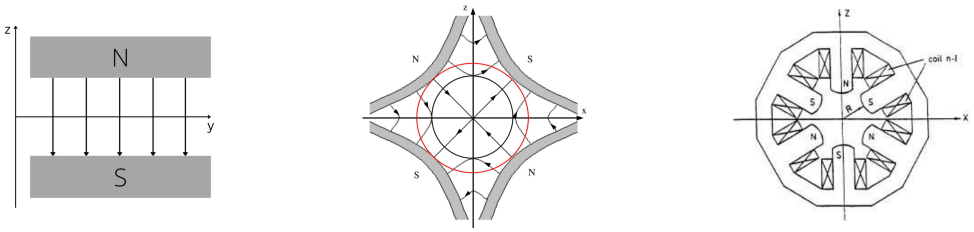

(a) Dipole magnet (b) Quadrupole magnet (c) Sextupole magnet

Figure 1.1: Types of magnets for particle accelerators.

A bunch of particles is described using the motion equation of a particle inside an electromagnetic field (eq.1.2); its main parameters are:

- Charge (Q): usually instead of the charge o the single particle, the charge of the total bunch is used.
- Current (I): expressed in Ampere (A); knowing charge and the duration of the bunch, it's possible to calculate the current as the ratio between these two quantities.
- Energy spread: parameter used to describe the quality of an accelerated beam, because it defines the ratio between the energy range of the particle beam and its mean energy ($dE/E.$). The higher is the energy spread, the lower is the beam quality.
- Emittance (ϵ): Property of the charged particle beam, used to evaluate its quality. It is an invariant for a given mean energy of the beam; the less it is, the better the beam behaves. It refers to the area occupied by the particles of the beam in a position-and-momentum phase space.

- Magnetic rigidity: it is the effect of magnetic fields on the motion of the charged particles. It is a measure of the momentum of the particle, and it refers to the fact that a higher momentum particle will have a higher resistance to deflection by a magnetic field. It is defined as $\rho = pc/q$, where p is the particle momentum, c the speed of light and q the charge of the particle.
- transverse length: transversal size of the bunch, usually measured in rms (root mean square). It describes the geometrical size of the beam.
- bunch length/duration: longitudinal length or duration of the pulse, measured in ps or μm (either defined as rms or FWHM).

To describe the general interaction of fields based on electric currents in specific devices and free charged particles which we want to preserve, guide and focus, we use as a starting point Maxwell's equations:

$$\begin{cases} \nabla E = \dfrac{\rho}{\epsilon_0}, & \text{(1.1a)} \\ \nabla \times \boldsymbol{E} = \dfrac{\partial \boldsymbol{B}}{\partial t}, & \text{(1.1b)} \\ \nabla \cdot \boldsymbol{B} = 0, & \text{(1.1c)} \\ \nabla \times \boldsymbol{B} = \mu_0 \boldsymbol{J} + \mu_0 \epsilon_0 \dfrac{\partial \boldsymbol{E}}{\partial t}. & \text{(1.1d)} \end{cases}$$

where ϵ_0 is the dielectric constant, and μ_0 is the magnetic permeability.
The trajectories of charged particles can be influenced only by electric and magnetic fields through the Lorentz force:

$$\vec{F} = m\frac{d\vec{v}}{dt} = q[\vec{E} + (\vec{v} \times \vec{B})] \tag{1.2}$$

with m is the particle mass, $\vec{v}$ is its speed, q its charge,$\vec{E}$ and $\vec{B}$ are the electric and magnetic fields.
The electric field accelerates the particles, while the magnetic field helps focusing or bending them. The particles will oscillate under the effect of both fields, in the transverse plan and in the longitudinal one.
In the transversal plan *betatron oscillations* are present, caused by the different momentum of the particles in the bunch; the oscillations happen along the orbit plan, and are corrected using quadrupoles.
In the longitudinal one, the *synchrotron oscillations* are present, generated by the spread of energy of the particles in the bunch: since the energy is different for different particles,

they will enter the cavities at different time and so different tension; the oscillations happen around the bunch centre.
The acceleration takes place in the RF cavities: as said before, RF cavities are chambers in which, thanks to EM fields present inside, can boost the particles and increase their velocities. The field in an RF cavity is made to oscillate at a given frequency, and the particles of the beam need to be localized in bunches and properly phased with respect to the field so that the beam is accelerated.

1.2. Principles of Plasma Physics

Plasma in physics is called *fourth state of matter* and is defined as a special class of gas made up of numerous atoms and molecules, in which at least one of the electrons in an atom has been stripped free, leaving a positively charged nucleus, called an ion.
Another definition of the plasma can be that a plasma is a quasi-neutral gas of charged and neutral particles which exhibits collective behavior.
Plasmas are rather ubiquitous: in the cosmos, 99% of the visible universe—including stars, the interstellar medium and jets of material from various astrophysical objects—is in a plasma state. Closer to home, the ionosphere (the ionized part of the upper atmosphere of Earth), extending from around 50 km to 1000 km, provides vital protection from solar radiation to life on Earth. Terrestrial plasmas can be found in fusion devices (machines designed to confine, ignite and ultimately extract energy from deuterium–tritium fuel), street lighting, industrial plasma torches and etching processes, and lightning discharges[1].
It may be produced in two ways: by heating a gas to an extremely high temperature, such as 3000K, or by applying electric fields of sufficient intensity to the gas; in this second way to generate a plasma, two processes are present: ionization and recombination.
Ionization means that an atom acquires a negative or positive charge by gaining or losing electrons, and recombination means that positive ions capture a free energetic electron to form new neutral atoms. Important ionization mechanisms include collisional ionization, multiphoton ionization and optical field ionization. In both processes of generation of the plasma, the atoms and molecules of the gas may become ionized, and the general behaviour starts being dictated by electromagnetic forces acting on the free ions and electrons.
The Plasma was first described in 1922 by Irving Langmuir, and offer two main characteristics for practical applications: first, they can reach temperatures and energy densities higher than those produced by ordinary chemical means; second, plasmas are able to produce, even at low temperatures, energetic species that can initiate chemical reactions that are difficult or impossible to obtain using ordinary chemical mechanisms [3]. Since then

the plasma has been studied for different types of applications, from solid state physics to nuclear fusion, and, as it will be described later, also for particle accelerators.
In order to be considered a plasma, an ionized gas must have a sufficiently large number of charged particles to shield itself electrostatically within a distance smaller than other lengths of physical interest [32]. In fact, one of the most important properties of a plasma is its tendency to remain electrically neutral in any given macroscopic volume element, so the ability to shield out electric potentials that are applied to it, by adjusting the charges inside. The quantitative measure of this distance is the so-called *Debye length*.
It is possible to write that, in thermal equilibrium (the condition under which two substances in physical contact with each other exchange no heat energy), the electron density follows a Boltzmann distribution

$$n_e = n_i \exp e\phi(r)/k_B T_e \tag{1.3}$$

where n_i is the ion density, e the electron charge, k_B is the Boltzmann constant, and $\phi(r)$ is the potential created by the external force, while T_e is the electron temperature. Combining this distribution with the Poisson's equation,

$$\nabla^2\phi(r) = -\frac{e}{\epsilon_0}(n_i - n_e) \tag{1.4}$$

it is possible to obtain a linearized solution for the potential created, as

$$\phi_D(r) = \frac{e}{4\pi\epsilon_0}\frac{\exp(-r/\lambda_D)}{r} \tag{1.5}$$

where λ_D is the Debye length define before

$$\lambda_D^2 = \frac{\epsilon_0 k_B T}{n_0 e^2} \tag{1.6}$$

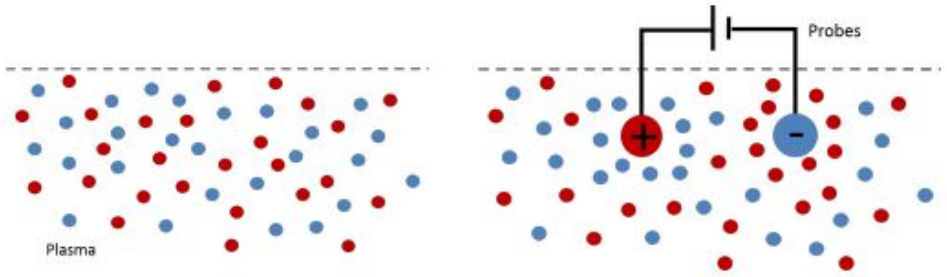

Figure 1.2: After some time, the ions in the ball's vicinity will be repelled and the electrons will be attracted, leading to an altered average charge density in this region[1]. The Debye length is the distance at which this effect is shielded.

The Debye length assumes that the plasma is initially neutral, i.e., n_e=n_i; if the dimensions L of the system is much larger than λ_D, then whenever local concentrations of charge arise or external potentials are introduced into the system, these are shielded out in a distance short compared with L, leaving the bulk of the plasma free of large electric potentials or fields[32], an so the plasma can then be assumed to stay extremely close to neutrality; this condition is called *quasi-neutrality*.
An important characteristic of plasmas is the so called *collective behaviour*, which means that motions depend not only on local conditions but on the state of the plasma in remote regions as well. This property will so intend that a net charge imbalance $\rho = e(Zn_i - n_e)$ (where Z is the charge number) will immediately give rise to an electrostatic field according to Gauss's law

$$\nabla \cdot \boldsymbol{E} = \frac{\rho}{\epsilon_0} \tag{1.7}$$

and to a current density

$$\boldsymbol{J} = e(Zn_i v_i - n_e v_e) \tag{1.8}$$

due to the different velocities of ions (v_i) and electrons(v_e). This in turn induces a magnetic field according to Ampères law,

$$\nabla \times \boldsymbol{B} = \mu_0 \boldsymbol{J} \tag{1.9}$$

It is these internally driven electric and magnetic fields that largely determine the dynamics of the plasma, including its response to externally applied fields through particle or laser beams as, for example, in the case of plasma-based accelerator schemes.
Each particle in a plasma can act as a test charge and carry its own shielding cloud. The concept of Debye shielding developed above requires the presence of a sufficiently large number of particles so that "density" can be defined in a statistically meaningful way[32]. A useful parameter in this connection is the number of particles in a Debye sphere, given

as

$$N_D = n_e \frac{4\pi}{3} \lambda_D^3 \tag{1.10}$$

A prerequisite for the collective behaviour condition to be applied is that $N_D \gg 1$, which signify that the Coulomb force, which in a plasma extends only about a Debye length from the source, has a long range influence, as a result of the Debye shielding cloud. An alternative way of expressing N_D is via the so-called *plasma parameter*:

$$g = \frac{1}{n_e \lambda_D^3} \tag{1.11}$$

When the plasma is perturbed by an external force, the local charge separation gives rise to an electric field E, that acts to reduce the charge separation by pulling the electrons back to their initial locations, so that they will be accelerated back to their initial positions. However, as they acquire kinetic energy in this process, their inertia carries them past their neutral positions. The plasma once again becomes non-neutral, and again an electric field is set up, now pointing in the opposite direction to retard their motion. Now the electrons accelerate in the opposite way as before, go past their equilibrium positions as a result of their inertia, and once again the charge displacement is set up. In the absence of any damping (due, for example, to collisions of the electrons with ions or other electrons), this oscillatory motion would continue forever [32].
To describe the movements of the electrons, the equation of motion for a single electron in the presence of an electric field is used:

$$m_e \frac{d^2x}{dt^2} = q_e E_x \tag{1.12}$$

Considering Gauss's law (1.7) applied to a closed shape, the electric field can be defined as:

$$E_x = -\frac{x n_e q_e}{\epsilon_0} \tag{1.13}$$

Substituting it into the equation 1.12, we have:

$$m_e \frac{d^2x}{dt^2} + \frac{x n_e q_e^2}{\epsilon_0} = 0 \tag{1.14}$$

It's now possible to introduce a characteristic frequency with whom the electrons oscillates, called $plasma frequency$ (w_p) and defined as:

$$w_p = \sqrt{\frac{n_e q_e^2}{\epsilon_0 m_e}} \tag{1.15}$$

The three conditions a plasma must satisfy are therefore:

- λ_D « L, for an ionized gas to be a plasma.
- N_D » 1 or g«1, so that there's dominance of collective effects over collisions between particles.
- $\omega\tau > 1$, where τ is the mean time between collisions with neutral atoms, so that the plasma behaves like a plasma rather than a neutral gas.

Another important variable in plasma physics is the *plasma temperature* T (usually measured in eV, where $1eV = 11605K$); the temperature in plasma physics is an equilibrium concept, and we may not always be faced with equilibrium situations. In such cases, a true temperature cannot always be assigned, although it is still possible to use the term in the sense of average energy. It should be noted that by temperature it's meant the quantity sometimes called "kinetic temperature," simply the state of energy of the particles. A high value of T does not necessarily mean a lot of heat, since the latter also depends on heat capacity, determined also by the number of particles. As an example, the electron kinetic temperature inside a fluorescent lamp is ∼11 000K, but it does not feel nearly as "hot" when one holds the tube while it is lit.
Since the plasma temperature measures essentially the energy of the electrons, the plasma can have several temperatures at the same time, since often the ions and the electrons have separate Maxwellian distributions (see eq. 1.16), corresponding to temperatures T_i and T_e.
To describe the two possible temperatures present in a plasma, it's needed to define two classes of plasmas: *cold plasmas* and *hot plasmas*. The first kind of plasmas are partially ionised gases, characterized by the fact that the temperature of heavy species (neutral particles and ions) is close to room temperature (25°C–100°C). Instead, the electrons temperature is much higher. Hot plasmas, on the other hand, approach a state of local thermodynamic equilibrium (LTE) and with the temperature of both electrons and ions being extremely high.
The need to define the class of cold plasmas can come about because the collision rate among ions or among electrons themselves is larger than the rate of collisions between an ion and an electron. Then each species can be in its own thermal equilibrium, but the plasma may not last long enough for the two temperature to equalize. When there is a magnetic field **B**, even a single species, say ions, can have two temperatures. This is because the forces acting on an ion along **B** are different from those acting perpendicular to **B** (due to the Lorentz force). The components of velocity perpendicular and parallel

to **B** may then belong to different Maxwellian distributions with temperatures $T_{\parallel}$ and $T_{\perp}$ [10].

It is good to have in mind an average temperature, so that it's possible to study the plasma; usually, taking into account the Maxwellian distribution

$$f(u) = A \exp\left(-\frac{1}{2}\frac{mu^2}{k_B T}\right) \tag{1.16}$$

and calculating the average kinetic energy of the particles from f(u) as follows:

$$E_{avg} = \frac{\int_{-\infty}^{\infty} \frac{1}{2} m u^2 f(u)\, dx}{\int_{-\infty}^{\infty} f(u)\, dx} \tag{1.17}$$

it's found an E_{avg} of:

$$E_{avg} = \frac{3}{2} k_B T_{av} \tag{1.18}$$

Knowing also that the kinetic energy is related to the thermal velocity of the particles as

$$v_{th} = \sqrt{\frac{2E_{av}}{m_e}} \tag{1.19}$$

the maximum temperature of typical plasma for acceleration experiments will not exceed 10 eV. In this way, the thermal velocity of the electrons does not pass the speed of light at which the plasma waves excitation propagates; therefore, the temperature does not affect the acceleration process.

To summarize the different properties and parameters described before, it is possible to divide the plasma in different classes, as it can be seen in fig.1.3.

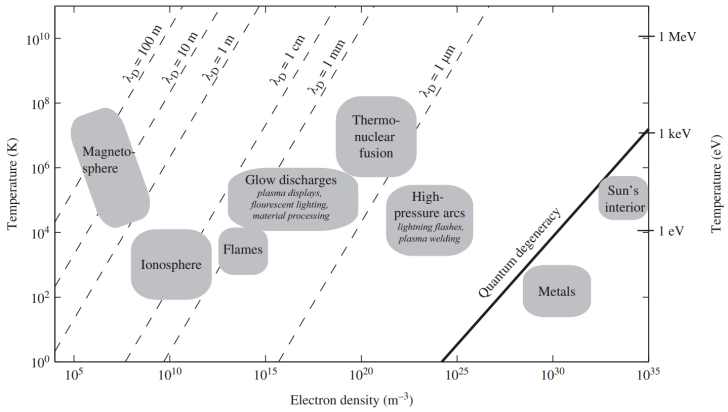

Figure 1.3: Range of temperature, electron density, and Debye length for typical plasma phenomena in nature and in technological applications[32].

1.3. Plasma Acceleration Physics

The primary limit of the traditional acceleration technology is the small accelerating gradient per meter which compounds the length and material cost of building more powerful accelerators. The small accelerating gradient is due mainly to the maximum RF energy which can be tolerated by the accelerating structure before the structure degrades due to field emission. To overcome this problem, studies on other acceleration techniques have been done, and Plasma Based Acceleration is one of the most promising ones.
Plasma acceleration schemes date back to early theoretical work in the 1950s, when Budker and Veksler proposed using plasma collective fields to accelerate charged particles more compactly. In the 1970s and 1980s the work performed by Tajima and Dawson led to laser and beam driven plasma wakefields being proposed. From that moment, research into plasma based acceleration schemes has made great progresses, particularly over the last two decades, due to further advances in driver technology, target design and improved understanding of the underlying physics through the development of advanced simulation techniques. The drive beam, whether a laser or particle beam, generates a plasma 'wake' with phase velocity close to the speed of light, which allows a relativistic 'witness' beam to remain in an accelerating phase of the wake and gain energy over long distances[2].
The principal innovation in plasma based accelerators is the size of them, compared with the acceleration gradient they can reach: if a conventional accelerator has the size from tens of meters to kilometres, a plasma accelerators have sizes much smaller, and therefore they are more practical in many aspects and many applications. In addition of the advantage of the size, plasma based accelerators are able to accelerate the particles up to the order of GV/m, a gradient that conventional accelerators are not capable of reaching.
In a plasma accelerator the role of the accelerating structure is played by the plasma. Instead of being a problem, electrical breakdown is part of the design because the gas is broken down to begin with. The power source is not microwave radiation but is either a laser beam or a charged particle beam. Plasma-based accelerators use the strong electromagnetic fields that may be supported by plasmas to accelerate charged particles to high energies in near unrestricted oscillating mode structures, allowing for several accelerating and focusing configurations.
The mechanism of the acceleration for plasma accelerators is analogous to the water wave behind a moving boat, so the electromagnetic fields driven by a laser pulse or a particle bunch is known as the plasma wakefield; in this case, the plasma is the medium, and the wakefield is generated by a "driver"(fig.1.4).
The process works in this way: A plasma as a whole is electrically neutral, containing equal amounts of negative charges (electrons) and positive charges (ions). A pulse from an

intense laser or particle beam, however, creates a disturbance in the plasma. In essence, the beam pushes the lighter electrons away from the heavier positive ions, which in turn get left behind, creating a region of excess positive charge, called "*bubble*"(fig. 1.5) and a region of excess negative charge.

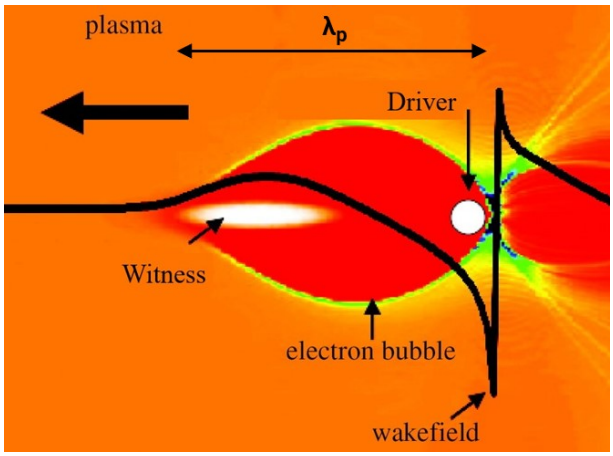

Figure 1.4: Scheme of the plasma acceleration process. The driver creates the wakefield and the bubble; the witness is shot with a certain delay between zero and the time at which it will end outside the bubble[2].

The disturbance forms a wave that travels through the plasma at nearly the speed of light. Subsequently, the electrons, attracted by the field generated by the ions, start to oscillate around the axis, creating a wave that is able to accelerate the bunch of electrons, called "witness". If the witness is placed in the bubble, it can behaves, using the same analogy of the boat and the waves, as a surfer on the wave, who continues to move and accelerate; if the timing is not correct, the surfer, and in plasma acceleration, the witness, will not be accelerated.

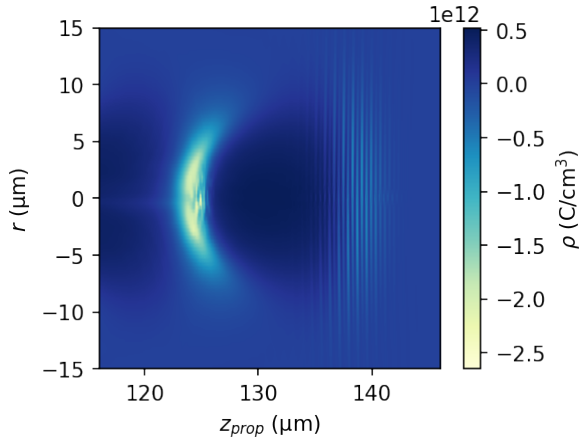

Figure 1.5: Bubble in relativistic regime, simulated using the FBPIC code by M. Kirchen and R. Lehe. It is possible to see the bubble in dark, while all the electrons (in a lighter colour because of the negative charge) are on the wake at the end of the bubble.

The electrons oscillations in the plasma, also called plasma waves, have a range of wavelengths and so a range of velocities, called group velocities. The phase velocity associated to the drive will be really close to the speed of light c; the wavelength of the driver is so equal to:

$$\lambda_p = \frac{c}{\omega_p} \tag{1.20}$$

The maximum electric field and maximum acceleration rate are determined by the maximum amplitude of oscillation supported by the plasma. When this boundary is reached, the plasma wave is said to break; the bubble created by the driver will be completely empty of electrons, and so the regime of acceleration becomes non linear, a condition not optimal for acceleration. The electric field associated with this regime, and so the maximum value inside the bubble, is called the *cold wave − breaking limit*.
Wave breaking in a plasma occurs when elements of the plasma electron fluid that started out in different positions overtake each other while moving back and forth during the passage of the wave. For both non-relativistic and relativistic plasmas, this overtaking happens when the peak fluid velocity equals the phase speed of the plasma wave. A direct consequence of this is that a large fraction of the plasma electrons get trapped in and accelerated by the plasma wave [31].
The maximum electric field for avoiding the wave breaking is calculated starting from of the electron density n_e, written as a fraction of the ion density n_i:

$$n_e = Z n_i \tag{1.21}$$

Where Z is the atomic number of the gas used. Using the Maxwell's equation:

$$\int E \cdot ds = \int \frac{\rho}{\epsilon_0} dV \tag{1.22}$$

an expression for the electric field is found as:

$$E = \frac{nex}{\epsilon_0} \tag{1.23}$$

Then, knowing the definition of plasma frequency from eq.1.15, it is possible to write E as:

$$E = \frac{\omega_p^2 m_e x}{e} \tag{1.24}$$

Since the maximum field happens for the plasma wavelength λ_p, it is possible to substitute the x with this quantity to obtain an expression for the maximum electric field as:

$$eE_{max} = m_e c^2 \frac{\omega_p}{c} \tag{1.25}$$

Inserting the eq.1.15 into the equation above, it is possible to say that the electric fields attainable by the plasma before the wave breaking phenomenon is:

$$E \simeq 96\sqrt{n_e[cm^{-3}]} \quad [V/m] \tag{1.26}$$

Assuming a plasma with a density of $10^{18} cm^{-3}$, a wave with maximum electric field peaks in the order of $100 GV/m$ can be generated, being three orders of magnitude more intense than the accelerating gradient in a conventional accelerator powered by microwaves. The length of the accelerating structure in a plasma-based accelerator is approximately the plasma wavelength in the linear regime[25].
Different particles can be accelerated in a plasma based accelerator: ions, protons and electrons can be accelerated through different mechanisms and different techniques; the most important ones of electron acceleration are the beam driven and the laser driven; combined, also a third technique can be implemented, as AWAKE project does. In case of ions and proton acceleration, less traditional method are implemented, using the interaction of a laser with a target to generate the ions.

1.3.1. Ion acceleration

Ions acceleration is made by the emission of protons from laser-irradiated metallic targets. The Bragg peak that ions have in their path makes them very suitable for highly

localized energy deposition, and so very useful in many applications, above all medicine. Other applications are laser triggering and control of nuclear reactions, production of warm dense matter, "fast ignition" of inertial confinement fusion targets, and injectors for ion accelerators.
In the technologies used nowadays the interaction is with solid target, where the penetration of the laser pulse depends not only on the electron density but also on the target size when the latter becomes close to or smaller than one wavelength[27].
The interaction between the laser and the target is shown in fig.1.6, where it is possible to see the fast ions produced by the interaction between the laser and the target.

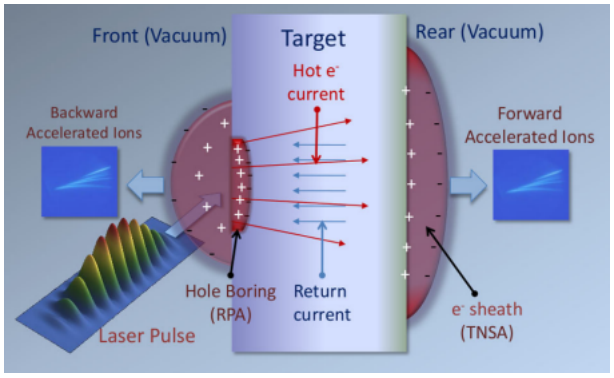

Figure 1.6: Some of the possible acceleration mechanisms in the interaction with a thick solid target[27].

Since the laser pulse cannot penetrate into solid-density regions, the absorbed energy is transported to these regions mostly by energetic (commonly named either hot or fast) electrons which may be generated during the interaction through several mechanisms.
Different ion acceleration procedures are used at the moment to accelerate protons; the most important one is the TNSA (Target Normal Sheath Acceleration).

TNSA

While TNSA can in principle accelerate any ion species present in surface layers, in most experimental settings this results in preferential acceleration of light ions (protons, carbon and oxygen ions).
Acceleration through this mechanism employs thin foils (typically from a few mm to tens of mm thickness), which are irradiated by an intense laser pulse. In the intensity regime of relevance the laser pulse can couple efficiently energy into relativistic electrons, mainly through ponderomotive processes.
While a limited number of energetic electrons will effectively leave the target, most of the

hot electrons will be backheld within the target volume by the space charge, and will form a sheath extending by approximately a Debye length λ_D from the initially unperturbed rear surface[9]. The acceleration is most effective on protons, which can be present either in the form of surface contaminants or among the constituents of the solid target as in plastic targets[27]. A scheme of how the process works can be seen in fig.1.7.
The highest TNSA energies reported are of the order of 60 MeV, obtained with large PW systems, and available data. The properties of the beams accelerated via TNSA are quite different from those of conventional RF beams, to which they are superior under several aspects. The beams are characterized by ultralow transverse emittance (as low as 0.004 mm-mrad), and by ultrashort (∼ps) duration at the source[9].

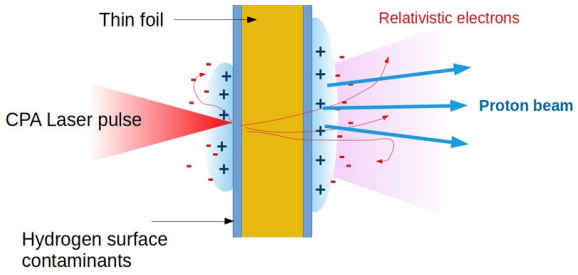

Figure 1.7: TNSA scheme.

1.3.2. Electron acceleration

Both mechanisms of electron acceleration are based on the creation of a wakefield; it can be created by sending a relativistic proton or electron bunch into an appropriate plasma or gas; this type of accelerator is called PWFA (particle wakefield acceleration). It requires a bunch with relatively high charge and thus strong fields. The high fields of the bunch then push the plasma electrons out from the center, creating the wake. Similar to a beam-driven wake, a laser pulse can be used to excite the plasma wake, and in this case the accelerator is called LWFA (laser wakefield acceleration). As the pulse travels through the plasma, the electric field of the light separates the electrons and nucleons in the same way that an external field would.

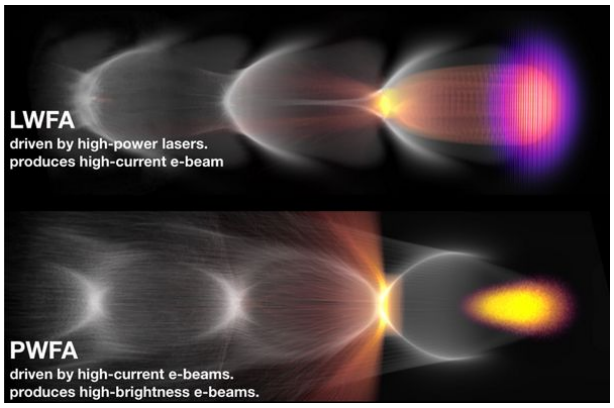

Figure 1.8: Particle-in-cell (PIC) simulations for an LWFA (top) and a PWFA (bottom). The figures show a laser and and electron-beam driver driving a plasma-electron density wave. The density of electrons being injected is also shown. In both simulations injection is triggered by means of induced ionization. In a hybrid LWFA | PWFA both plasma acceleration principles are combined for the production of superior quality beams from a particularly compact setup. Copyright: DESY Hamburg (Germany).

Electron driven PWFA

In this case, a driver bunch of ultra-relativistic electrons or protons is sent through a stationary plasma (fig.1.9). It allows a constant phase relation between accelerating driver beam and accelerated witness beam, and long acceleration distances in a single plasma wakefield stage. This permits large energy gains to be reached while the relative position and the conditions experienced by the accelerated witness beam inside the bubble remain essentially constant.

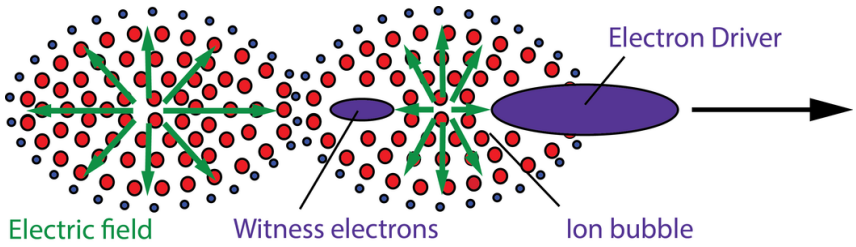

Figure 1.9: Scheme of the wakefield generated by the driver. The electron bunch expels the plasma electrons, creating an ion bubble with accelerating electric fields.

The space charge of the drive bunch displaces the plasma electrons transversely and excites the plasma electron oscillations at the plasma frequency ω_p. Although the wakefield structure and plasma response after the first full wave period is similar for both the positively and negatively charged driver bunch, the plasma response at the location of

the driver is different. In the case of a negatively charged drive bunch, e.g., an electron bunch, the repulsive Coulomb force initially expels plasma electrons from the bulk of the driver bunch[25].
In PWFA the wave is generated by the Coulombian repulsion of a charged beam; the electron expulsion generates the bubble, and the recombination region of expelled electrons generates an high accelerating gradient; a trailing bunch wisely placed in the wake can so acquire an high amount of energy. The equation of motion of the wave will be:

$$\frac{d\boldsymbol{p}}{dt} = -e\boldsymbol{E} \tag{1.27}$$

that, coupled with the continuity equation and one of the Maxwell's equations give us the fluid description for plasma electrons and immobile ions in a PWFA:

$$\left(\frac{\partial}{\partial t} + \omega_p^2\right) n_1 = \omega_p^2 \frac{q}{e} n_b \tag{1.28}$$

where n_1 is the plasma electron density, while n_b is the bunch density.
There are two regimes in which the PWFA can work: linear or nonlinear. In both cases it is possible to use the QSA (Quasi-static approximation) in which the plasma time scale is a lot lower than the beam time scale, the beam is considered as "frozen" when plasma response is calculated and the plasma density perturbation is local.
The linear regime, where the bunch density is very small compared to the plasma, has the advantage that the plasma oscillation may be resonantly driven, but has the notable drawback that the focusing is nonlinear in radial coordinate and the same dependence would apply for the provided acceleration.
In the nonlinear regime, called blow-out regime, the plasma response to a beam that is much denser than the ambient plasma is violently nonlinear, as the plasma electrons are ejected from the path of the intense driving electron beam, resulting in an electron-rarefied region. The plasma is no longer able to screen the beam and the perturbation theory, that assumes $n_1 \ll n_0$, is no longer valid. This region contains only (nearly stationary) ions, and thus possesses linear electrostatic focusing fields that allow high quality propagation of both the driving and accelerating beams [29]. Under these conditions, the plasma response is very nonlinear, the plasma wavelength λ_p depends on the wakefield amplitude and large wave-breaking spikes are excited at the end of the first plasma oscillation[26].

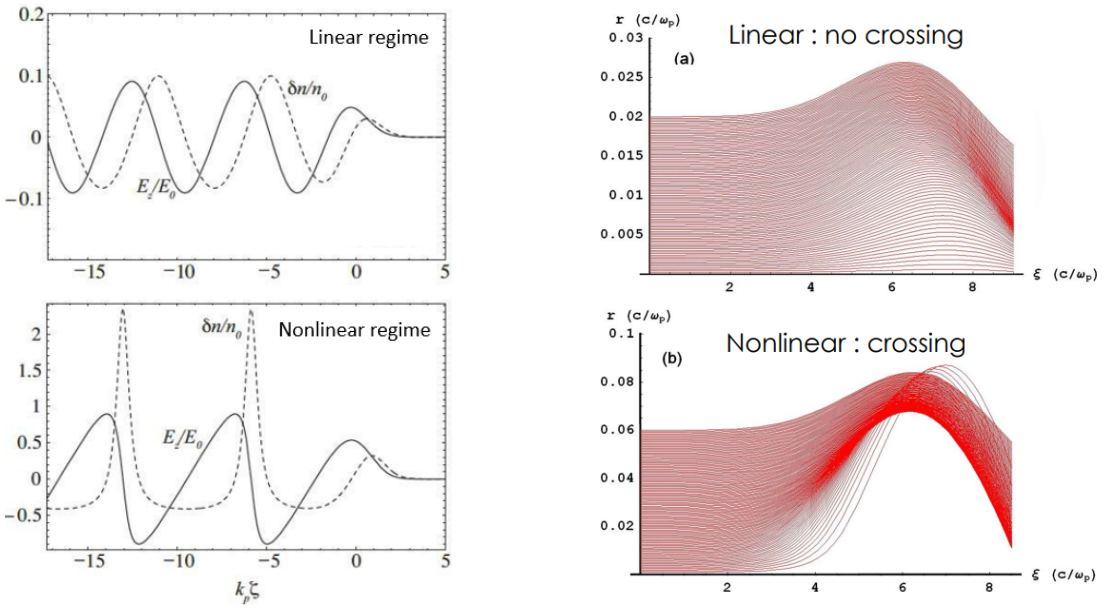

(a) (b)

Figure 1.10: a) differences in the electron density and electric field trend over in space of the two regimes. b)Plots of trajectories for electrons at different initial radial position. It is possible to see that there is a transition from no crossing to crossing[34].

Whether it is a relativistic or non relativistic blowout, a key property of these wakes is that particle crossing (or transverse wave breaking) occurs, and the fluid theory becomes inadequate to describe the response of plasma electrons (fig.1.10b). A fully kinetic approach is required.

To overcome the limitations both regimes have, it's possible to operate in the so-called quasi-nonlinear regime. It requires operations where one uses beam with relatively low charge and longitudinal and transverse beam size smaller than a plasma wavelength, σ_r, $\sigma_z << \lambda_p \sim 200\mu m$. In this case, the beam density may exceed that of the plasma, producing blowout (strongly non linear regime), but due to the small total charge, producing a disturbance that behaves in many ways as linear, having frequency essentially that of linear plasma oscillations.

An important topic in PWFA is the matching of the beam with the plasma; in fact, it is crucial that the two are matched, in order to preserve the quality of the beam and improve the acceleration. The beam is said to be matched in the absence of beam envelope oscillations, which represents the best conditions for quality preservation; instead, if the focusing term is not balanced by the emittance term, we observe betatron envelope oscillations, the beam is said to be mismatched to the plasma.

LWFA

In a laser-plasma accelerator, mentioned for the first time by Tajima and Dawson, an intense laser beam is used to drive a relativistic plasma wave, within which are formed strong longitudinal electric fields able to accelerate beams of charged particles. This approach has been used to generate quasi monoenergetic beams of electrons from plasma accelerators driven in plasma channels or gas jets to energies that, in the last years, have approached values of 8 GeV/m [21].
In LWFA the generation of the wave is due to the ponderomotive force, and so the motion equation has an expression different in the case of non relativistic ponderomotive force or relativistic ponderomotive force. In non relativistic regime F_P is written in the following expression:

$$\vec{F_P} = -\nabla U_P \tag{1.29}$$

Where U_P is the ponderomotive energy.
In the relativistic regime, it is possible to find the expression for the energy through the laser parameter:

$$\frac{d\boldsymbol{p}}{dt} = -\frac{1}{2}\frac{mc^2}{\langle\gamma\rangle}\nabla\langle\boldsymbol{a_0^2}\rangle \qquad\qquad \boldsymbol{a_0^2} = \frac{e\boldsymbol{A}}{m_e c^2} \tag{1.30}$$

with a_0 the laser strength parameter, defined as the peak amplitude of the normalized vector potential $\boldsymbol{A}$. The electric force of the plasma wave can never exceed the ponderomotive force of the laser; for LWFA in the nonlinear regime ($a_0 >> 1$) the maximum wakefield amplitude will be:

$$\frac{E_{max}}{E_0} = \frac{a_0^2}{\sqrt{1+a_0^2}} \tag{1.31}$$

Also in LWFA two regimes are present: in the linear regime, the plasma waves are sinusoidal as in PWFA, with a wavelength equal to λ_p, and the amplitude of the plasma wave scales linearly with laser intensity. In the nonlinear regime the plasma wave has a sawtooth shape, while the plasma wavelength increases owing to relativistic mass shift.
To be injected and trapped, an electron must reach the velocity of wake, and several possible methods are use to inject it: external injection from another accelerator (conventional or plasma), self-injection and controlled injection. The invention of the chirped-pulse amplifier enabled the use of high-power lasers with a pulse width approximately equal to the wavelength of a high-density plasma wave, and so the LWFA started to being developed. For short, high-intensity pulses ponderomotive force expels all electrons from region behind laser pulse; its condition is $a_0 > 2$ and $c\tau \sim \lambda_p\sqrt{a_0}/\pi$, with τ the timelength of the laser pulse; in this case the bubble is generated behind the laser pulse.
The scheme of a LWFA is the following (see fig.1.11): a high-power laser is applied into

the plasma and acts as the generator of the plasma wave. Then a ultra-intense, ultra-short ($\omega_L >> \omega_p$) laser pulse is focused into the plasma; electrons start to oscillate while the positively charged ions remain in place and pull back the expelled electrons, since they are too heavy to follow the electrons. If the laser pulse is shorter than the duration of this plasma oscillation, a fully blown out bubble without electrons is created behind the laser. If the conditions for the creation of this bubble regime are satisfied, strong fields in laser direction occur. Electrons are so confined or introduced in the wakefield, and remain within the focusing accelerating phase of the wave, gaining energy from the wakefield.

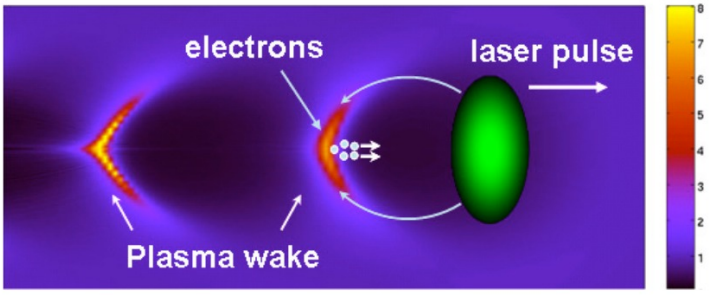

Figure 1.11: Scheme of a LWFA

Despite huge advantages that the LWFA brings, it is subjected to several factors that limit the energy gain for LWFAs: electron dephasing, laser depletion, laser diffraction as well as various laser-plasma instabilities. PWFAs usually use highly relativistic particle bunches from conventional accelerators as the driver, thus it do not significantly suffer from the dephasing effect in the acceleration distance of interest. The quality of the beam is higher in the case of PWFA than in LWFA, since the angular spread in the second case is too high. The efficiency is also higher, because there are still no high quality lasers for this type of applications. LWFA would be cheaper and more compact than the PWFA, but nowadays this particle driven type of plasma accelerator is the most developed one due to the less difficulties in the development and use of the machine.

AWAKE technology

The Advanced Proton Driven Plasma Wakefield Acceleration Experiment (AWAKE) aims at studying plasma wakefield generation and electron acceleration driven by proton bunches, currently being built at CERN. Its innovation lays in the combination laser and beam driven acceleration; in particular, it is the first proton driven wakefield accelerator.
Plasma wakefields are typically excited either by a relativistic particle bunch or an intense laser pulse. The distance over which the bunch or pulse can drive high gradient wakefields depends on its stored energy; in 2009, Caldwell proposed to accelerate witness electrons

in plasma wakefields driven by a Large Hadron Collider (LHC) type proton bunch. The bunch consists of $3x10^{11}$ protons with a particle momentum of 400 GeV (19.2 kJ)[20].
The plasma source used is a plasma cell of 10m length, made of a rubidium vapor source, ionized by a short laser pulse that precedes the proton bunch. The vapor cell ends have a continuous flow through orifices at each end, so that a n uniform gas distribution can be ensure. The density gradient in the plasma cell is controlled by the temperature difference of the Rb sources at each end of the plasma cell.
AWAKE uses a short-pulse Titanium:Sapphire laser to ionize the rubidium source.that can deliver up to 500 mJ in a 120 fs pulse envelope.
First, the laser is injected into the plasma; passing through the plasma, it creates a long bunch of protons that separate in microbunches. These microbunches will serve as the wakefield for the electron bunch, that will be sent in the gas cell with a frequency to match the timing of the proton bunches. In order to optimize the electron injection and avoid the ramps created by the ionization of the plasma by the laser, it is applied an oblique electron injection, as shown in fig.1.12.

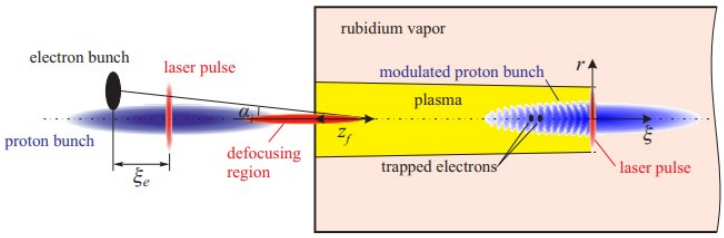

Figure 1.12: The oblique injection of the electrons into the plasma [20].

The laser-driven wakefield provides strong linear transverse focusing of the electron beam. On exiting the plasma this is lost and the beam diverges due to its finite emittance.

2 | Electron plasma accelerators sources

One of the most important component of an electron plasma accelerator is the plasma source; inside it, an acceleration up to GV/m takes place, so it's important to understand and choose the right type of source for every purpose.
In literature many types of plasma sources are investigated, since for different purposes different configurations and characteristics in the plasma are needed. Nowadays the most important ones are the gas jet, the gas cell and the discharge capillary; the implementation of these devices is different, and also the range of densities that can be performed inside is different.

2.1. Gas Jet

Laser wakefield accelerators rely on a plasma to act as both electron injector and accelerator. This plasma is created via ionization of a gas target and in order to permit a laser pulse to propagate. A gas jet primarily consists of a high-pressure gas valve and an individually designed exit nozzle; the laser is focused onto the gas that flows freely into the vacuum chamber.
Controlling the gas flow by the use of a sonic or a supersonic nozzle is essential to provide the desired interaction density profile. For example, changing the gas pressure will vary the initial neutral density, while changing the nozzle diameter will change the plasma length.
The typical configuration shown in fig.2.1 is composed of a gas flow coming from the gas jet, that will be completely ionised by an ultra-short, high-intensity laser pulse focused into a jet of gas, coming from the nozzle; through this procedure, it is created a plasma channel within the jet. The gas used is typically helium as it is a low atomic number gas that is easy to ionise, but mixtures of it with other gases are often used to increase the charge of the bunches generated. Gas jets are the most common type of gas target used for laser wakefield acceleration for many reasons. first, they are much simpler to align

due to their open geometry; this property offers good accessibility for diagnostics, which is interesting for prototyping and proof-of-concept setups. But furthermore their stability and durability makes them a frequent choice for permanent setups[12].

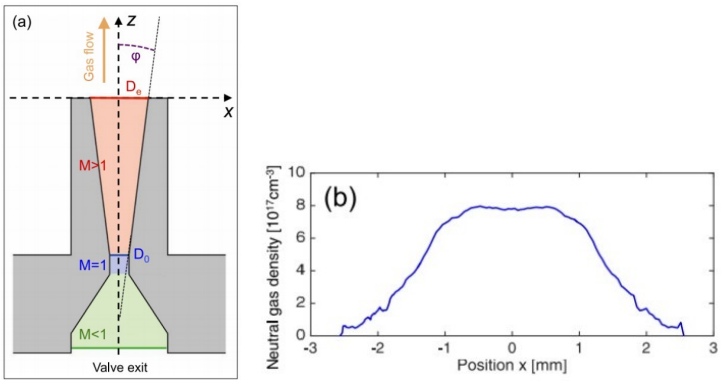

(a) (b)

Figure 2.1: An example of a supersonic gas jet. (a) A fast valve releases a pulse of gas from a backing reservoir through a constriction and in to a conical nozzle. The jet is tailored by choice of inner diameter D_0, exit diameter D_e and opening angle Φ. M represents the Mach number in each region. (b) Optimising the nozzle parameters produces a flat top density profile above the nozzle, as illustrated[16].

The main disadvantage is the large volumes of gas they eject, even when operated in pulsed mode, which is prohibitive for high repetition rate operation, larger than 10Hz. Ripples in the gas density profile, which can be caused by imperfections on the nozzle surface, can caused unwanted self-injection and acceleration of dark current[16].
Gas jet are used also in PWFAs, since utilizing LWFA beams as PWFA drivers in a staged LWFA-driven PWFA (LPWFA) combines the unique features of each plasma acceleration method in a compact geometry with a twofold potential. First a laser driven stage is present, to generate high peak-current drive electron beams; then, a thin foil is positioned at the entrance of the PWFA, to reflect the spent laser pulse, whereas the electron beam passes through the foil and drives a purely beam-driven wakefield, as it is shown in fig.2.2. In contrast to the self-ionized regime, creating a pre-formed plasma environment allows the whole drive beam to contribute to the plasma wakefield formation, thus transferring more energy to the plasma and driving a larger amplitude wakefield[24].

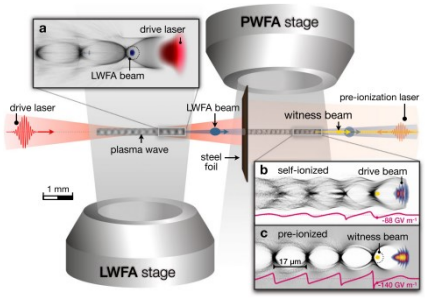

Figure 2.2: Schematic overview of the layout. [24]

2.2. Gas cell

To generate stable electron beams from the laser wakefield acceleration (LWFA), the plasma source must provide a stable plasma density. A stable plasma density can be achieved in a gas cell when a high-power laser pulse propagates in the gas cell, making it a good plasma source. Plasma cells are devices composed by a long cylindrical channel with a small diameter; since a suitable gas target for LWFA should have a tunable density and length, with a uniform density profile, gas cell is used for this purpose.
It has no electrodes or high voltages to produce plasma, tunable dimensions and different configurations. It is a box with a pinhole at each end to allow the driver to enter and exit the cell. The cell is filled with gas in the few tens of mbar to 1 bar range to give molecular densities in the range between 10^{17} and 10^{19} cm^{-3}. This significantly reduces the gas load to the chamber compared to gas jets. Like gas jets, laser ionisation is required. The pinholes should be sufficiently large as to reduce damage from higher order modes in the focal spot, as their erosion changes both the gas density and profile. Multiple designs of adjustable length gas cells exist. The length is variable, and goes from 0 up to a few centimeters[16]. The use of gas cells has been shown to contribute to the stability of electron production as the gas confined in the cell is relatively homogeneous. There are different types of gas cells; in the last decade two configurations have been most developed. The first configuration is shown in fig.2.3; the cell design employs two separate gas feedlines to provide different gases at the same time. A square cross-sectional capillary hole is formed by placing two thin (350 μm) sapphire plates between two thick (2 mm) sapphire plates. This configuration allows to provide an upward plasma density tapering in the range of 10^{18} and 10^{19} cm^{-3}, which has a potential to enhance the electron beam energy in laser wakefield acceleration experiments.

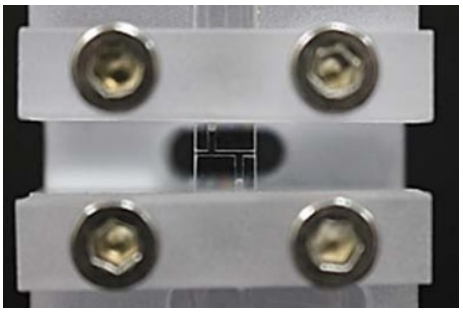

Figure 2.3: Detailed pictures of the first configuration for capillary gas cell[23].

The second configuration is used at ELISA (ELectron Injector for compact Staged high energy Accelerator), where multi-stage LWFA is studied.
The design of the gas cell is reported in fig.2.4, where it is possible to note the tunable length of the cell. Changing the diameter of the plate apertures allows one to control the shape of the gradients of the density profile along the laser axis, while changing the cell length allows to have a density profile more uniform or curve, to use it for different applications.

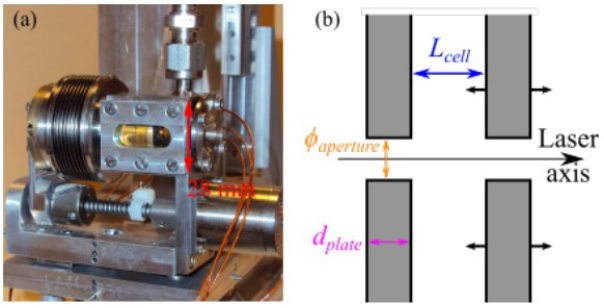

Figure 2.4: (a) Photograph of the ELISA gas cell.(b) Schematic longitudinal cut of the gas cell[5].

2.3. Plasma capillary

Plasma capillaries are the type of plasma sources studied in this thesis. They are generally 3D-printed, made out of rigid materials, like plastic or Sapphire.
Compared with other plasma sources, as plasma jets or plasma cells, gas filled capillaries allow to control the properties of the plasma channel locally by varying the geometrical characteristics or by timing the discharge with the beams to wait for the desired plasma profile during the interaction. This let to have homogeneous plasma profile even at low densities of the order of 10^{15} -10^{18} cm^{-3}, the one requested for beam driven plasma accelerators.

Discharge capillaries are an attractive method to confine plasma. In this technique, a capillary is filled with gas via small holes located some millimetres from each end of the capillary. A pulsed discharge current of several hundred amperes, and several hundred nanoseconds duration, is driven through the capillary via coaxial electrodes at each end of the capillary ionizing it. The plasma density distribution along the capillary depends strictly on the capillary geometry and so simulations of the capillary behavior is not straightforward due to the high number of parameters to take into account, such as the shape and the composition of the electrodes and the capillary[14].
A real picture of a generic capillary can be seen in figure 2.5, where the capillary used at BELLA (Berkley, USA) is shown.

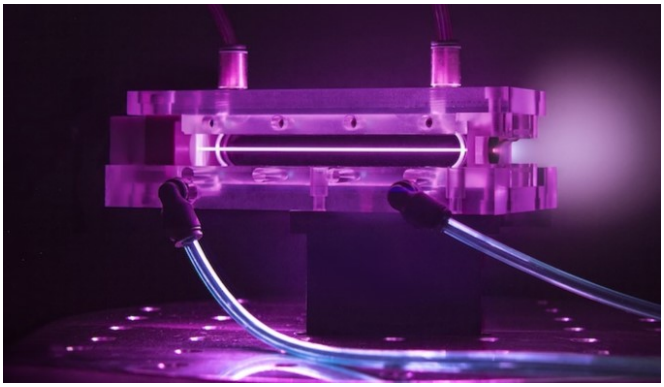

Figure 2.5: A 9 cm-long capillary discharge waveguide used in BELLA experiments to generate multi-GeV electron beams. The plasma plume has been made more prominent with the use of HDR photography. Credit: Roy Kaltschmidt

Variation in plasma density along the interaction length results in a variation of the accelerating structures, and so it must be controlled and properly tailored to preserve the quality of the accelerated beam. Gas-filled capillaries are well-suited devices to control plasma density up to centimeter scale length; this technology also ensures a stable and repeatable plasma density distribution during the interaction with the drivers.
Tailored longitudinal and radial plasma density profiles can aid in the matching of externally-injected charged particle beams, preserving transverse and longitudinal beam quality and allowing extended stable wakefield propagation. Profile shaping can facilitate the realization of internal injection, correction of dephasing and hosting mitigation [15].
The effective utilization of the capillary plasma source requires a comprehensive understanding of the gas density distribution within the capillary. To characterize the capillary density profile, different types of diagnostic can be used; in particular, in section 3.3, it will be explained the Stark Broadening technique, a type of diagnostic used during the experiments carried on in the thesis.

Different capillaries with different shapes are used around the world; some examples are the ones used at SPARC_LAB in Frascati, Italy(fig.2.6a), the one of DESY in Hamburg, Germany (fig.2.6b) and the one use at BELLA at Berkeley, California (fig.2.6c). These capillaries are all different, but they all have in common the discharge that is needed to generate the plasma, the gas inside, that can be Hydrogen but also a different one, and a channel where the beam passes.
All the three models of capillary shown in fig.2.6 are composed of a pair of electrodes, inlets and a channel, that can be tailored in different shapes; also the length can be tune, from a few cm up to half a meter. All the different configurations are used to obtain different electron density profiles inside the capillary, useful for different applications.

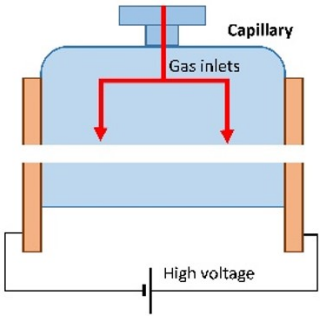

(a) SPARC_LAB capillary [26].

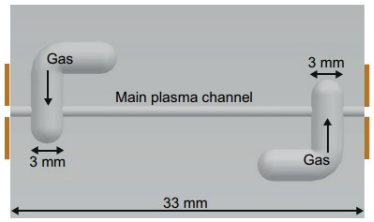

(b) DESY capillary[15].

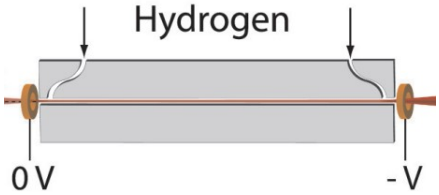

(c) BELLA capillary[18].

Figure 2.6: Designs of capillaries used in different laboratories.

2.3.1. Capillary as active plasma lens

An attractive method to use the gas filled capillary is to focus the electron beams through the creation of a radially symmetric field, so using it as an *active plasma lens*.
In fact, according to the Ampère law, the discharge induces an azimuthal magnetic field B_ϕ whose strength is directly proportional to the flowing current I_0:

$$\frac{\partial B_\phi}{\partial r} = \frac{\mu_0 I_0}{2\pi R^2} \tag{2.1}$$

with μ_0 the vacuum permeability. Then, the magnetic field will generate a Lorentz force that, depending on the direction of the current flow, will be directed towards the axis or the walls of the channel, and so it will focus or defocus.
A scheme of how it works can be found in fig.2.7. Such a magnetic field can focus high-energy beams over distances of centimetres, rather than metres as is the case for conventional magnet-based techniques.

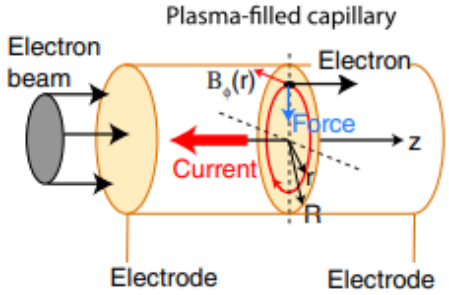

Figure 2.7: Schematic concept of the focusing force in an active plasma lens[33].

An ideal APL (active plasma lens), assuming a cylindrical channel filled with plasma of uniform conductivity, can provide radially symmetrically uniform focusing field. The principle of a APL is that a proton beam collinearly propagating along an actively externally current I is radially focused. The interaction of charged particles with plasma has important influences on focusing, in fact the APL can effectively focus beams in a state where the plasma medium cannot significantly affect the intrinsic characteristics of the beam, such as emittance and energy; this use is still theoretical and not tested yet.
Since beam injection and extraction from a plasma accelerating module is still one of the crucial aspects to be solved for the plasma-based acceleration of high quality electron beams, plasma lenses are currently enjoying a renaissance worldwide to demonstrate their integration in conventional transport beam lines without affecting the beam quality and, in particular, avoiding emittance degradation[11].
State-of-the-art quadrupoles are not strong enough compared to transverse plasma gra-

dients to limit the emittance growth that might occur because of the abrupt transition between plasma and vacuum. At the exit of the plasma-accelerating module, the beam size is a few micrometers, therefore with typical values for the normalized emittances of $\sim$ 1 mm mrad, the angular divergence of several mrad and the betatron function of few millimeters for GeV beams[11]. In the future, plasma lens technology can replace conventional devices (like solenoids and quadrupoles) with more compact structures.

2.3.2. Optimization of discharge capillary for electron plasma acceleration

As it has been explained in the sections before, plasma discharge capillaries have a lot of applications and ways of usage. In fig.2.6 different geometries have been shown, each with qualities and problems to solve. The objective of the work done at SPARC_LAB test facility was to improve the properties of the plasma source used right now in the accelerator, and to study the dependence of the plasma density inside the channel on different parameters and conditions.
The aim of this study is to improve the acceleration process, to enhance the shot-to-shot stability of the source and to find new solutions for new applications of the discharge capillary, as the use of it as an active plasma source.
Starting from the capillary used right now, the goal is to arrive at a m-scale long capillary, that will be used in the future in the EuPraxia project. A prototype of this capillary has been already done, and is shown in fig.2.8. It is 40cm long, with different inlets and a cylindrical channel with a diameter of 2mm.

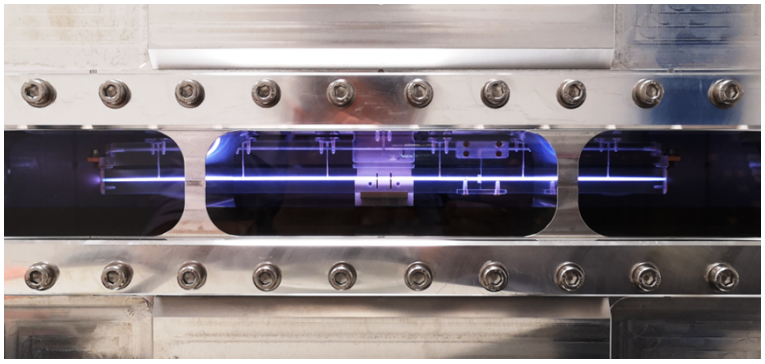

Figure 2.8: EuPraxia capillary prototype[26].

3 | Experimental setup

3.1. Overview of SPARC_LAB facility

SPARC_LAB (Sources for Plasma Accelerators and Radiation Compton with Laser And Beam) facility at LNF is a part of the laboratories that aims to study and perform plasma acceleration. It is based on the combination of the high−brightness ($\approx 10^{15}$A m^{2}rad^2) SPARC photo injector with the highintensity ($\approx 10^{19}$W/cm^2) FLAME laser. The joint presence of these two systems allowed the investigation of several plasma acceleration schemes, e.g. self and externalinjection, laser and beam driven, and a wide spectrum of interdisciplinary leading−edge research activities based on novel radiation sources such as FreeElectron Laser (FEL), both in Self Amplified Spontaneous Emission (SASE) and seeded schemes, and high peak power THz radiation both in the broadband and narrow−band range.

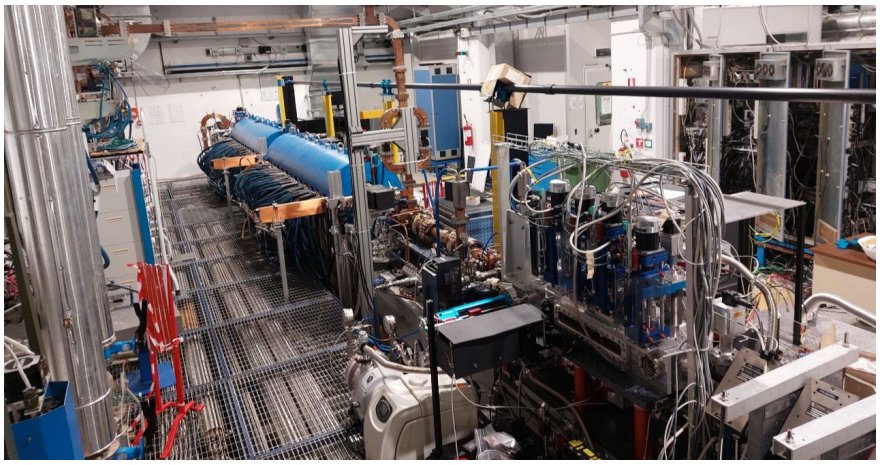

Figure 3.1: SPARC_LAB real photo. It is possible to see the layout until the vacuum chamber inside which the capillary is placed.

The work on plasma is motivated, in the framework of the EuPRAXIA project, by the EuPRAXIA@SPARC_LAB user facility that foresees the realization of the first ever plasma

beam driven facility at LNF.
The structure of SPARC starts with a laser driven RF photoinjector gun, where the electrons are accelerated up to 5.6 MeV, followed by the main linac consisting of two travelling-wave (TW) S-band structures and a TW one operating at C-band (f_{RF} = 5.71 GHz), with a total accelerating gradient can raise the beam energy to 170 MeV. The electron beam is produced by a photo-cathode laser and is working in single pulse mode at a 10 Hz repetition rate.

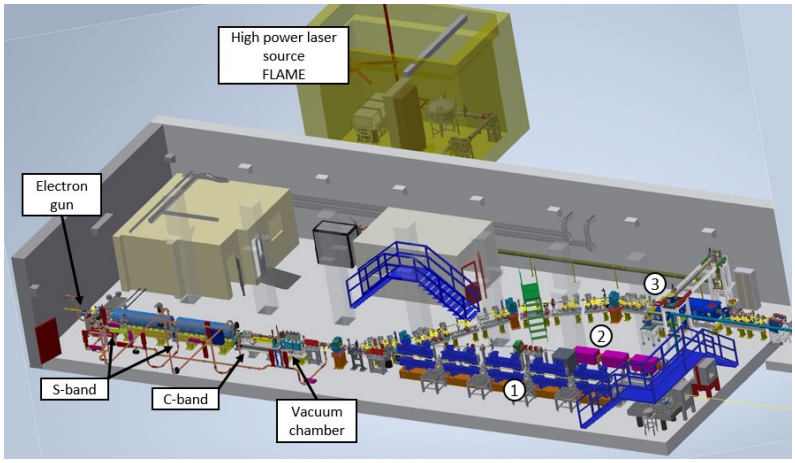

Figure 3.2: SPARC_LAB layout. Different beamlines follows the COMB, devoted to FEL physics (1), beam diagnostics (2) and X-rays production in the Thomson interaction chamber (3)

The photocathode is composed by a 1.6 cell RF gun operated at S-band (2.856 GHz, of BNL/UCLA/SLAC type) with a high peak field on the cathode (120 MV/m) generating 5 MeV electron beam. The laser is a TW-class Ti: Sapphire system which has two laser access points: one at 70° of incidence from viewports beside the photocathode and one at 3° of incidence with an off-axis mirror inside a vacuum chamber at about 0.5 m from the cathode. Quantum efficiency is typically in the order of 10^5 for our copper cathode and we measured intrinsic emittance of 0.7 mm mrad /mm. A four-coil solenoid assembly approximately 20 cm in length is inserted after the RF gun. This element is crucial for emittance minimization to have high brightness electron beam, in a configuration where a double minimum in emittance is generated along the line [26].
The SPARC photo-injector has a wide flexibility and is able to provide very different working points for the electron beams in terms of charge and duration, that thus peak current, with an overall high-quality on the transverse phase-space with relatively small projected emittances. The beam energy can be tuned in a wide range, from 5∼MeV to

180 MeV, by acting on the RF system of the accelerating sections; the two S-band sections are able to accelerate up to 20MV/m, while the C-band section is able to accelerate around 40MV/m. On top of that, a slightly off-crest operation can be used to reduce the final energy spread or properly manipulate the beam LPS. The wide tunability in terms of beam duration is ensured thanks to the on-crest or RF compression, by means of velocity-bunching (VB), operation of the first accelerating section. With VB the longitudinal compression is indeed achieved by slightly accelerating the tail of the beam while decelerating its head. This leads to a rotation of the beam longitudinal phase space that is simultaneously chirped (with a varying frequengy between the head and the tail of the laser pulse) and compressed[26].

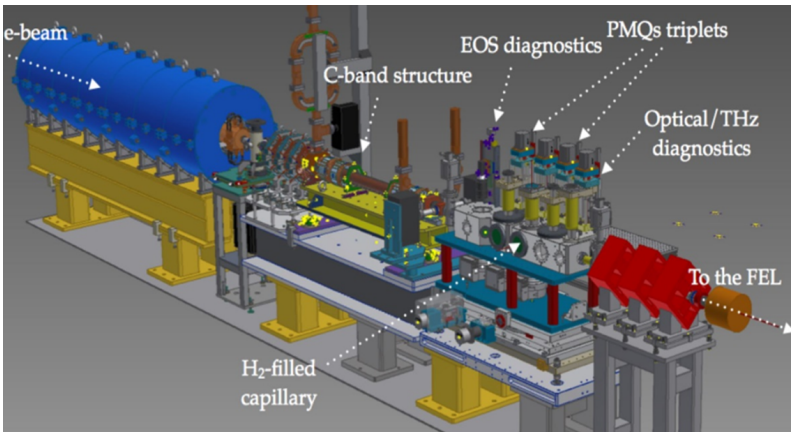

Figure 3.3: Layout of the SPARC photo-injector and the plasma interaction chamber.

The gun is crucial for emittance minimization to have high brightness electron beam, in a configuration where a double minimum in emittance is generated along the line[26]. The first two S-band sections are surrounded by Solenoid coils, which provide additional magnetic focusing for more reliable control of the beam envelope and the emittance oscillations following RF compression first-rate; each solenoid is composed by a long iron joke containing 13 coils forming a long solenoidal magnetic field. After the solenoid there is a small diagnostic station for beam characterization in transverse dimension, energy, charge and emittance.
For the S-band LINAC it is used a SLAC constant gradient design Solenoid with an accelerating field of 20 MV/m, with a length of 6m. A third C-band section of 1m allows an higher gradient (>40 MV/m), since it works in the microwave frequency range.
A Plasma Chamber, where the plasma acceleration actually happens, is placed after the LINAC (fig. 3.4); since the particle-driven plasma acceleration tests exploit different configurations, such as one or more driver bunches creating a pulses train similar to a comb

shape, the chamber is named COMB. It consists on a vacuum chamber with the plasma source inside; a detailed description can be found in section 3.2.2.
As it can be seen in fig.3.2, there are three different beam lines located downstream the main magnetic spectrometer. The first one is dedicated to the Free-Electron Laser (FEL) by means of six magnetic undulators. The second one consists of a dogleg line and hosts two THz undulators devoted to users applications. The third one is currently under development and will be devoted to LWFA experiments. The details of these beam lines are reported in the following paragraphs. The parameters of the beam used at SPARC_LAB are listed in the table 3.1.

parameter	value
Number of bunches	1-5
Delay between bunches	0.5 ps-20 ns
Charge	10 pC-2 nC
Duration	20 fs-10 ps
Energy	5-180 MeV
Energy spread	0.1-5 MeV
Normalized emittance	0.3-10 μm

Table 3.1: Range of electron beam parameters that can be obtained with the SPARC photo-inejctor.

The Frascati Laser for Acceleration and Multidisciplinary Experiments (FLAME) shown in fig.3.2 is a compact femtosecond laser system able to provide pulses with a maximum energy of 7J with a peak power of 200TW and 10Hz repetition rate, based on the design of Amplitude Technology's Pulsar system and configured with custom front end and modular choice of pump lasers. The system is a Titanium-Sapphire laser based on the so-called Chirped Pulse Amplification (CPA).
The laser FLAME is equipped of a clean room, hosting the front-end, the high-power multi-pass amplifier and a compact laser compressor; and two experimental areas, the Guiding Experimental Measurement (GEM) Area and TW Experimental Target (TET) Area, dedicated to different experimental campaigns amongst them gas-solid target interaction, high-power laser guiding for LWFA experiments and plasma characterization experiments.
Major components of the SPARC LAB accelerator used for characterizing electron beams, in addition to the accelerating structures, are: electro optical sampling (EOS) diagnostic,

a terahertz (THz) diagnostic, the RF-deflector (RFD) to measure the longitudinal phase space of the beam. The EOS diagnostic is located next to the plasma chamber, before the plasma capillary for evaluating the longitudinal beam properties before the acceleration in order to be matched with the plasma properties. By using a single shot measurement, it is possible to reach a resolution of $20 - 50$ fs and monitor the distance between driver and witness bunches. The THz source is placed inside the plasma chamber downstream of the plasma, which is a multi−shot measure device and can be used to evaluate the longitudinal beam dimension with a resolution of about 10 fs. The RFD system after the plasma interaction chamber is embedded. This system, estimates the longitudinal dimension of a beam with a resolution of 30 fs. A combination of the RFD and a bending magnet, placed downstream on the transport line performs direct measurements of the longitudinal phase space[28].

3.1.1. Plasma chamber for acceleration experiment

The vacuum chamber installed at the end of the C-band accelerating structure is dedicated to host the plasma source for acceleration, and it is called COMB chamber by virtue of the multi-driver acceleration technique that can be implemented inside it. It has the main constraint on the vacuum system represented by the limit value of 10^{-8}mbar that has to be maintained outside the chamber at the C-band side.

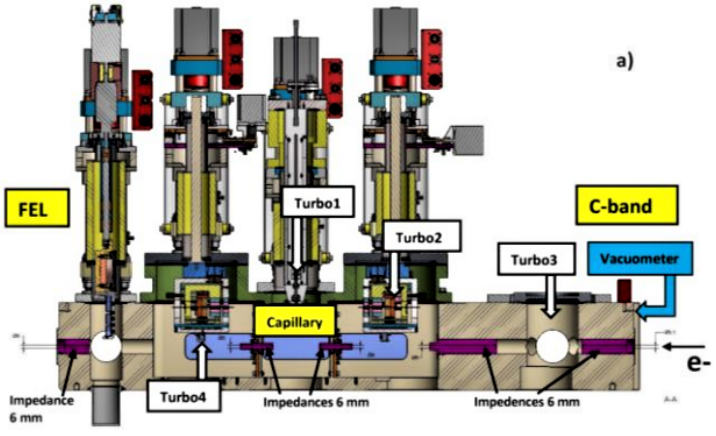

Figure 3.4: Structure of the COMB chamber

This request strongly affects the entire plasma structure, both chamber geometry and pumping system, since during the plasma formation at densities useful for the acceleration we need to reach pressure up to 50 mbar inside plasma sources installed in the vacuum chambers. Inside the chamber an Hydrogen-filled capillary is fixed, where the

gas injection is controlled by means of an electro valve and a mechanical regulator placed between the hydrogen gas tank and the plasma source itself; the structure of the COMB chamber is shown in fig.3.4.
The chamber outline aims to provide the plasma channel system a transverse and longitudinal diagnostics, and permanent quadrupole magnets to match the beam at the vacuum-plasma interface and the extraction from plasma. In order to adjust the beam transverse dimensions to the plasma properties, a permanent magnet quadrupole (PMQ1) is installed at the entrance of the capillary. Then, at the exit of the plasma source, in order to catch the accelerated beam, a second permanent magnet quadrupole (PMQ2) has to be used.
As said before, the main problem related to the COMB chamber is the mantainment of the value of vacuum: in order to preserve the vacuum level during the whole process of plasma formation and acceleration, several pumps are mounted on the vacuum chamber. The pumping system is composed of 4 turbo pumps and 5 Scroll pumps mounted on the chamber, with parameters listed in table 3.2.

parameter	off-line
Turbo pumps (l/s)	1780 l/s
Scroll pumps (m^3/h)	150 m^3/h

Table 3.2: Vacuum parameters during vacuum test (off-line) and during operating conditions (on-line)[7].

3.2. Plasma Diagnostic Lab

The Plasma Diagnostic Lab, called PLASMA LAB, is the part of SPARC_LAB facility in which plasma source development and diagnostic take place. The main activity concerns theoretical studies and experimental developments of devices used to confine the plasma. The overall apparatus of the lab consist in a vacuum chamber, in which a he plasma source used for particle acceleration experiments at SPARC_LAB test facility composed of thin capillaries is placed, and an apparatus needed in order to create, confine and characterize plasmas for plasma-based accelerators. The capillary is connected at the extremities to two electrodes in order to generate the plasma through high voltage pulses able to ionize gases at pressures in the range 10-100 mbar. The two electrodes are connected outside the vacuum chamber with a high-voltage pulser circuit, a gas dispenser, with H_2 or another type of gas, and three pumps used to generate the vacuum at which the chamber works. The high-voltage source is composed of a switch circuit able to produce short electrical

pulse of 1 μs duration and a high-voltage generator used as the power supply device of the first one. Voltage and current amplitude can be selected by using these circuits. For the gas discharge, it is possible to control the pressure at which the gas enter the inlets of the capillary.
The vacuum system is made of two scroll pumps and one turbopumps, since the vacuum level has to be maintained below 1x10^{-6} mbar in the experimental chamber before every shot.
The overall experimental apparatus is presented fig.3.5.

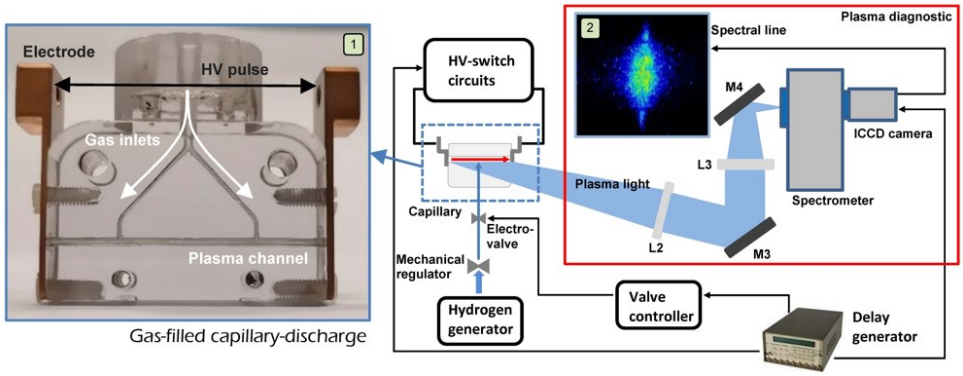

Figure 3.5: Scheme of the plasma module for plasma-based accelerators used at SPARC_LAB test-facility for which the plasma source is a gas-filled discharge capillary[6].

3.2.1. Plasma source

Typical capillaries used for SPARC_LAB experiments are realised through 3D-printers with a particular transparent plastic material named VeroClear, which is particularly suitable for plasma diagnostics like spectroscopic or interferometric analysis. Two Copper electrode plates are placed on the short side of the capillary through pairs of tiny screws and coupled with a high voltage discharge pulser for providing current, as shown in fig.3.6b.
It is possible to study the longitudinal and transverse plasma density distribution, inside and outside the channel, in order to study the interaction with the electron beams to be accelerated. The capillary itself can be also modelled changing different parameters, as the diameter of the channel, the number and distance of the inlets, the length and the shape of the channel; different types of capillary are shown and compared in this dissertation, in order to optimise the plasma distribution and consequently to maximise the efficiency of acceleration.

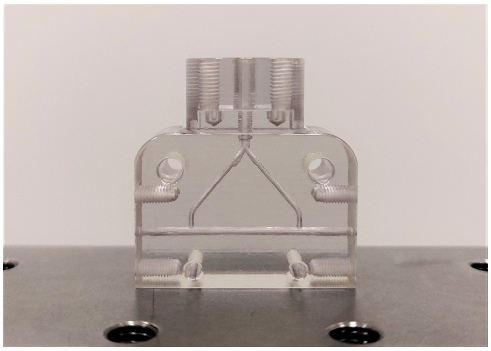

(a) A generic capillary

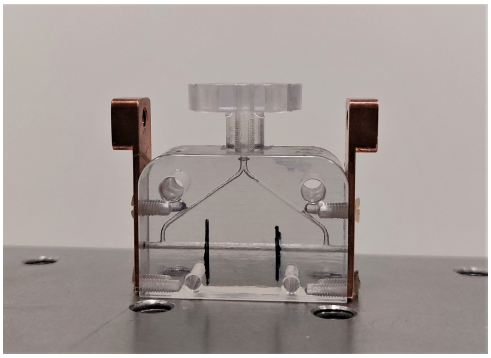

(b) Connection with the electrodes

Figure 3.6: Images of real capillaries used for characterizing the plasma behaviour and then at the SPARC_LAB accelerator for plasma acceleration experiments.

The capillary is then placed inside the vacuum chamber and connected to the gas injector; in this thesis, when the value of pressure is shown, it relates to the pressure at the connection between the gas tube and the capillary.
The generation of the plasma consists in different steps: initially, a gas injection inside the capillary is generated; thereafter, an electric impulse is sent to the two electrodes. The voltage will ionize the gas inside the channel, and so will generate the plasma. This procedure is repeated with a tunable frequency in the order of 1-10 Hz, and with an intensity of the impulse and a pressure of injection of the gas tunable too.

3.2.2. Plasma formation system

The plasma formation system is composed by two parts: the discharge circuit, used to generate the current inside the channel, and a gas injection system, needed to inject the gas inside the source; a scheme of the system is shown in figure3.7.

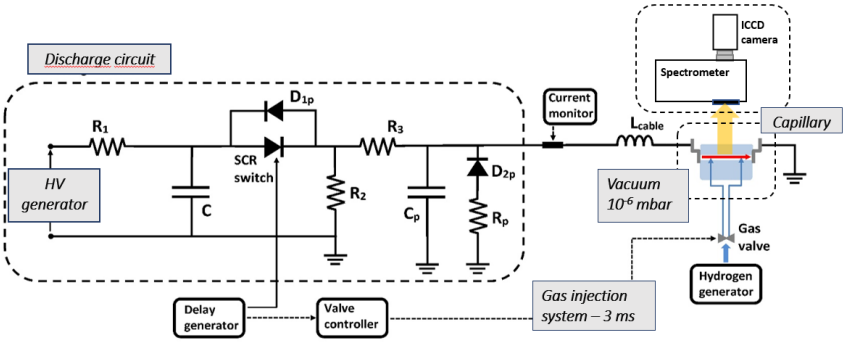

Figure 3.7: Scheme of the plasma formation system.

The discharge apparatus is composed of two parts: a high voltage generator that supplies a switch circuit based on the charging and discharging of a capacitor through the plasma capillary; also, the solid state switch circuit, together with the electronic gas valve, controls the repetition rate of the plasma formation within the capillary[6]. The high voltage discharge includes several components: first of all, a delay generator controls the timing of gas and HV discharge, in order to synchronise them; the delay generator is then connected to all the other parts of the experimental setup: the valve controller, which governs the gas injection inside the capillary's channel, the HV pulser and the image acquisition system, formed by an imaging spectrometer (SpectraPro 275) equipped with an intensified CCD camera (Andor Istar 320) where the images are taken; finally, a gas source is used to produce hydrogen to be ionized.
The gas injection circuit is needed for the plasma to form into the capillary. Hydrogen is produced by the electrolysis of water by using the NM Plus Hydrogen Generator. The gas pressure inside the channel is imposed outside the vacuum chamber by using a pressure regulator set to 100 mbar. The valve is typically open 3 ms to have uniform filling of 3-5 cm long capillaries, and then the discharge takes place 10 µs after its closure.
The high-voltage power source produce the gas ionization along the capillary channel. For each pressure value set inside it, in the range 10-100 mbar, by means of the mechanical valve, voltage and current can be imposed to select the ionization level and so the plasma density requested for the acceleration experiments. The typical current profile measured for 3cm long capillaries with 1 mm in diameter is shown in figure 3.8. A requirement for the current profile is that the voltage curve needs to be clean and well define, so that also the current is precise. The relation can be seen in fig.3.8.

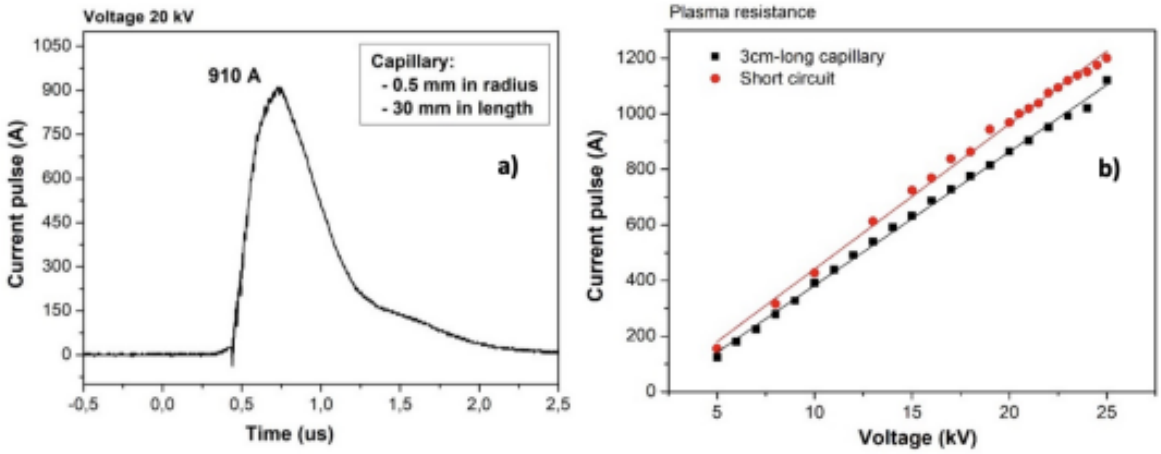

Figure 3.8: a) Current pulse produced by high-voltage pulse circuit; b) Relation between the voltage applied and the current in the capillary.

The possibility to use a gas filled discharge capillary to accelerate and to focus an electron beam and, at the same time, preserving the beam quality, is related to the capability to reach high values of the peak current. In fact, both the ionization degree and the radial uniformity of the plasma electron density depend on the plasma temperature that can be reached inside the capillary's channel, which in turn depends on the plasma current produced during the plasma creation[6]. The temperature reached in the capillary is calculated through the following formula [8]:

$$T[eV] = 5.7 \left[\frac{I_{peak}(kA)}{R_{ch}(mm)} \right]^{2/5} \tag{3.1}$$

where I is the peak current pulse measured in kA, R_{ch} represents the capillary radius measured in mm and Te is the electron temperature.
Temperature, pressure and plasma electron density represent the parameters needed to understand the plasma evolution and match it with the acceleration experiments. The plasma electron density is related to its behaviour in terms of stability, uniformity and repeatability, which in turn depends on the high-voltage pulse and the geometric properties of the structure. Therefore, the plasma characterization inside the gas-filled capillary-discharge is performed in terms of longitudinal and transverse electron density distribution.
The plasma density directly depends on the Hydrogen pressure set inside the capillary's channel, which in turn will determine the voltage pulse that has to be used to produce the gas ionization; from the Paschen curves it is possible to determine the minimum HV to apply for producing plasma (fig. 3.9).

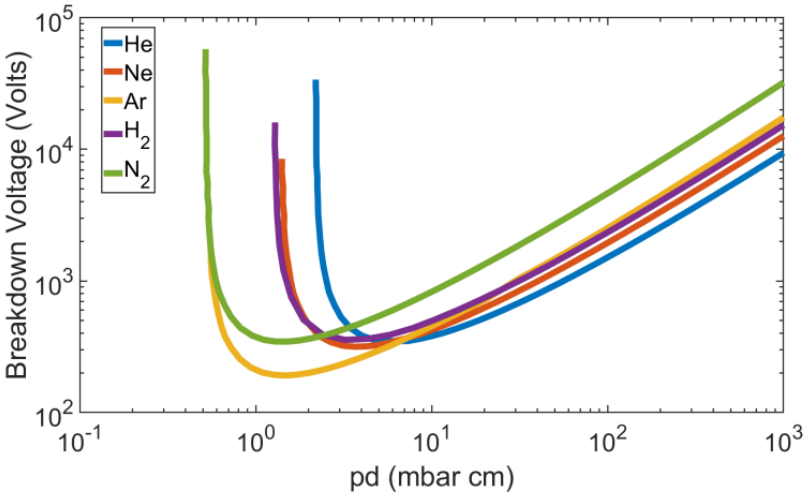

Figure 3.9: Paschen curves for different gases

According to Paschen's curves shown in fig.3.9, the ionization of a gas column can be obtained by applying voltages larger than the breakdown voltage, which are proportional to product of length d and the internal pressure P; in addition, the plasma density can be imposed by using appropriate values of the neutral gas density before the ionization. In the system described, the neutral gas pressure inside the capillary's channel has established by the mean of an electromechanical regulator in the range 10–100 mbar [4].

3.2.3. Plasma diagnostic system

The plasma diagnostic is done by a spectrometer connected to a ICCD camera so that images can be acquired. Outside the vacuum chamber there's an optic line, used to send the light produced by the plasma discharge insid ethe spectrometer.
The series of lenses and mirrors is used for guiding the light towards 1 cm entrance slit of the ICCD camera; it consists in different mirrors to direct and bend the light, and two focusing lenses to diminish the light beam.

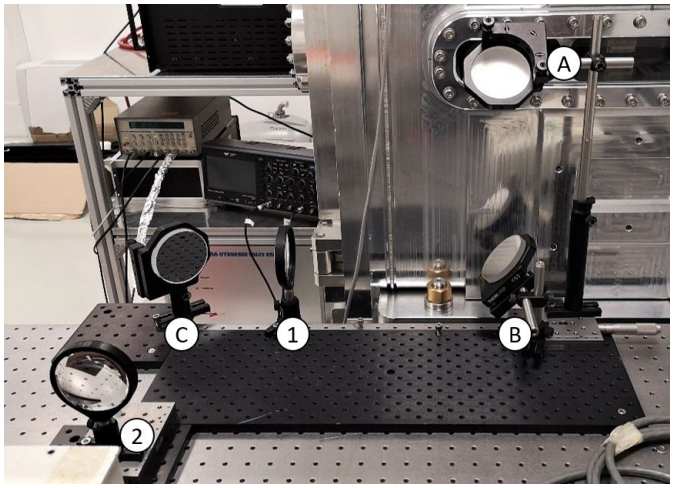

Figure 3.10: Optic line of the experimental setup for studying plasma properties of the source.

First, the light produced by the plasma goes outside the vacuum chamber through a window; then, positioning mirrors A and B (fig.3.10) in a proper configuration, the light is bend to the direction of the lens 1 (fig.3.10), where it is focused to lower the dimension. After been bent by the mirror C (fig. 3.10), the beam is focused again by the lens 2 (fig.3.10) so that its dimension lower to a dimension of 1cm, to enter the ICCD camera.
The calculations to find the right distances between the lenses and the mirrors follow the

thin lenses law:

$$\frac{1}{f} = \frac{1}{p} + \frac{1}{q} \tag{3.2}$$

where p is the distance before the lens and q is the distance after the lens.
Knowing that magnification of the image, beyond being the ratio between the image and the starting element is also $M = q/p$, and knowing the focal length f of the lens, it's possible to calculate the position between the starting point and arriving point of the light at which the lens needs to be placed to have a certain magnification.
The ICCD camera then acquires the images and show them on the computer: through a dedicated Labview virtual instruments, it's possible to tune the parameters of the image. The most important ones are the delay from discharge trigger at which the spectrum is acquired, and the gate width, which let us decide how much light we want to acquired; usually the gate width is set under 100ns, so that just the plasma light is acquired, and not also the surrounding light. In addition, it is possible to work on different hydrogen spectral lines, H_α and H_β, depending on the spectal resolution and line intensity we need to use. The image produced by the ICCD camera have two dimensions: 255 pixels represent the longitudinal y-axis of the capillary, while the 1024-column pixels convey the spectral information of the wavelength broadening.

3.3. Data acquisition

The light emitted by the plasma allows the reconstruction of the electron density, using a spectroscopy on the hydrogen spectral lines, generated due to different effects. Ionized hydrogen emits in visible range four lines of the so-called Balmer series. The broaden of those lines depends on many mechanisms:

- Natural broadening, present due to the Heisenberg principle.
- Doppler broadening, caused by thermal particle motion, depends on plasma temperature and the mass of the emitting species.
- Stark broadening, caused by the emitter interaction with the electric field produced by nearby charges.

Natural broadening is a consequence of the Heisenberg principle; This is one of the basic principles of quantum mechanics, and is characteristic of particle waves behavior. The principle, in its energy-time version, states that in a physical phenomenon the product of the uncertainties ΔE and Δt assumes the minimum value:

$$\Delta E \Delta t \approx \frac{\hbar}{2\pi} \qquad \Delta E = \hbar \Delta \nu \tag{3.3}$$

$$\Delta\nu \approx \frac{1}{2\pi\Delta t} \tag{3.4}$$

with $\hbar$ the reduced Plank constant, equal to 6,58284392·10^{-16} eV s.
From Heisenberg's relation it can be deduced that ΔE $\neq$0 (would be null in the case of infinite lifetime) and therefore also the frequency of the photon emitted has an intrinsic uncertainty, and so the wavelength too.
Doppler broadening is caused by the distribution of velocities of atoms and molecules that produce a typical enlargement of the spectral lines. Different velocities of the emitting (or absorbing) particles result in different Doppler shifts, the cumulative effect of which is the emission (absorption) line broadening. The broadening only depends on the frequency of the spectral line, the mass of the emitting species, and their temperature and does not relate to the plasma density, as it can be seen in eq.3.5:

$$\Delta\lambda = \frac{2\lambda_0}{c}\sqrt{\frac{2kT\ln 2}{M_a}} \tag{3.5}$$

where k is the Boltzmann constant, M_a is the mass of the emitting particles. These two broadening mechanisms produce spectra with distributions that can be approximated with a Gaussian profile.
Due to the low plasma temperature and the Heisenberg uncertainty principle, the Doppler and the natural broadening of the spectral line are negligible comparing other broadening effects. In fact, at the temperature at which plasma acceleration works, the broadening due to Doppler and natural broadening is in the order of ∼0.1nm, while the Stark broadening is in the order of 10nm. Therefore, the most dominant line broadening governing the Balmer lines is dominated by the Stark effect.

3.3.1. Stark broadening

Every chemical element has a specific characteristic emission spectrum, observed when light is emitted by a gas, and the spectrum is visible as bright-colored lines on the Black background (fig.3.11). Energy is released when an electron drops from an upper to a lower orbit, causing the atom to emit electromagnetic radiation. The light emitted has a wavelength corresponding to the energy difference between the two-electron energy levels. In case of Hydrogen, the emission spectrum is divided into several spectral series, with wavelengths in different spectral regions, from UV to IR, as shown in table 3.3.

Series	Spectral region	Wavelengths (nm)
Lyman	UV	<400
Balmer	VISIBLE	400-700
Paschen	near IR	>700

Table 3.3: Hydrogen spectral lines

For particle acceleration, the plasma formation is obtained by means of a current discharge inside a neutral gas contained inside thin plastic capillaries. In these conditions, if the neutral gas is Hydrogen gas at low pressure, when this light passes through the spectrometer's grating, four narrow bands of bright light are observed, at wavelengths in between the interval of the Balmer spectral series (fig.3.11).
The equation commonly used to calculate the Balmer series is a specific example of the Rydberg formula:

$$\frac{1}{\lambda} = R_H \left(\frac{1}{2^2} - \frac{1}{n^2} \right) \tag{3.6}$$

where R_H is the Rydberg constant, equal to 10973731.57 m^{-1}; The transitions are named sequentially from 3 to 2 H_α, 4 to 2 is H_β, 5 to 2 is H_γ, and 6 to 2 is H_δ.

Figure 3.11: Hydrogen emission spectrum lines in the Balmer series. In red H_α (656.2 nm), in aqua H_β (486.1nm), in blue H_γ (434.0 nm), in Violet H_δ (410.1 nm).

Stark effect is responsible for the broadening of spectral lines by charged particles in plasma due to the presence of an external electric field; the local electric fields from the free charges which surround the emitters are capable of modifying the emission process, giving rise to shifts in the emission frequencies or changes in the phase of the radiation, which are observed, as a whole, as a phenomenon of broadening and shift of the lines. This is an effect determined by the intensity of the local electric fields, thereby enabling us to find the density of charged particles in the plasma[17]. Instead of emitting light at wavelengths of Balmer spectral lines (Balmer alpha line H_α corresponding to 656.2 nm, Balmer beta line H_β corresponding to 486.1 nm, etc.) as it can be seen in fig.3.11, the

emission happens in an interval of wavelengths centered in the emission wavelength, with a theoretical distribution shown in fig.3.12, very similar to the real one, shown in fig.A.1.

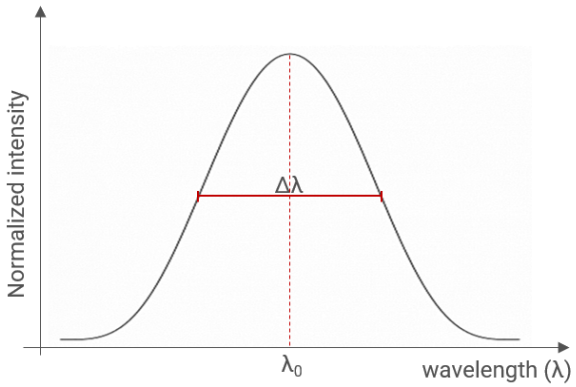

Figure 3.12: Theoretical distribution of intensity due to stark broadening.

The spectrum of light emitted by a plasma can be so used to obtain information about the plasma density, throught the following relation:

$$n_e[cm^{-3}] = 8.02 \cdot 10^{12} \left(\frac{\Delta\lambda_{1/2}}{\alpha_{1/2}} \right)^{3/2} \tag{3.7}$$

According to this equation, a wider (thinner) spectral line corresponds to a larger (smaller) plasma density. In the formula, $\Delta\lambda_{1/2}$ is the full width at half maximum (FWHM) of the Stark-Broadening spectral width in angstroms, and $\alpha_{1/2}$ is a function of the electron density and the temperature, tabulated in [19].

3.3.2. Spectrum acquisition

The calculation of the longitudinal profile is made using the relation between n_e and the FWHM he plasma electron density as a function of the spectral line width, written in eq. 3.7. The technique used to analyse every spectrum is explained in A, and it is based on the Stark broadening described before.
The ICCD camera view can be found in fig.3.13, and shows hoe, for different delays, the acquisition is different.

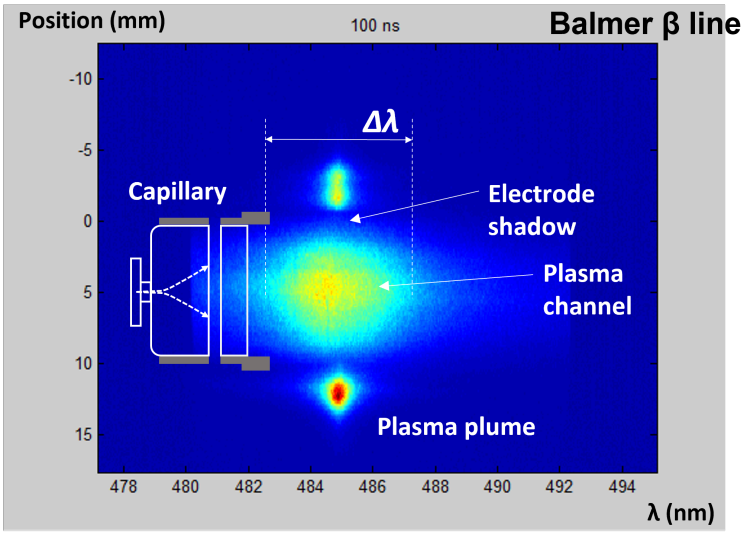

Figure 3.13: ICCD camera view, on the right the profile of the longitudinal position highlighted in red.

The longitudinal dimension of the spectral line describes the longitudial density profile along the capillary. The shadows shown in figure 3.13 represent the electrode traces, which can be used to calibrate the longitudinal axis from pixel to millimiters unit. In addition, as it will be seen in fig. 4.1 in chapter 4, in the capillaries there are to vertical and centered black lines; these are used, as the electrodes shadows, to calibrate the analysis software and change unit from pixel to millimeters.
In picture 3.14 it can be noticed two side lines; these lines represent the oxygen that is present in the gas discharge, since the hydrogen is generated by electrolysis, and there can be some remains in the gas; it also shows the chemical composition of the capillary $(C_5O_2H_8)_n$), since there is a track of C_{III}, O_{II} and O_{III} ions between the wavelengths of 420 nm to 550 nm, and so it is visible in the spectra.
With this technique, and the possibility of delay tuning, is possible to obtain a longitudinal and a temporal characterization; the longitudinal one is made from the analysis of the line broadening along the longitudinal coordinate of the capillary, while the time dependence of the plasma density is obtained by measuring the longitudinal profiles at several delay time with respect to the starting point of the discharge.
In fact, plasma density inside and outside the capillary will change during the current pulse: such a behaviour it is very important to select when inject the electron bunch, because different densities will accelerate differently.

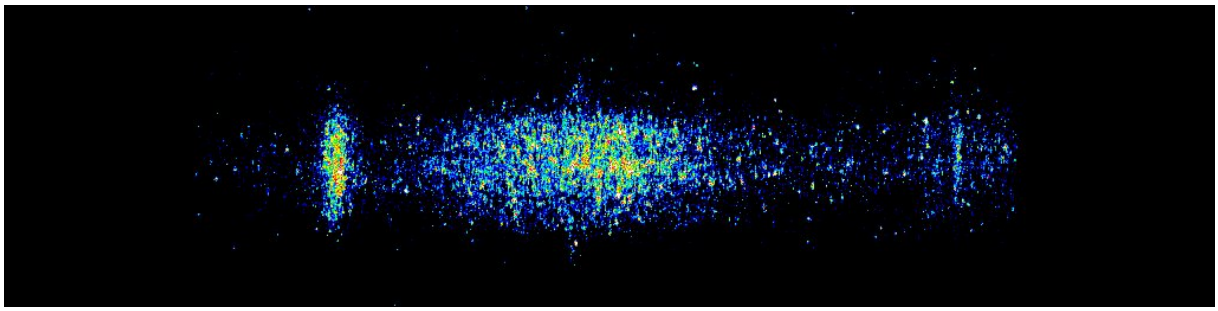

Figure 3.14: Real longitudinal H_β spectrum acquired by ICCD camera; capillary n. 5 from table 4.1 at 7kV, pressure at the inlet of 800mbar, delay of 2200 ns.

v

4 | Measurements and results

The experimental study presented in this thesis work concerns the optimization of hydrogen-filled discharge capillaries, aimed at improving the acceleration of particle beams at SPARC_LAB facility. Different capillary configurations, shown in fig.2.6, are designed and tested in the Plasma Diagnostic Lab, described in section 3.2 facility to investigate how the plasma properties are affected by the capillary geometry and experimental parameters.
For every capillary, different pressures, delays and voltages have been analysed, to explore their impact on the density magnitude and distribution. Moreover, using different gases, can highlight how elements with different atomic number behave as plasma gas source. Different geometrical alternative to the design used at SPARC_LAB have been also investigated. First, the diameter of the channel have been changed; secondly, an analysis of the effect that the distance between the gas inlets and number of them have on the density profile as been done. As last geometrical parameter, also different shapes of the channel and their effects on the density distribution have been investigated.

n°	**length (mm)**	**diameter (mm)**	**n.inlet**	**inlets distance (mm)**	**channel shape**
1	30	2	2	15	cylindrical
2	30	1	2	15	cylindrical
3	30	1	2	9	cylindrical
4	30	1	2	12	cylindrical
5	30	1	2	24	cylindrical
6	30	1	1	-	cylindrical
7	30	1-2	1	-	cigar shape
8	30	1-3	1	-	flared

Table 4.1: Capillaries tested, pictured also in fig.4.1.

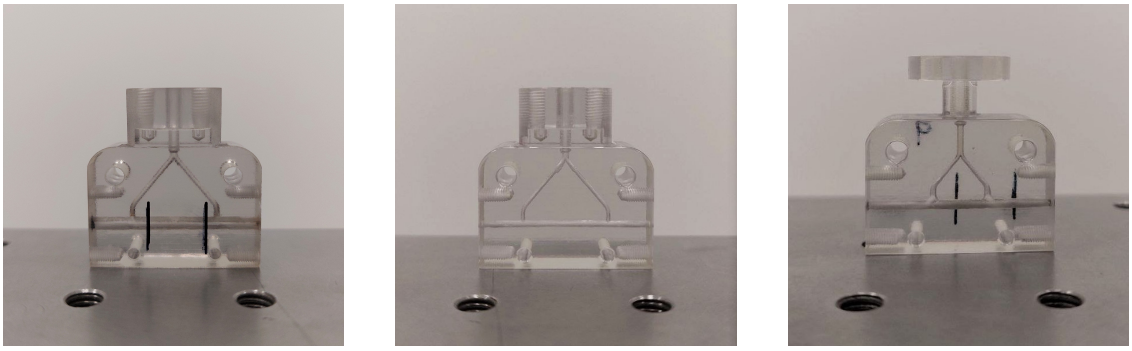

(a) n°1. (b) n°2. (c) n°3.

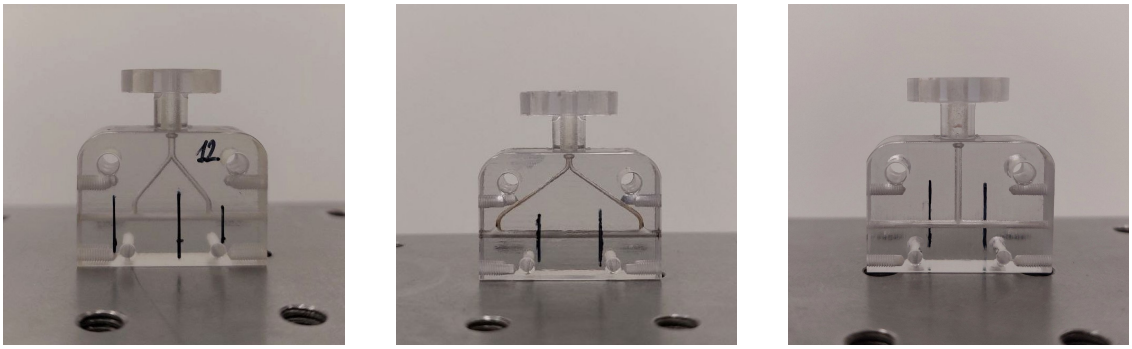

(d) n°4. (e) n°5. (f) n°6.

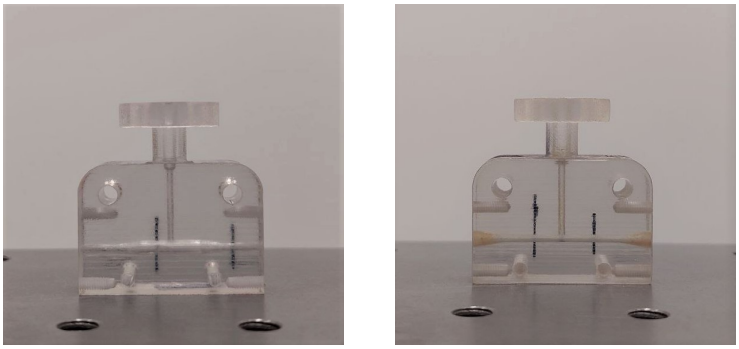

(g) n°7. (h) n°8.

Figure 4.1: Tested capillaries for parameters and geometry comparison.

Every capillary has two lines drawn, so that the data analysis calibration (see AppendixA) can be made. They are tiny and don't affect the diagnostic on them.
All the measurements of every capillary with the same parameters have been made the same day,so thatthey couldn't affect the measurements.
The average error is around 5-10%; it is relatively high, but it's possible to lower it decreasing the gate width of the measurement. The gate width is the time width the camera stays open and acquires the image; the higher it is, the most light it acquired. Increasing it, the light acquired is not just the plasma one, but also the one from the reflection on

the chamber walls and other external lights, as it can be seen in fig.4.2. Decreasing it, a problem rises in the acquisition, since the ICCD camera is not able to acquired enough light to generate good images.

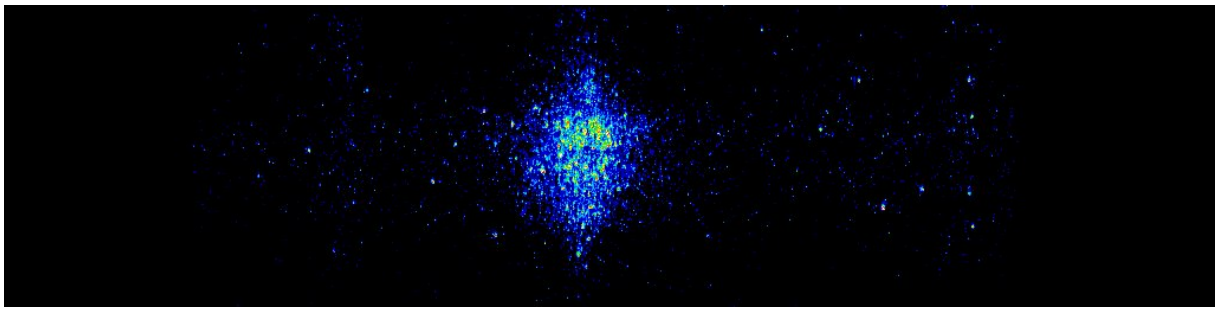

(a) gate width: 50ns.

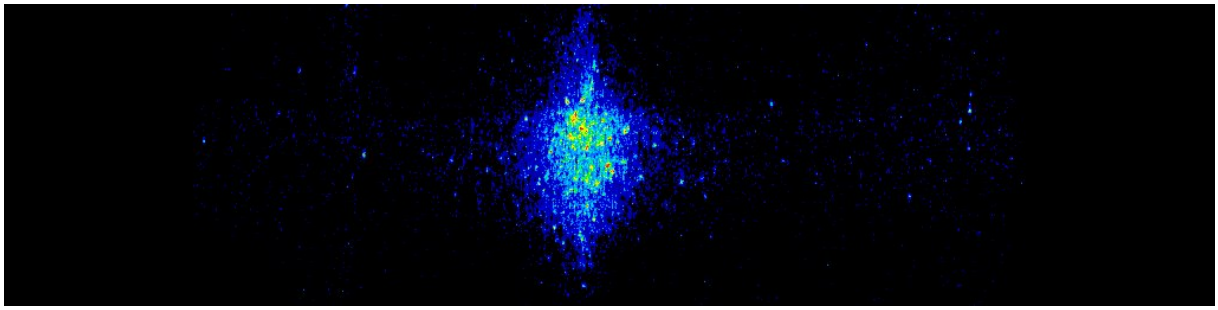

(b) gate width: 100ns.

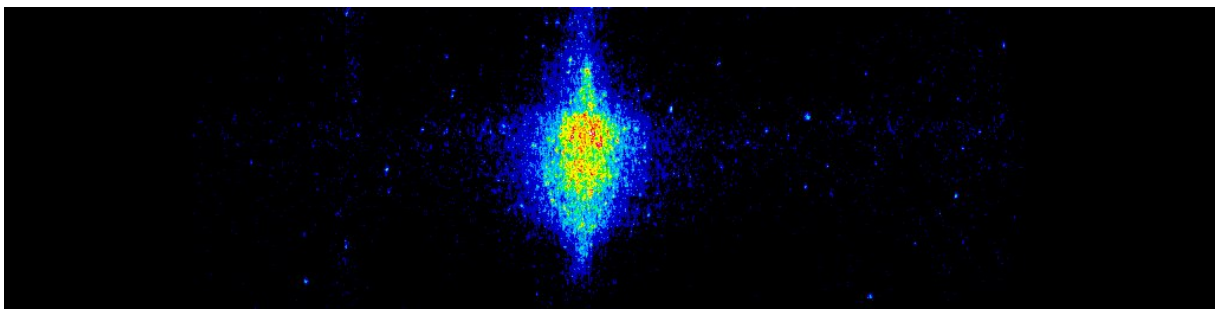

(c) gate width: 300ns.

Figure 4.2: Different gate widths tested. Capillary n°1, Pressure=800mbar, Voltage=10kV, Delay=2500ns.

The starting point of the study is the capillary inside inside the accelerator of SPARC_LAB, with the same design the capillary is the n°50.
The parameters and conditions inside SPARC, expressed in table 4.2, are different than the ones in the diagnostic lab, since the two discharge circuits are different. The experimental setup used for the experiments performed works around 10^{16-18} cm^{-3}, voltage

current tunable and a vacuum value around 10^{-6} mbar.
The bunch enter the capillary with an energy of 500 MeV, and get out after 30mm with an energy gain of 1.1GeV/m; with the measurements performed the goal is to increase both the energy gain and the quality of the bunch.

parameter	Working point
Driver delay*	$\sim 2\mu$s
Current	200 A
Pressure	(?) mbar
Gas used	H_2
Vacuum	10^{-8} mbar

Table 4.2: Working conditions in the vacuum channel at SPARC_LAB.
* with respect to the discharge, approximated value.

4.1. Measurements

Different parameters had been tested during the study of the capillaries, to fully characterize the plasma electron density along the channel.
Two types of characterization have been done: the first one is a spatial analysis, that aims to show how the density behaves along the axis, coincident with the trajectory where the particle beam propagate; knowing this profile, it is possible to see the behavior of the plasma, and so predict the behavior of the bunches inside the channel. This is an important matter, because, at it has been seen in chapter1, the bubble size depends on the frequency, and therefore on the density.
After a longitudinal characterization, a temporal on is made, since knowing the density during time permits to know with which delay is better to shot the bunches and improve the acceleration.
In the next sections, a qualitative characterization of the source used in the accelerator at SPARC_LAB is given to describe the two types of performed on all the tested capillaries. Note that the values are not the ones used for the acceleration process, but different to diagnose and characterize the source.

4.1.1. Longitudinal density profiles

In this section, the plasma sources characterization by means of the longitudinal density profiles is presented. The longitudinal profiles will be reported using the Balmer beta line, since the Balmer alpha line does not show the exact density, but an higher one.
Different kinds of gas-filled capillaries have been used to study the effects of their geometric properties (inlets, channel shapes, etc.), in addition to the operating conditions used to produce the plasma inside them, as the voltage pulse, pressure, etc.
The actual measurements will be shown in section 4.2, but the description of a generic profile will be given here.

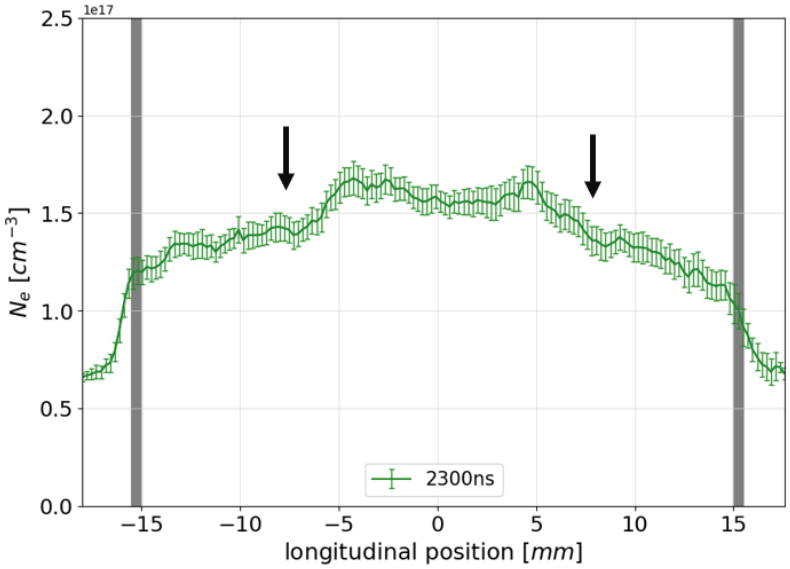

Figure 4.3: Longitudinal profile.

The longitudinal profile shown in fig.4.3 is centered at zero, so the two electrodes are placed at -15 mm and 15 mm. Outside the electrodes the density decreases because of the spread in the vacuum; these are the plumes, and nowadays a lot of study is focused on them, to understand how the bunch behaves when it leaves the capillary. The accuracy outside the electrodes is low due to the too little light that the spectrometer is able to acquired; in fact, in some of the measurements, the density at the plumes has a lot of error and is not so reliable.

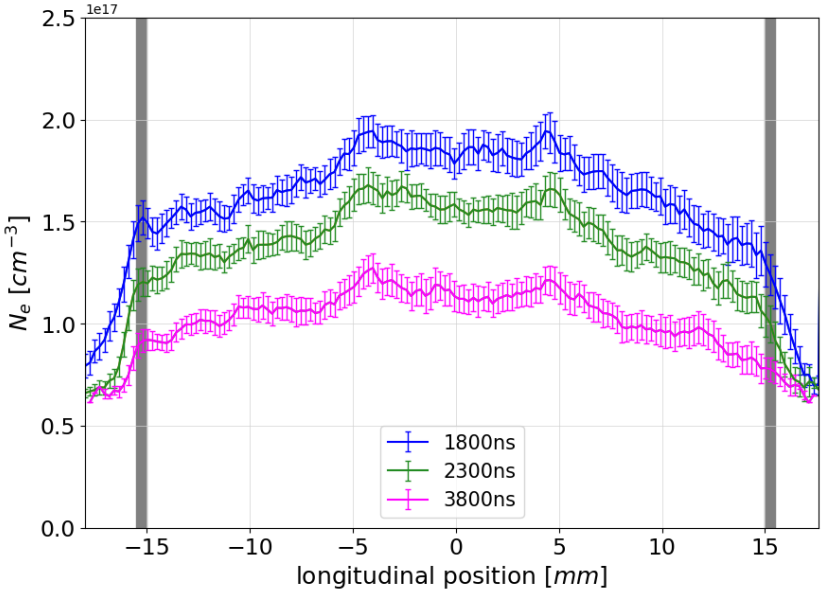

Figure 4.4: Evolution of the profile during time.

In figure 4.3 it is possible to notice some small depression of the density; those arise from the inlets, since in that point the gas density is lower because able to spread in two directions instead of one. This depression is bigger at lower delays, while at higher delays it almost disappear. As it can be seen in the graph 4.4, different delays show how the longitudinal profile behaves in time. At first the profile is not completely developed, and so not uniform; after the peak, it stabilize and it's possible to study the shape of the profile.

4.1.2. Time Graphs

After studying the longitudinal trend of the capillaries, the trend over time is analysed. This is a very important matter, since the timing of injection of the beam depends on this. In fact, depending on the delay at which the driver and the witness are shot, there will be a different density in the channel, as it is possible to see in fig.4.4.

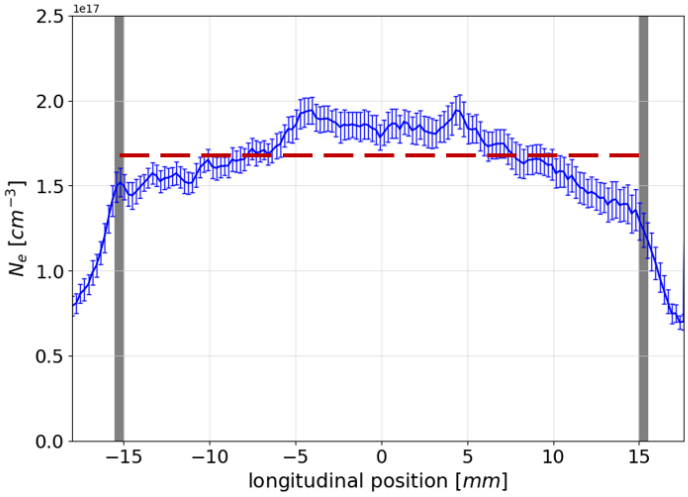

Figure 4.5: Longitudinal profile of one of the capillaries analysed, and the average value taken between the electrodes.

By delaying the camera trigger after the discharge, it is feasible to peruse the temporal evolution of the plasma density, and understanding the temporal evolution of the plasma density assists us in controlling the stability and reproducibility of the plasma. An average value between the two electrodes is calculated, and so its standard deviation; this process, shown in fig.4.5 is made for every delay analysed, to generate a curve of the trend of the density.

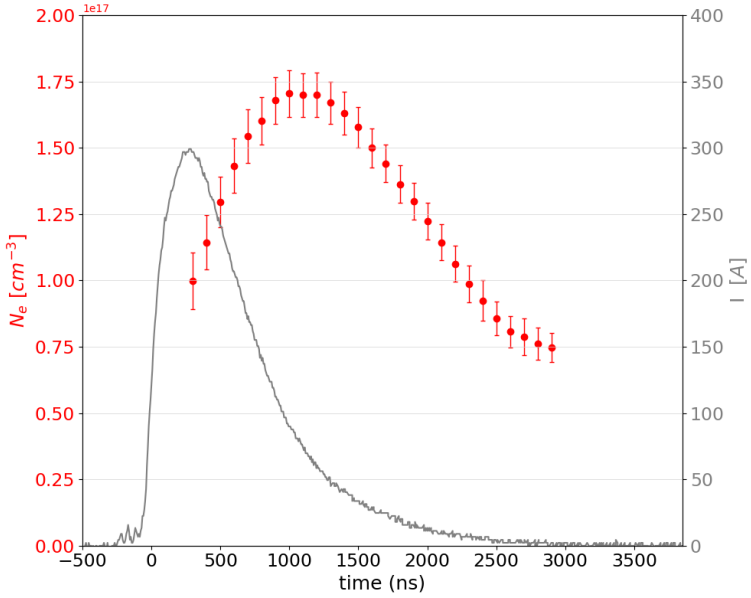

Figure 4.6: Trend over time of the density.

In graph4.6 the current is also shown; the pulse is shorter than the time evolution, but recombination effects inside the channel make the plasma die slower than the current pulse.
After the peak, the density time evolution can be approximated to an exponential one, and through computational tool it is possible to study the trend even after the experimental diagnostic is not able to acquired datas.

4.1.3. H_α and H_β

A first choice to make when performing the measurements is to decide which Balmer series to use. AMong the Balmer spectral lines, H_α and H_β are the ones usually used for this kind of analysis.
The two lines are have a very different broadening on the Balmer lines; in fact, has been study by Hans Griem in [19] how the broadening of the spectral lines is directly connected to the electron plasma density; the graph 4.7 shows the relation between the $\Delta\lambda$ and the electron density.

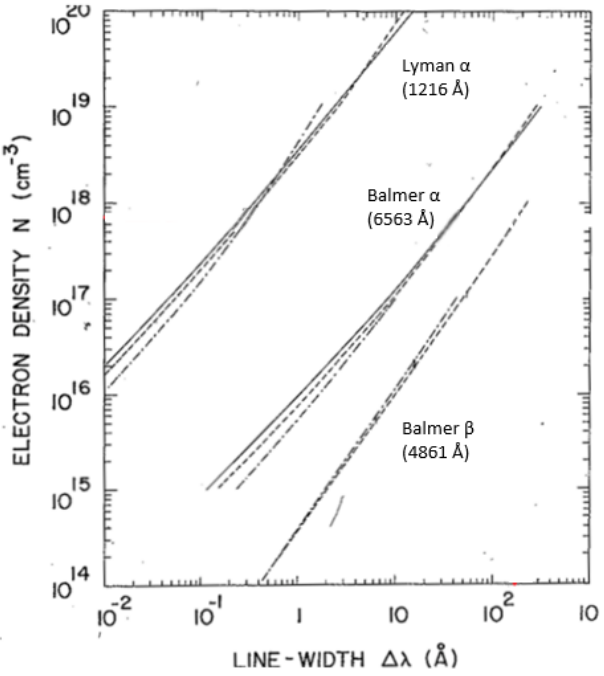

Figure 4.7: Relation between linewidth and electron density[19].

When comparing the spectra acquired, as the ones in fig.4.8, at first H_α seems to be the obvious choice when measurements are performed, since at the wavelength of 656nm the only spectral lines present are the one of the Hydrogen; in fact, the side lines mentioned

in section3.3.2 are not present, as is possible to see in fig.4.8, and so the fitting process described in AppendixA is easy to be made.
The absorption spectral line profile follows the emission line profile, so the measured spectral line width is broadened by maximum absorption of the central line. Since the self absorption is associated with the fact that the radiation emitter and absorber are the same kind of atoms, the line broadening will be severe for pure composition plasma such as our hydrogen plasma[22]. The possibility of self absorption in the H_α emission line is relatively higher than that of H_β emission line, since the self-absorption is more probable in close to the ground state. Consequently, the additional line broadening of the H_α emission line by the self-absorption effect can lead to over-estimation of the electron density. As the H_α emission line gives a significantly higher density due to the self absorption problem, H_β emission line may be good candidate for more accurate electron density measurement.

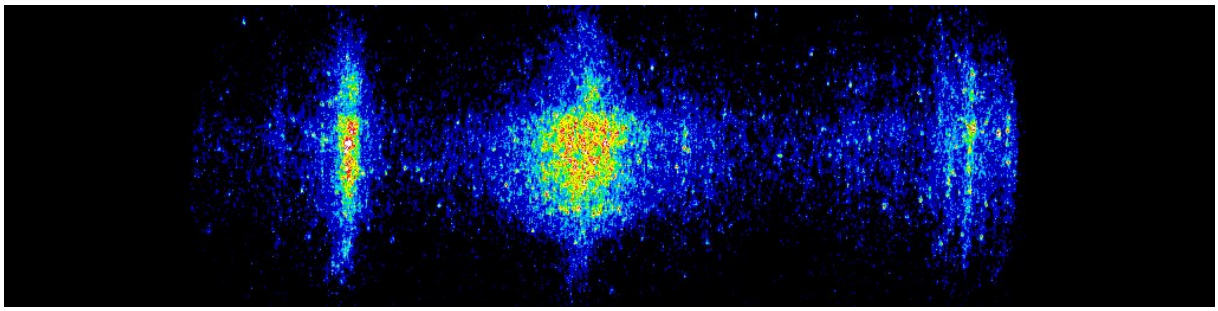

(a) H_β.

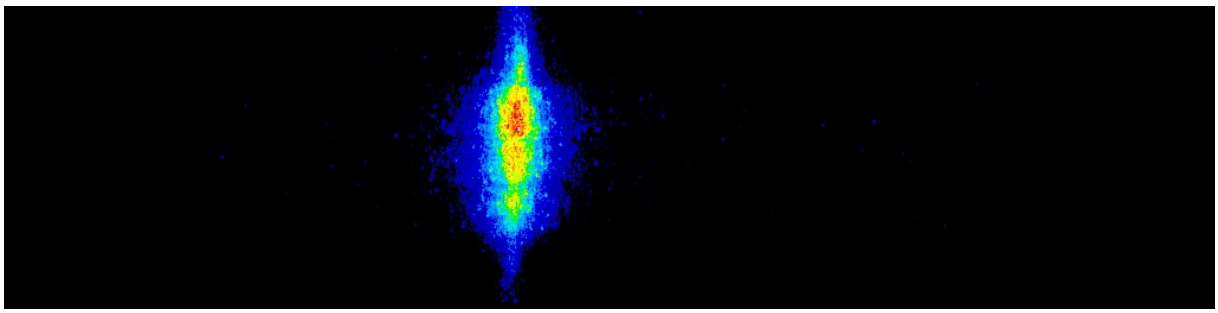

(b) H_α.

Figure 4.8: Acquired spectra of H_α and H_β.

The analysis on the two spectra, presented in fig.4.8, is very different. In case of H_β, the spectra can be seen being disturbed by the broaden spectral lines of other elements, and so the procedure to find the right fitting function (the general procedure is explained in AppendixA) is more difficult to be made. In the other case, with H_α, the spectrum is clear, and so making the fitting become easier. The two spectra in fig.4.8 will generate different longitudinal profiles, with a different error and accuracy. Two examples are

shown in fig.4.9; there it can be noted how the error generated using H_β is higher than the one using H_α. At the same time, as explained before, H_α profiles show an higher density than the real one, almost the. Because of that, usually H_β spectral line is used for the spectroscopy and analysis of discharge capillaries.

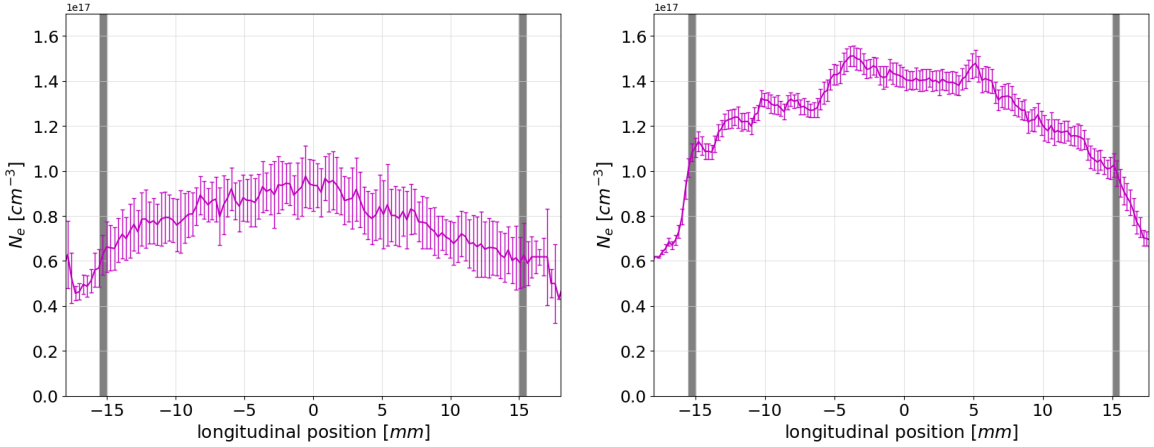

(a) H_β. (b) H_α.

Figure 4.9: Longitudinal profiles acquired with H_β and H_α.

4.2. Results

4.2.1. Parameters comparison

The first thing to understand when deciding to use a plasma capillary for electron plasma accelerators is the conditions in which the process work; the plasma density distribution inside gas-filled discharge capillaries, as longitudinal profiles or average density values, can be modulated by changing the operating conditions, in terms of gas pressure and high-voltage applied to the electrodes for creating the plasma. Knowing how the density changes - in terms of intensity and uniformity - when the environment changes is needed to decide how to tune the intensity to reach the values wanted for the acceleration.
In this section, the effects of the voltage pulse on the plasma distribution will be described.

Current

Measurements on different currents have been carried out on every capillary presented in tab.4.1 and analysed in the thesis. In all of them was possible to see how the current increases the intensity of the density, but doesn't change neither the trend of longitudinal behavior and the temporal one.

Measurements from just one of the capillaries are shown in fig.4.10, since it has been seen from all the measurements that the behaviour of all the capillaries is analogue.
As it can be seen in the graphs 4.10, the density distribution along the capillary axis is similar for every current; this means that increasing the current doesn't change the longitudinal distribution trend. The only thing that changes is the intensity, that is higher for an higher current, and so a little more curved; in fact, the longitudinal density profiles have a more uniform behavior when the voltage assumes lower values.

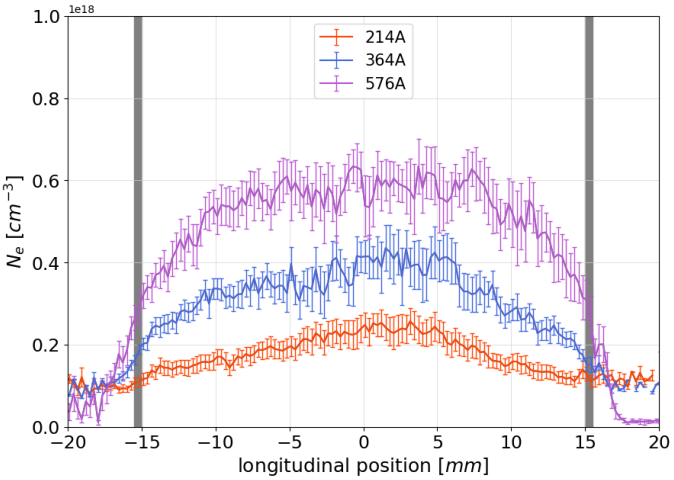

Figure 4.10: Capillary 2 from table 4.1, pressure 800mbar, 1400ns of delay, different currents.

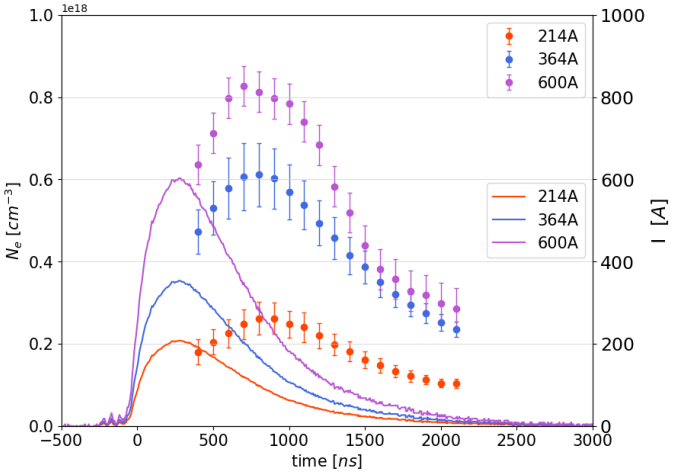

Figure 4.11: Capillary n.2 from table 4.1, pressure 800mbar, different currents.

The time analysis shows that the trend is analogue, with a more prominent peak for higher currents, as it can be seen in graph 4.11.

Pressure

When the gas is generated the pressure with which shot is of 4bar, with a pulse lasting for 3ms, with a frequency of 1Hz that can be increased. This pressure is too high to be able of having a pulsed gas discharge inside the capillary, so it is lower during the transport from the generator to the capillary. Between the gas generator and the inlets are present two valves that control the pressure of injection inside the inlets; tuning the pressure changes the gas density inside the channel, and so the electron density when the HV discharge takes place.
Measurements at 600-700-800 mbar have been done on all the capillaries; here just one of the analysis is shown, because the behaviour is the same for all the samples.

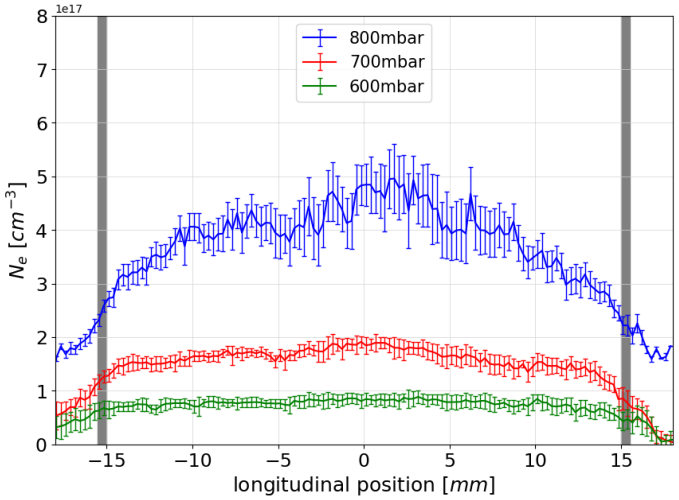

Figure 4.12: Capillary 2, 7kV of voltage, 1500ns of delay.

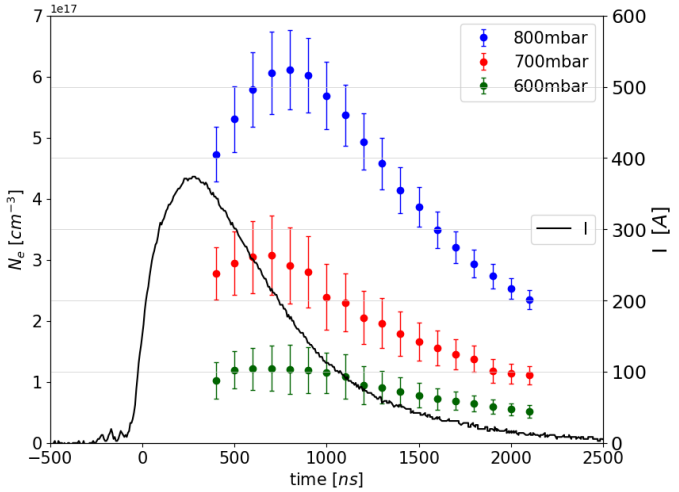

Figure 4.13: Capillary n.2 from table 4.1 at 7kV∼370A, different pressures.

In fig.4.12 is possible to see how the pressure changes the longitudinal distribution of the plasma electrons; with higher pressure, the longitudinal profile needs more time to completely develop, and has an higher intensity with respect to lower pressures.
The time behaviour is shown in fig.4.13, where is possible to notice that the peak at higher pressure is more prominent that a lower pressure. the density tends to stabilize before at lower pressure than at higher pressure, where the slop is still high at delays between 2100ns and 2700ns.

4.2.2. Different gases comparison

Different gases can be used to generate the plasma inside the discharge capillary. Every gas has its own characteristics, and behaves differently when a HV discharge is applied; heavier atoms have more electrons, and so the recombination time is different than for lighter atoms. At first, an analysis with the hydrogen is done, to set the starting point of this analysis.
As it is seen in the graph 4.14 and 4.15, the error bar is pretty low, since the α line is more accurate and with less errors, as described in section 4.1.3.
Since the Stark broadening technique is based on the analysis of the Hydrogen spectral lines, for this experiments a mixture of 5% of H_2 and another gas, in particular N_2 and Ar have been used. Moreover, since the quantity of Hydrogen present in the mixture is really low, the H_α line is used, and then the datas are calibrated to the real density. The following graphs are already normalized to the real density that would be acquired using H_β.

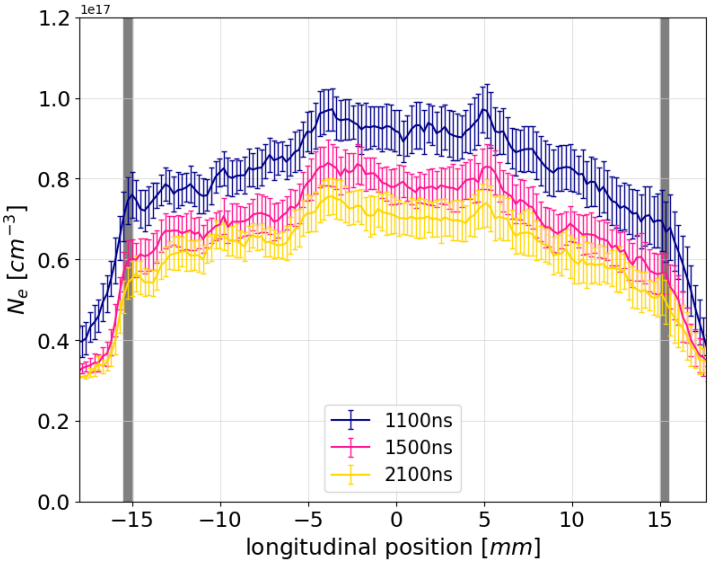

Figure 4.14: Longitudinal profile using H_2.

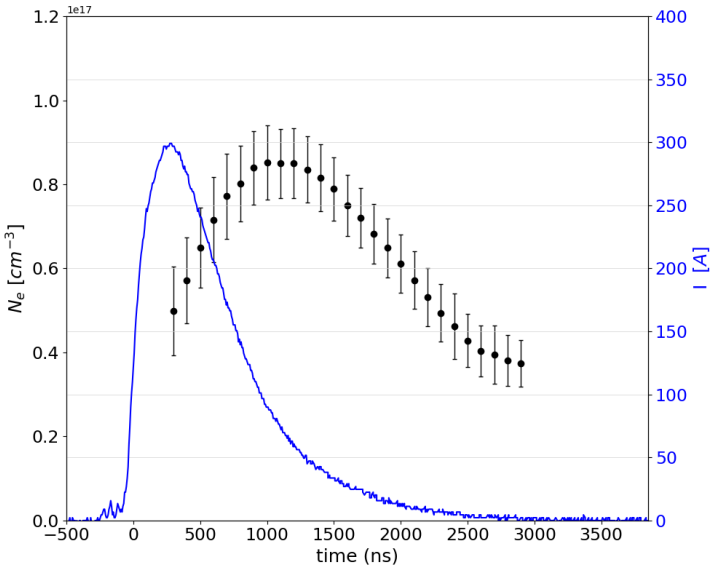

Figure 4.15: Temporal evolution using H_2.

The reason on using Nitrogen as an alternative of Hydrogen is the abundance of it in the atmosphere, since the air is made of 78% of Nitrogen. It would also be cheaper and safer to use than hydrogen gas.

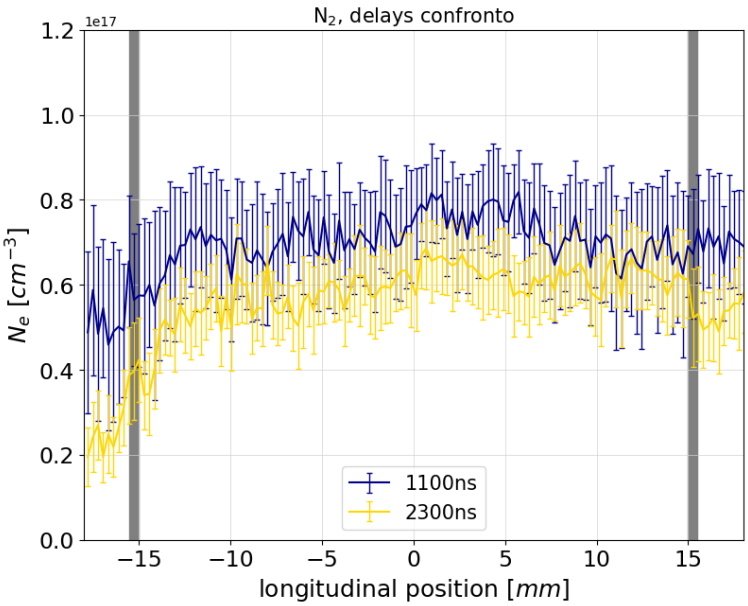

Figure 4.16: Longitudinal profile using N_2.

As it can be seen in graph 4.16, the measurements have a lot of error and are not linear, since the abundance of H_2 in the mixture is really low. The hydrogen spectral lines are really low compare with the other present due to nitrogen or carbon.

Time graph 4.17 shows that the recombination of atoms is slower, so the time evolution is also slow.

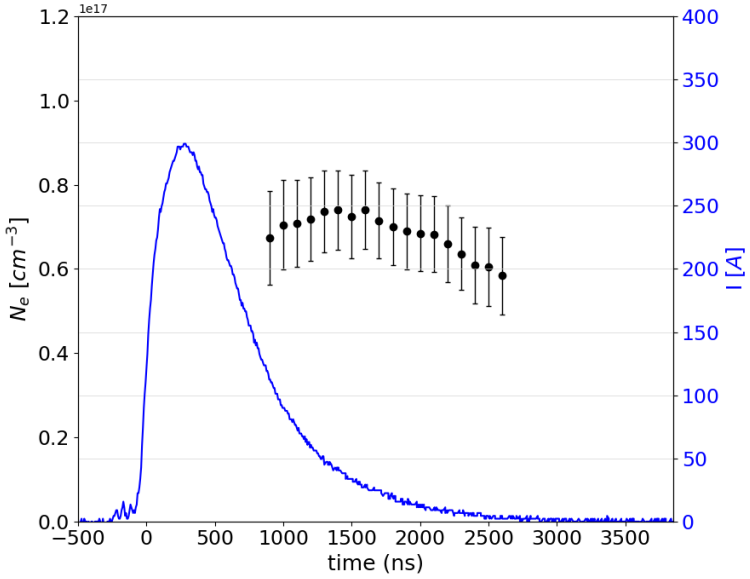

Figure 4.17: Temporal evolution using N_2.

The Argon mixture is the most difficult one to analyzed, since the broaden spectral line of the hydrogen are hidden between the argon spectral lines, really close to the hydrogen one in terms of wavelength.

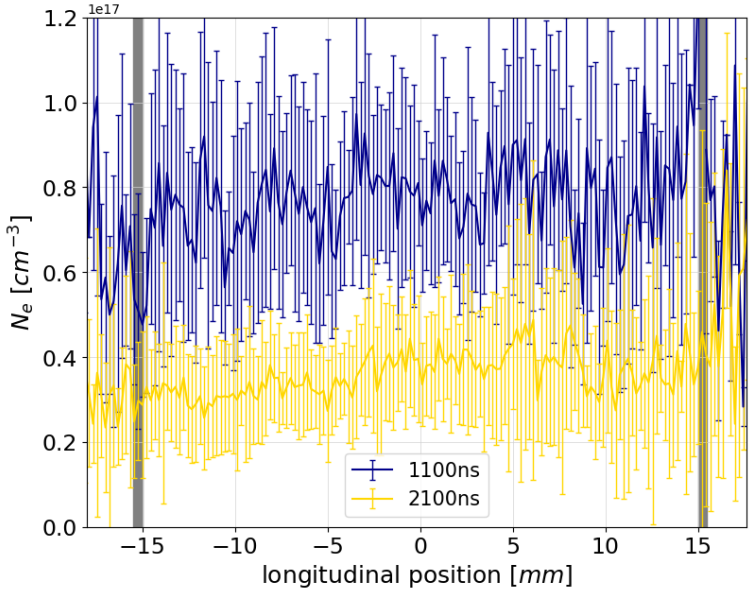

Figure 4.18: Longitudinal profile using N_2.

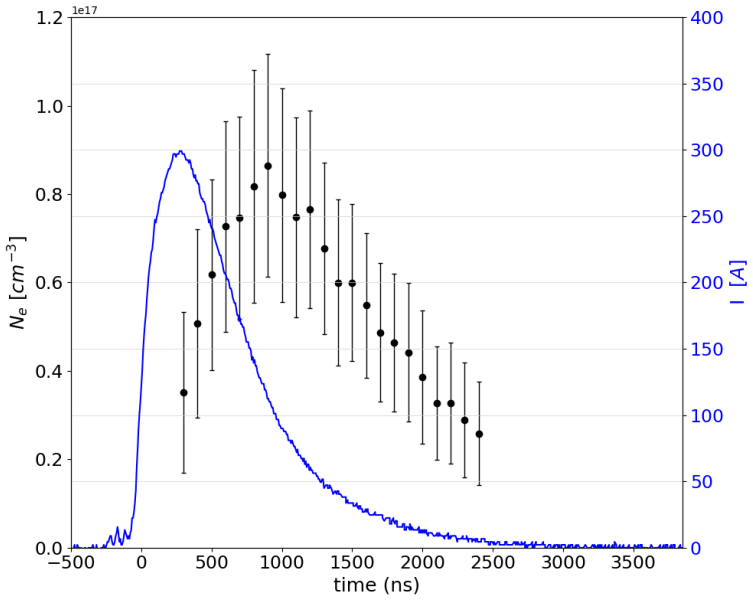

Figure 4.19: Temporal evolution using Ar.

The density profiles present in graph 4.18 have a high error and the datas are not so good, because of the problem just explained. Even with this obstacle, it was possible to outline a temporal evolution profile in graph 4.19, that shows a similar behaviour with respect to the hydrogen one. By the analysis of different gas spectra it is possible to say that, even if the diagnostic has low quality due to the low concentration of hydrogen present inside the gas mixture, the profiles obtained show that the two gases behave similarly to the hydrogen, and so can be good substitute in the accelerator.

4.2.3. Geometrical configuration comparison

Another set of measurement have been performed to investigate the role of the geometrical properties of the capillary on the electron plasma density distribution inside it. Indeed, the longitudinal electron density can be controlled by changing the position of the gas inlets, the dimension and the shape of the channel. By investigating the plasma evolution along the capillary, a comparison between different solutions for both capillary channel and gas inlets has been presented in this section. Also here, the plasma electron density profiles acquired are in the range of 500ns to 2300ns delays, at pressures of 600mbar and 800mbar, with HV dicharges of 5kV, 7kV, 10kV and 13kV applied. The comparison has been made on the fully developed profile, at 1500ns of delay.

Diameter

Two capillaries have been analysed and studied to understand how the dimension of the channel can affect the electron density. Has been seen that, while both the longitudinal profile and the time evolution of the density inside the capillaries was similar, the density was lower in case of a 2mm diameter than in the case of 1mm.
The plasma electron density profiles acquired with the Balmer beta line in the range of 500ns to 2300ns delays, at pressures of 600mbar and 800mbar, with HV dicharges of 5kV, 7kV, 10kV and 13kV applied. Here are shown just some of the results, since changing the parameters affect just the intensity but not the qualitative distribution.

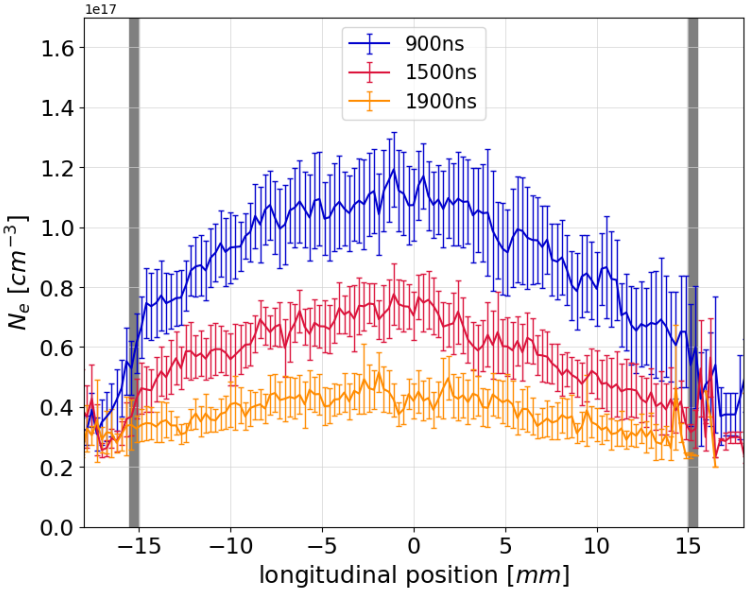

Figure 4.20: Longitudinal profile of capillary 1 at 800mbar of pressure and 7kV∼380A applied.

In both profiles at lower delays, as at the peak, the profile is not developed properly, in fact is not uniform, while at higher delays the density uniforms itself and also the error on the measurements decreases. The main difference in graph 4.20 and 4.21 is the order of magnitude in the density axis; while the two profiles seems similar, the electron density is different of an order of at least 4. This happens because , when the diameter is increased by a factor 2, the volume will increase by a factor 4; consequently, also the plasma density will undergo a decreasing by the same factor.

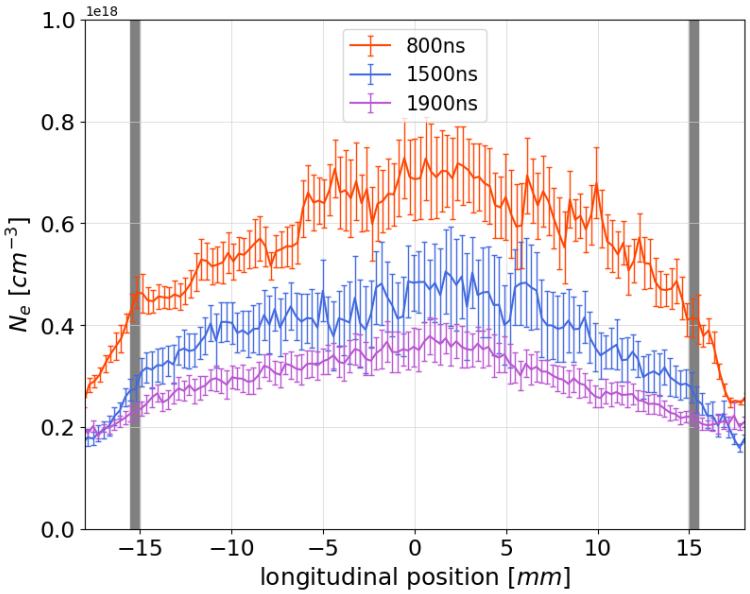

Figure 4.21: Longitudinal profile of capillary 2 at 800mbar of pressure and 7kV∼380A applied.

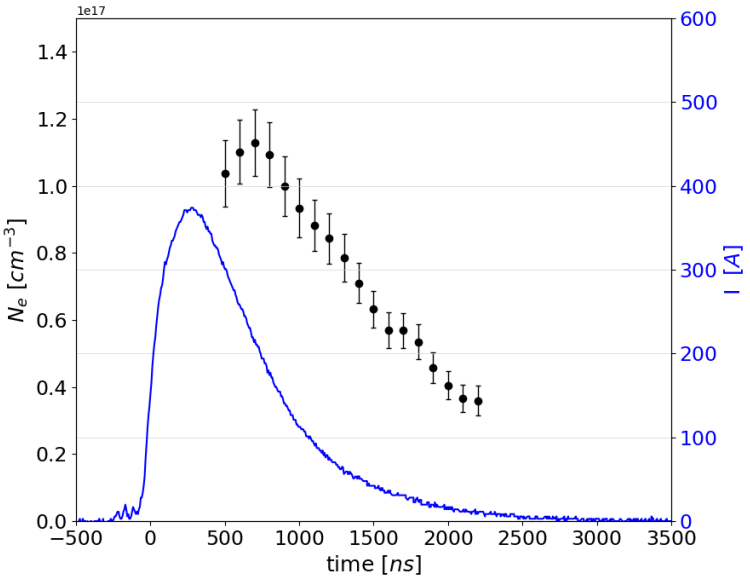

Figure 4.22: Temporal evolution of capillary 1 at 800mbar of pressure and 7kV∼380A applied.

The temporal evolution in graphs 4.22 and 4.23 of the two capillaries is qualitatively the same, just at different intensities, for the reason explained before.

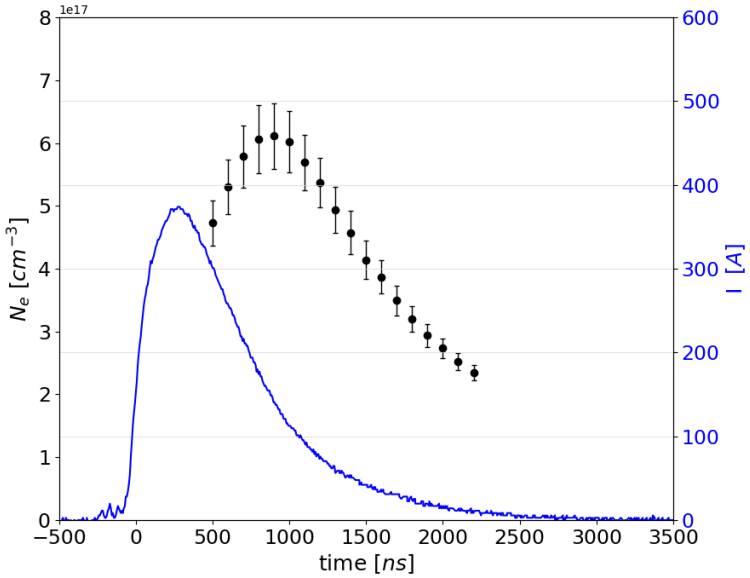

Figure 4.23: Temporal evolution of capillary 2 at 800mbar of pressure and 7kV∼380A applied.

Inlets distance

The number and position of inlets can change the electron distribution inside the channel; this is due to the spread of the gas from the inlets. At first it can be easy to think that, to have an uniform gas distribution inside the channel, placing the inlets close to the exit can improve the uniformity; this is not true, since the increased distance between the inlets produces a gas accumulation at the center of the capillary and a depletion at the edges that consequently provides a curved profile. Measurements and analysis on different capillaries have been performed, and the results are shown in fig.4.24 and 4.25.
As it can be seen in the graphs in figure 4.24, a more uniform distribution is achieved using a capillary with a distance between the centered inlets of 9mm, while with higher distances of the inlets the longitudinal profile is not plain anymore; increasing the distance, the curve becomes more prominent.

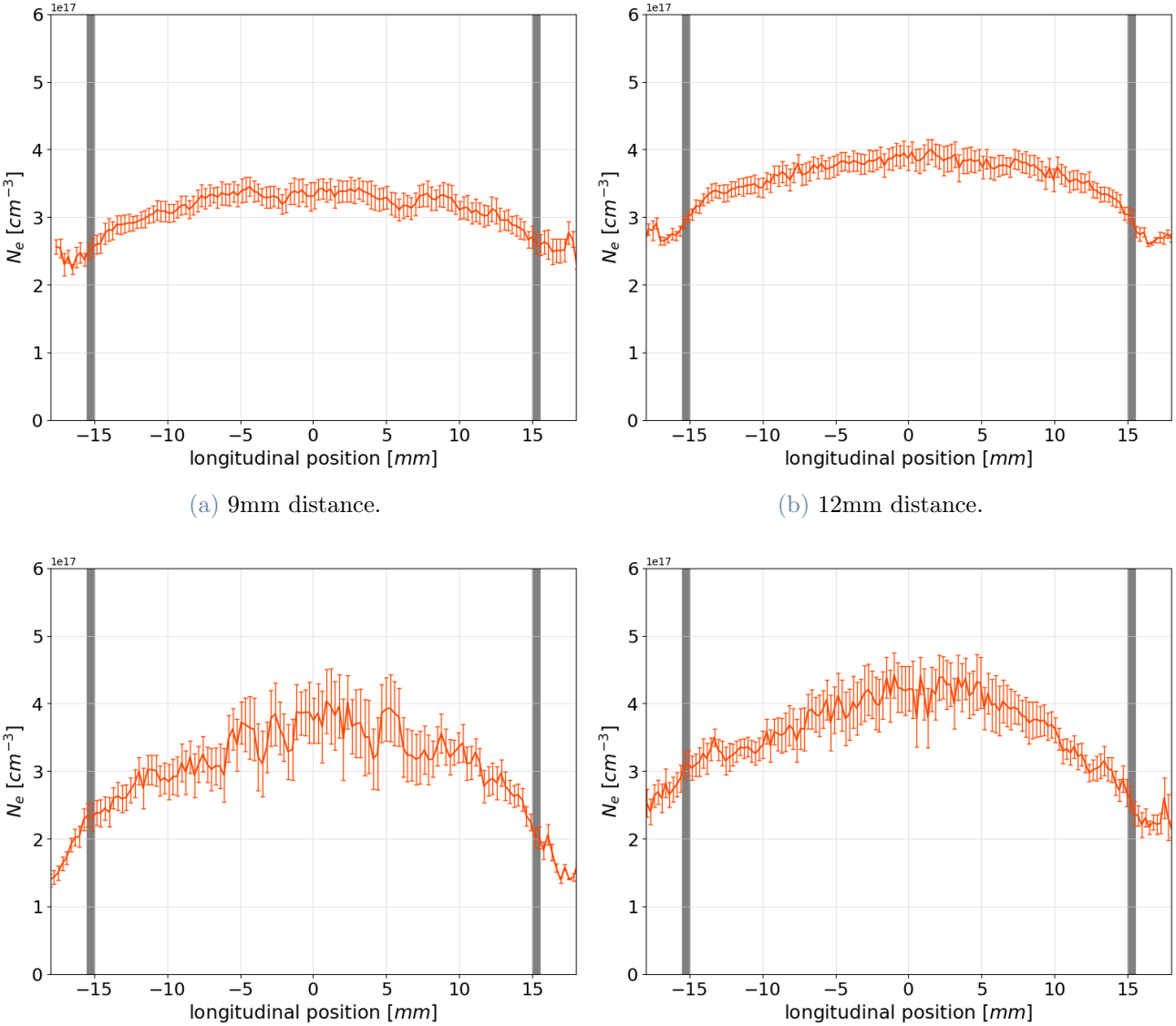

(a) 9mm distance.

(b) 12mm distance.

(c) 15mm distance.

(d) 24mm distance.

Figure 4.24: Longitudinal profile of capillaries 3(a), 4(b), 2(c), 5(d), at 800mbar of pressure and 7kV∼380A applied; delay of 1500ns.

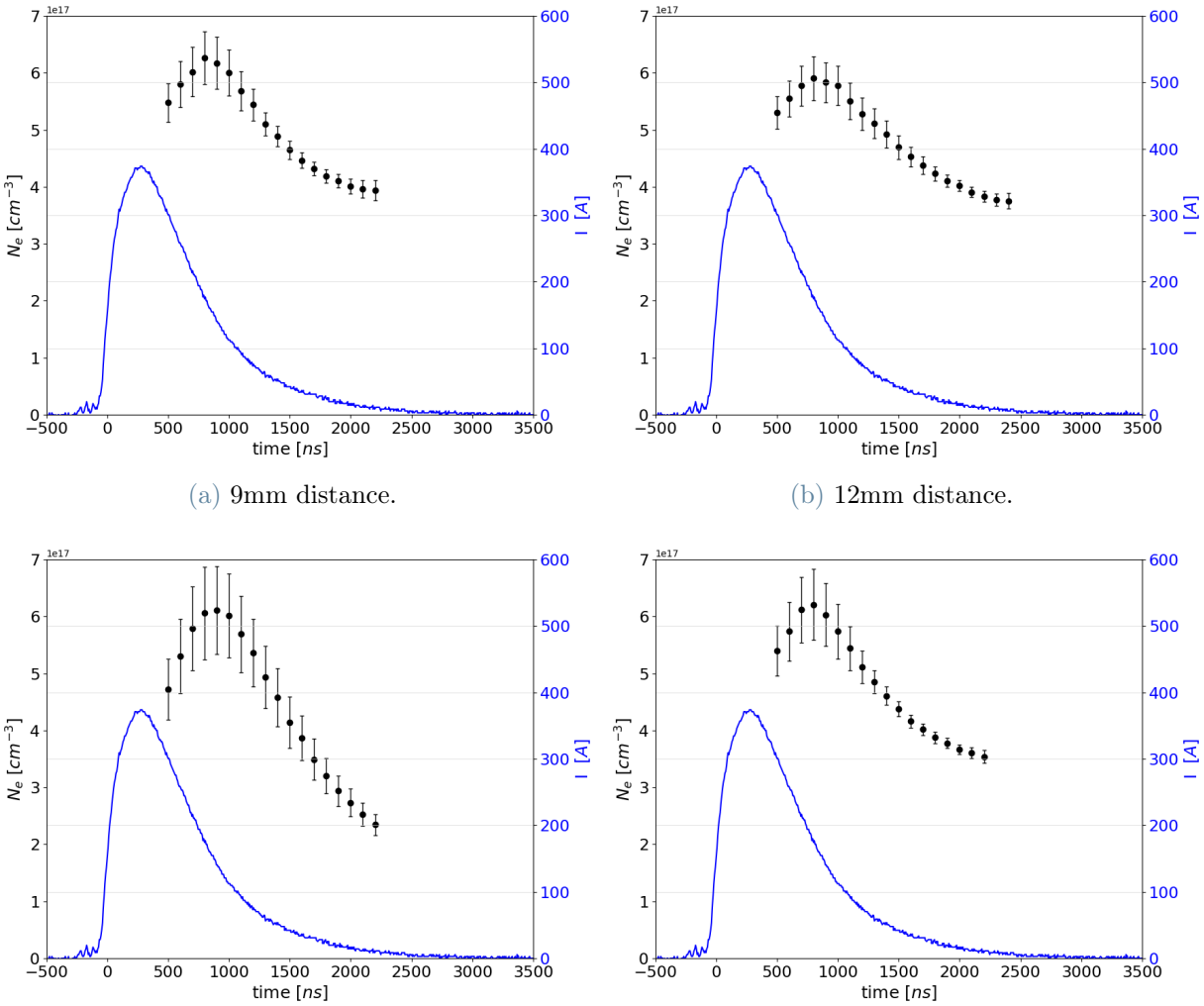

(a) 9mm distance.

(b) 12mm distance.

(c) 15mm distance.

(d) 24mm distance.

Figure 4.25: Time evolution of capillaries 3(a), 4(b), 2(c), 5(d), at 800mbar of pressure and 7kV∼380A applied.

For what concerns the time evolution, the behavior is similar; all the types of configurations show a peak around 1000ns of delay, and then a decreasing that can be described as an exponential one.

Number of inlets

Not just the positions of the inlets can be tune, but also the number of them can be changed. In a 3cm long capillary is not possible to increase the number of them, but is possible to decrease the number to just one inlet.

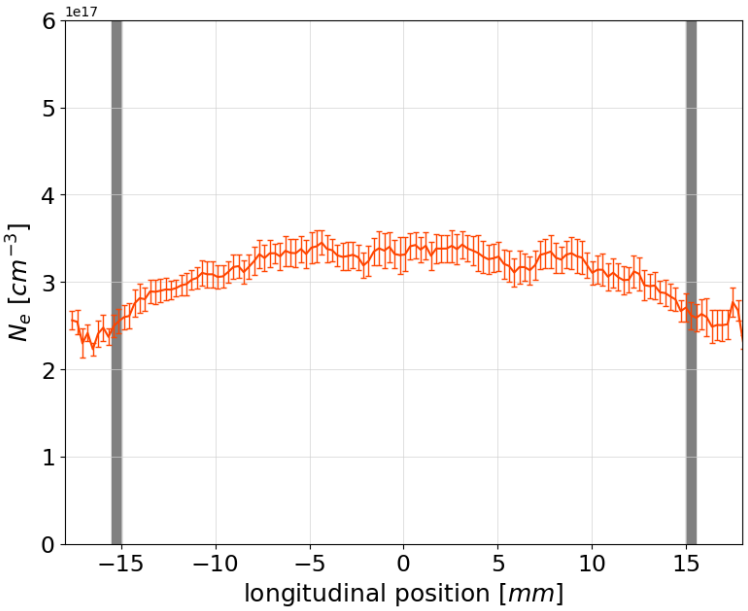

Figure 4.26: Longitudinal profile of capillary 3, 2 inlets, 9mm distance. 7kV∼380A applied; delay of 1500ns.

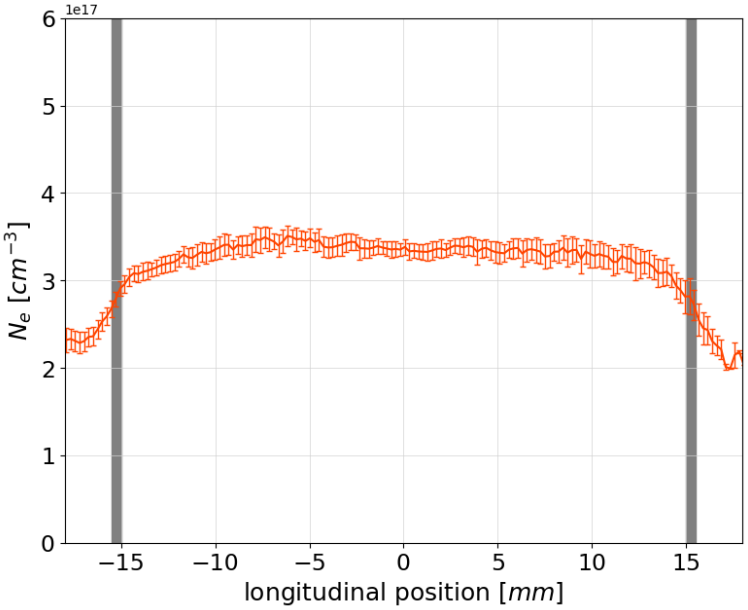

Figure 4.27: Longitudinal profile of capillary 6 with one inlet, 7kV∼380A applied.

Both from time evolution and longitudinal profile graphs of the two configurations not a real difference can be seen; in fact, as it is shown in graph 4.264.27, the capillary with two inlets at 9mm of distance, before addressed as the best option among the different distances possible, shows a fully developed profile really similar compared with the one

of the capillary with just an inlet.
Also the time evolution of both capillaries, shown in graphs 4.28 and 4.29, is pretty similar.

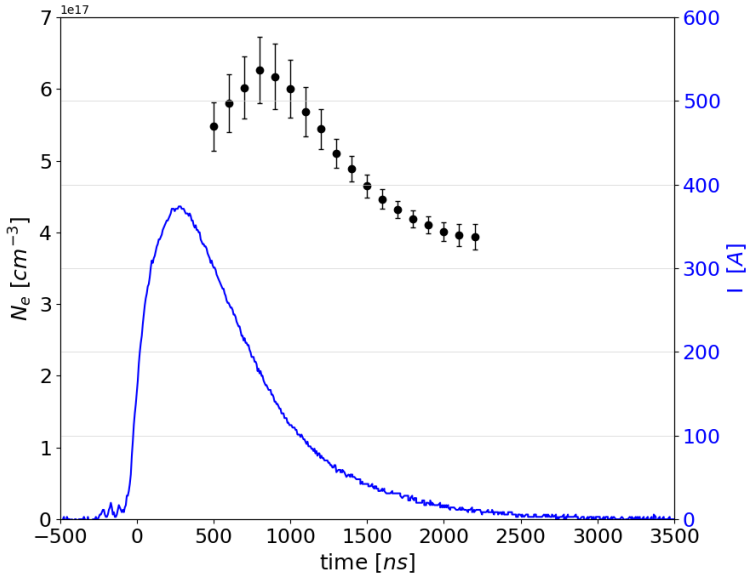

Figure 4.28: Temporal evolution of capillary 3, 2 inlets, 9mm distance. 7kV∼380A applied; delay of 1500ns.

In case of a cylindrical shape, the peak happens later; the reasons can be multiple, due to the configuration or the experimental setup.

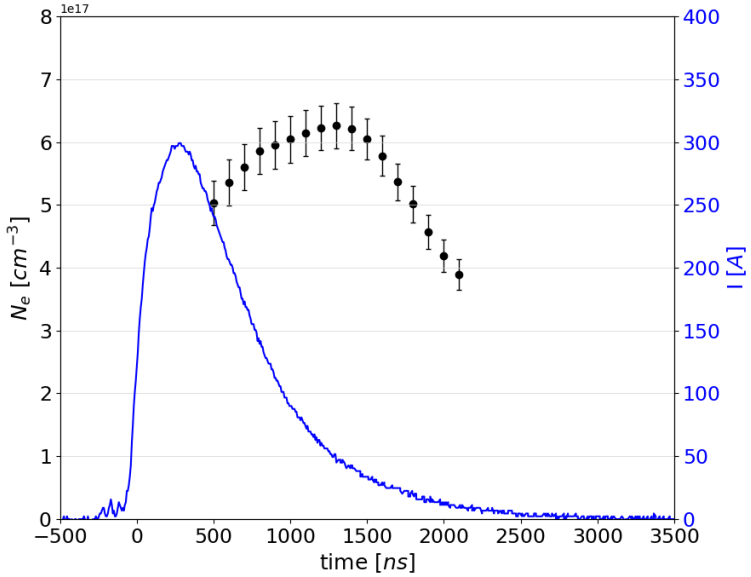

Figure 4.29: Temporal evolution of capillary 6 with one inlet, 7kV∼380A applied; delay of 1500ns.

Channel shape

As it has been seen in the comparison between the diameter, a change in the size of the channel reflects on a change in the electron density, but not in the longitudinal behaviour. Possible variations can be achieved changing the diameter of the channel in some sections; two possibilities have been analysed: an increasing of the diameter in the central part of the capillary and an increasing of the shape at the edges of the capillary.
In this section a comparison between capillaries 6, 7 and 8 from table 4.1 has been done, all at 300A of current, 800mbar.
Starting from the cylindrical shape, analyzed in graphs 4.30 and 4.31, it is possible to see the uniformity of the profile. Changing the shape of the channel in some points, other longitudinal profiles can be acquired.

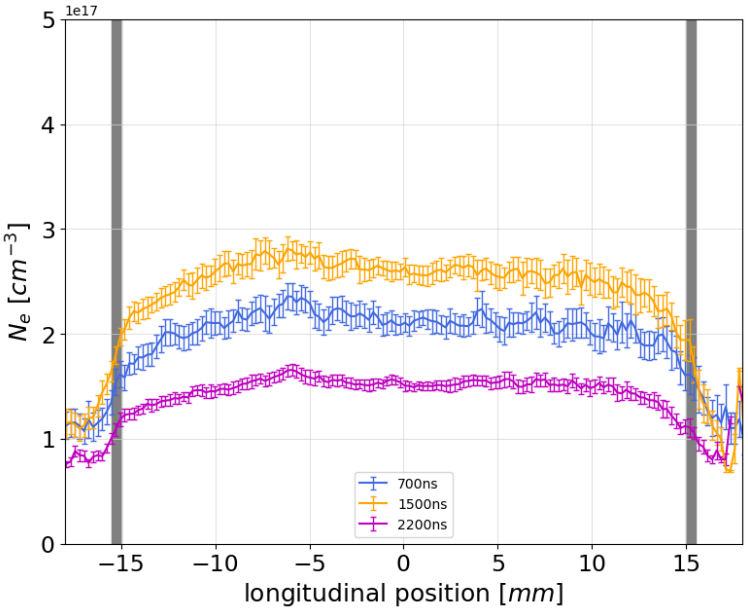

Figure 4.30: Longitudinal profile of capillary 6.

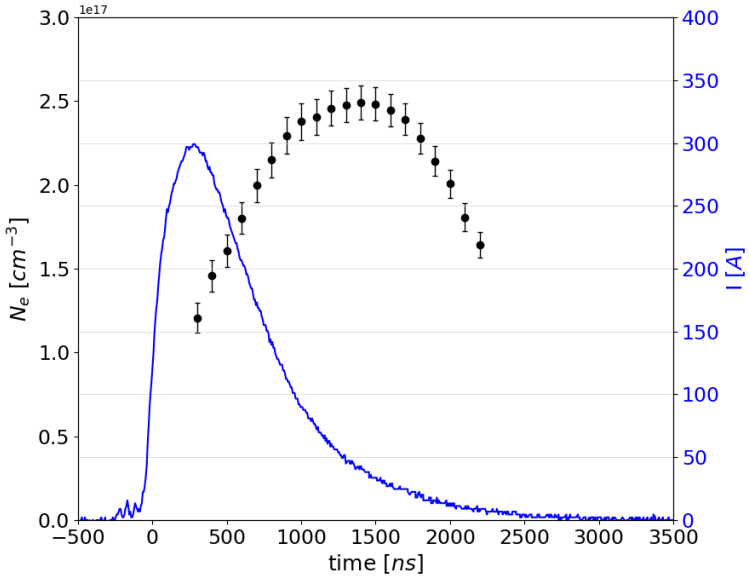

Figure 4.31: Temporal evolution of capillary 6.

After the analysis of this channel shape, different configuration have been implemented and investigated. The first one is a "cigar shape", visible in capillary 7 in fig.4.1g.

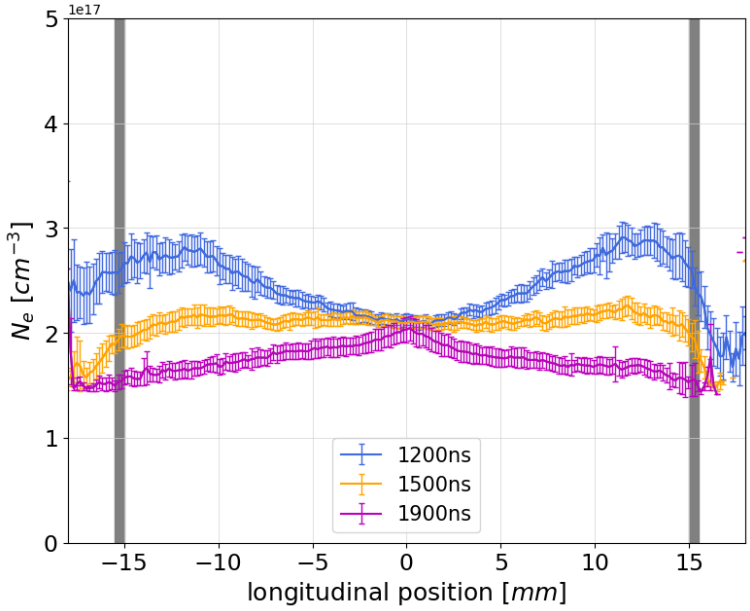

Figure 4.32: Longitudinal profile of capillary 7.

Capillary 7 has a channel shaped as a cigar; the increasing starts from 6mm from the left edge, and at 10mm the diameter reached is of 2mm; the same thing happens starting from the right edge, so that the length of the 2mm region is of 10mm.

In graph 4.32 is possible to see that the density at first is much higher in the border parts, while in the center, due to the larger section, the density is lower; during time the central part remains almost constant, while the borders uniforms, arriving at a uniform profile at high delays. The time evolution showed in 4.33 is qualitatively similar to the cylindrical one, so in terms of time there's no difference between the two capillaries.

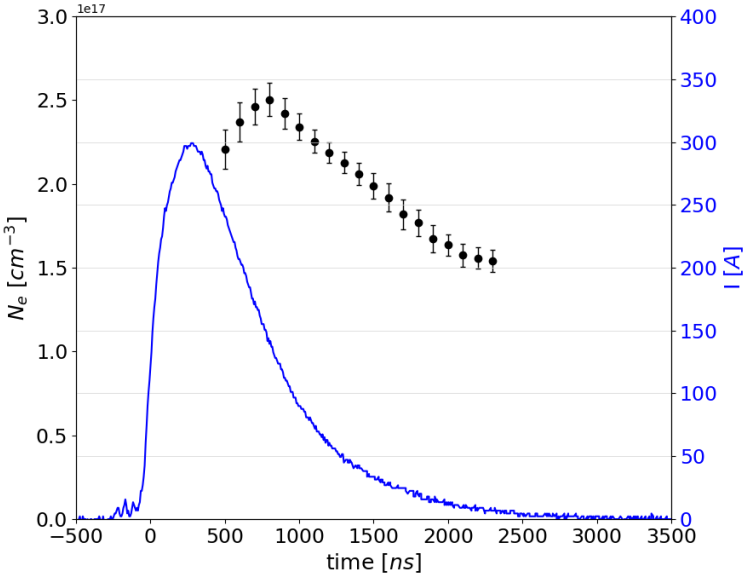

Figure 4.33: Temporal evolution of capillary 7.

Then capillary 8 is analysed; it has a 1mm big diameter, with a conic shape at the edges, that starts 5mm from the border and goes from 1mm of diameter to 3mm.
In this case, showed in graph 4.34, the smaller diameter in the center causes the density to be higher in the central region, creating to ramps at the borders. These ramps can be used to adapt the electron beams to the plasma within the capillary in order to preserve the quality of the beams. Also here, the time evolution of the density in graph 4.35 is quite similar to the other two configurations, so that the only change in the behaviour is the longitudinal one.

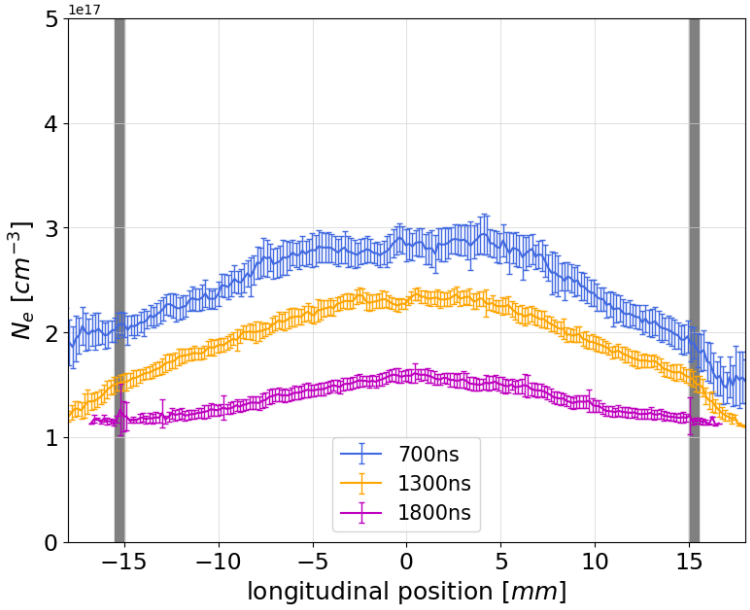

Figure 4.34: Longitudinal profile of capillary 8.

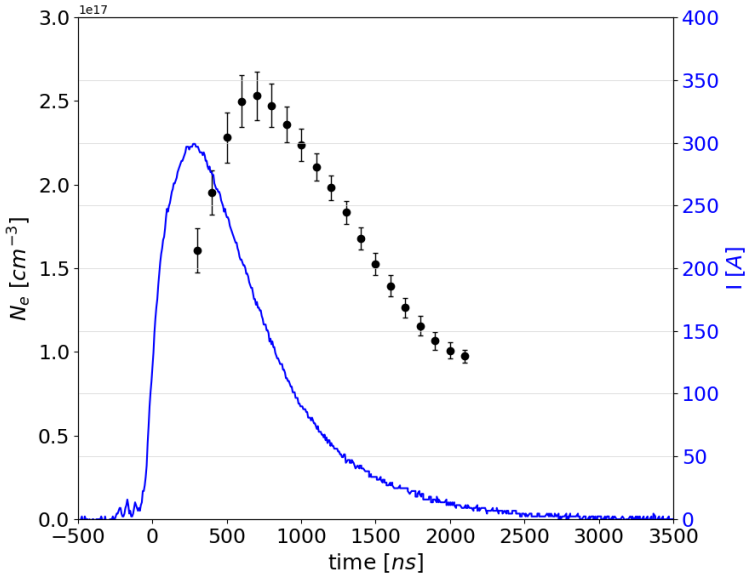

Figure 4.35: Temporal evolution of capillary 8.

The two different plasma distributions behaviors analyzed and obtained for various types of tapering of the capillary's ends represent another approach usable for controlling the plasma properties. These channeling configurations can also be effective for ruling the plasma density.

4.3. Segmented capillary

New technologies have been implemented to improve the acceleration process and also to take a look into the different applications that every configuration of source can have during the last years.
A new technology developed in the last months at SPARC_LAB is the segmented capillary prototype (fig.4.36); this source is a capillary of 16cm length, with a 2 mm diameter channel and multiple gas inlets, with the particularity of having a central electrode. This configuration permits to have different currents inside the channel, so that the density is tunable along the whole capillary length.
The three electrodes are connected to two different circuits, so that the two discharge are individually tuned and timed; in fact, it is possible to tune both the voltage and the delay with respect to the gas discharge; doing this, the density evolution during time of the two regions can be different too.
The goal with this configuration is the modulation of density and the possibility to reach m-scale plasma sources; this is done by synchronization of the charge pulses and the modulation of the current intensity.
Even if it is just a prototype, the characterization of this configuration showed really good results, leading the way to new possibilities of configurations.

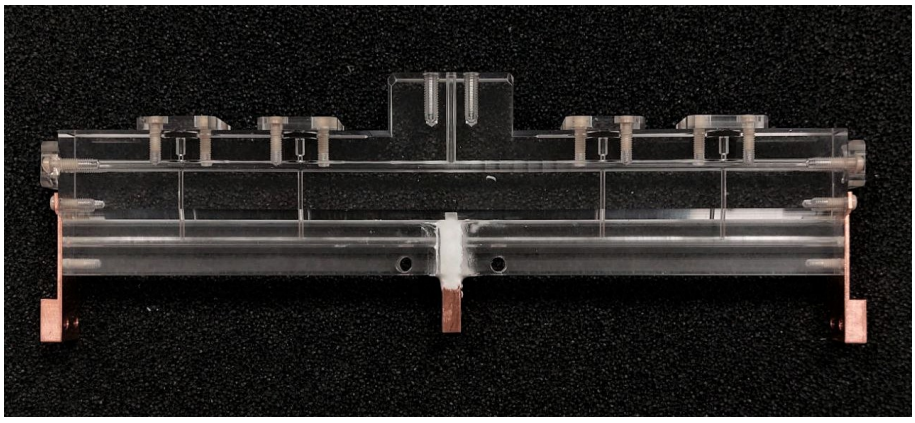

Figure 4.36: Segmented capillary geometry.

4.3.1. Measurements and results

The characterization on this capillary has been made both at different voltages (and so currents) in the two regions and with same voltages; a real photo of the capillary during the diagnostic is shown in fig.4.37.
Since the mirror of the optic line is not able to acquire all the length of the capillary, a

different acquisition technique has to be implemented. The optic line and spectrometer have been moved along the capillary, dividing it in 3 regions; then, the analyzed datas have been put together to generate a total profile of the capillary electron density.

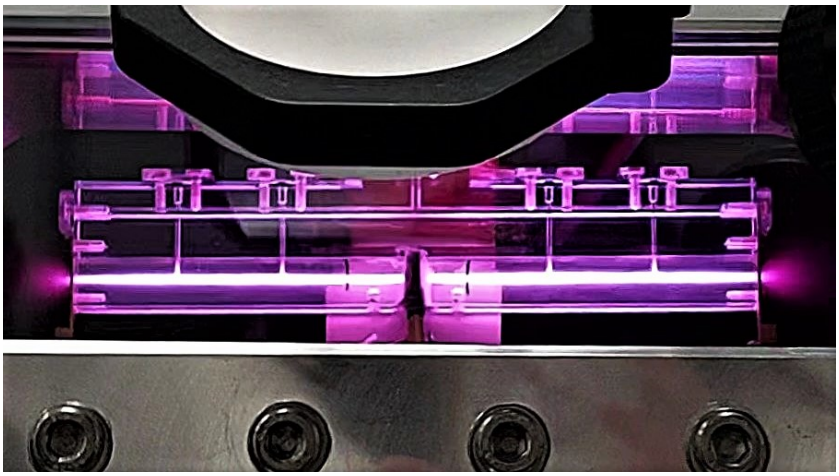

Figure 4.37: Segmented capillary during the characterization. It is possible to see the different intensity in the light emitted, meaning that also the density is different.

The first type of study concerns the possible uniformity of the density if the same voltage is applied in both regions; in this case, a voltage of 6kV has been applied, resulting in a current around 300A for both regions.
Measurements have been taken from 2000ns of delay to 3500ns, with a gate width of 150ns, managing to acquire enough light; the data analysis has been done following the procedure in Appendix A, with a proper changing in the parameters.
Using the same voltage for both regions, it has been notice that the synchronization of the current pulses can't be perfect, due to the different behavior of the two circuits used for the measurements.

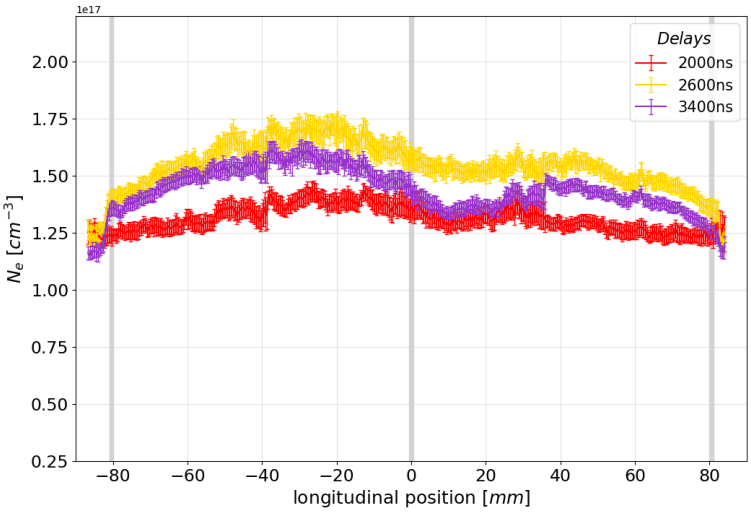

Figure 4.38: Longitudinal characterization of the electron density for different delays, same voltages case.

During time the two regions experiment not identical densities, even though the tuned voltage is the same; the temporal profile is almost identical (fig.4.39), but is not so easy to implement an uniform longitudinal profile (fig.4.38).

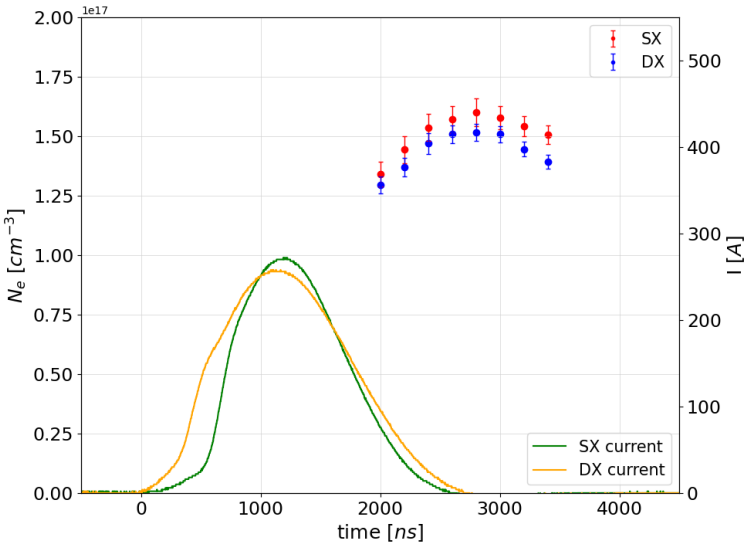

Figure 4.39: Time evolution of the average density in both regions of the capillary, same voltages case.

In the second case different voltages have been applied, with also a different delay in the current pulse. The two densities at first are really different, as it is possible to notice in graph 4.40. With time, plasma electrons in the most dense region tend to spread in the

other region. Then, when the density is uniform, the two regions behave as one and the density decreases in all the capillary.

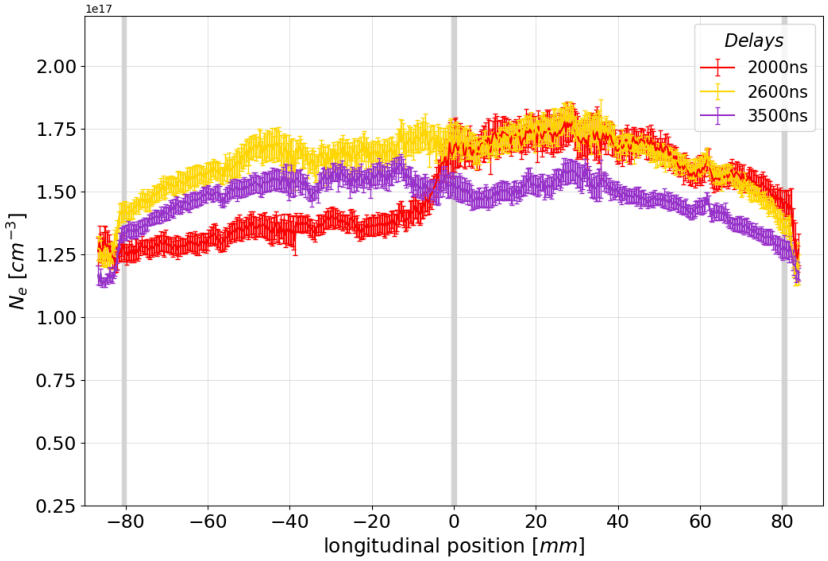

Figure 4.40: Longitudinal characterization of the electron density for different delays, different voltages case.

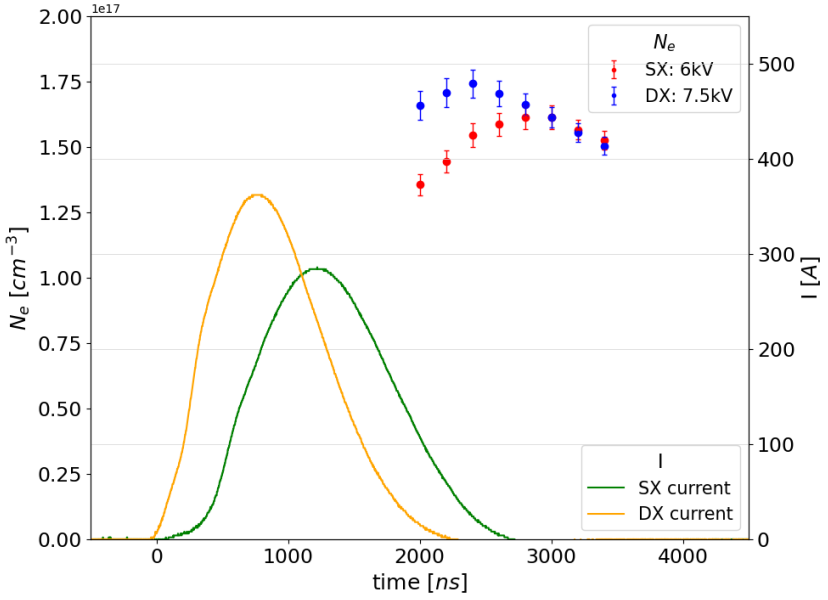

Figure 4.41: Time evolution of the average density in both regions of the capillary, different voltages case.

Since this capillary is just a prototype, measurements at high delays were not acquired, but it can be seen from graph 4.41 how, at a certain point, the densities are quite similar

in the two sides of the channel.
The characterization of this prototype shows how, applying all the knowledge acquired from the measurement and analysis of the capillaries before, new technologies can be developed. The density inside the capillary has been tuned by changing the current pulse to show how a ramp can be created inside the channel, to be used for different applications.

5 | Outlook and conclusions

5.1. Conclusions

Summing up, the thesis work describes the characterization of plasma-discharge capillaries for plasma-based acceleration of particle beams performed in the Plama Diagnostic Lab, part of SPARC_LAB project (INFN-LNF).
First, an overview on novel particle acceleration schemes was presented, including the physics of plasma acceleration mechanism and the state of art of plasma sources. Then, it has been shown how important it is to find the right work conditions and geometrical design to obtain a better electron density distribution inside the plasma source, in order to optimize the acceleration process. The first set of measurements showed how the density can be tuned by changing the work conditions as current and pressure. The density needed for the acceleration process can vary depending on the experiments and the applications. In addition, it has been studied the effect of the gas used on the uniformity and density inside the channel. Hdrogen is more dangerous since it is flammable and it is more difficult to maintain the vacuum if hydrogen is used, since the molecule is so small. In this part, it has been seen how Nitrogen and Argon are good candidates to replace the hydrogen used right now. On the other hand measurements obtained with argon and nitrogen were characterized by much higher uncertainty compared to the well known hydrogen.
In the second half of measurements, the effect of capillary geometry on the plasma distribution is investigated. First of all, the role played by the diameter and the channel shape on the plasma density spacial distribution and temporal evolution was studied. This is a very important tool that can be used for different applications.
In the end, a study on the dependence of the density on the position and number of the inlets has been carried on; the results show that, using two inlets positioned at low distance can lead to an improvement in the uniformity inside the channel.
In conclusion the thesis project reports a novel scheme for a plasma discharge capillary, composed by two segments with a shared central electrode that are fed by two independent electrical circuits. Experimental results showed that, by tuning the current and the

discharge delay, it is possible to modulate the plasma density inside the source to obtain different profiles used in different applications.

5.2. Future perspective

Based on these ideas, the present work may represent a starting point for future experimental developments.
The results obtained highlight the possibility to modulate the density inside the capillaries through the work conditions and the geometry of the source itself. This is a first step towards a m-scale long capillary, that will be used in the future in the EuPraxia project and future perspectives for improving the plasma acceleration process and the compactness of the accelerator itself.
For example, from the first design of a segmented capillary, that showed the possibility of generating different densities inside the same source, some advanced configurations can be implemented. Using a segmented capillary, in which two plasma lenses are included, can be the turning point for achieve the compactness needed in the process. This application of the discharge capillary can achieve very good results in scaling down the dimensions of the electron plasma accelerators used nowadays.
In the future, experiments on this kind of source will take place at SPARC_LAB, and improvements to the technology will be made.

Bibliography

[1] *Proceedings of the 2014 CAS-CERN Accelerator School: Plasma Wake Acceleration*. CERN, 2016, vol.1.

[2] F. Albert. 2020 roadmap on plasma accelerators. *New J. Phys.*, 23 031101, 2021.

[3] L. A. K. Alexander Fridman. *Plasma Physics and Engineering*. CRC Press, 2011.

[4] S. Arjmand, D. Alesini, M. P. Anania, A. Biagioni, M. Ferrario, and et al. Characterization of plasma sources for plasma-based accelerators. *PPLA*, 15 C09055, 2020.

[5] T. L. Audet, P. Lee, and e. a. G. Maynard. Gas cell density characterization for laser wakefield acceleration. *Nuclear Physics A*, 2018.

[6] A. Biagioni, D. Alesini, M. P. Anania, M. Ferrario, and et al. High-voltage pulser to produce plasmas inside gas-filled discharge capillaries. 2019.

[7] A. Biagioni, D. Alesini, M. P. Anania, M. Ferrario, and et al. Vacuum system design for plasma wakefield acceleration at `SPARC_LAB` test facility. 2021.

[8] N. A. Bobrova, A. A. Esaulov, J.-I. Sakai, P. V. Sasorov, D. J. Spence, A. Butler, S. M. Hooker, , and S. V. Bulanov. Simulations of a hydrogen-filled capillary discharge waveguide. *Physical Review E*, 65, 016407, 2002.

[9] M. Borghesi. Laser-driven ion acceleration: State of the art and emerging mechanisms. *Nuclear Instruments and Methods in Physics Research A*, 740, 6-9, 2014.

[10] F. F. Chen. *Introduction to Plasma Physics and Controlled Fusion*. Springer, 2016.

[11] E. Chiadroni, M. Anania, M. Bellaveglia, and A. B. et al. Overview of plasma lens experiments and recent results at sparc_lab. *Nuclear Inst. and Methods in Physics Research, A*, 909 16–20, 2018.

[12] A. Döpp, E. Guillaume, C. Thaury, and e. a. J. Gautier, Kim Ta Phuoc. 3d printing of gas jet nozzles for laser-plasma accelerators. *Review of Scientific Instruments*, 21 (3), pp.250-261. ff10.1063/1.4958649ff. ffhal-01347352f, 2016.

[13] Y. L. et al. Simple empirical analytical approximation to the voigt profile. *J. Opt. Soc. Am.*, Vol. 18, No. 5, 2001.

[14] F. Filippi, M. P. Anania, A. Biagioni, M. Ferrario, and et al. 3d-printed capillary for hydrogen filled discharge for plasma based experiments in rf-based electron linac accelerator. *Rev. Sci. Instrum*, 89 083502, 2018.

[15] J. Garland, G. Tauscher, S. Bohlen, and e. a. J. Osterhoff. Evolution of longitudinal plasma-density profiles in discharge capillaries for plasma wakefield accelerators. *Nuclear Physics A*, 2018.

[16] M. J. Garland, J. C. Wood, G. Boyle, and J. Osterhoff. Plasma sources and diagnostics. *Proceedings of the 2019 CERN-Accelerator school*, 2020.

[17] M. A. Gigosos. Stark broadening models for plasma diagnostics. *Journal of Physics D: Applied Physics*, 47 343001, 2014.

[18] A. J. Gonsalves, K. Nakamura, and J. D. et al. Multi-gev plasma acceleration results at bella. *IPAC2015*.

[19] H. R. GRIEM. *Spectral Line Broadening by Plasmas*. Academic Press, INC., 1974.

[20] E. Gschwendtnerb and E. A. et al. Awake, the advanced proton driven plasma wakefield acceleration experiment at cern. *Nuclear Instruments and Methods in Physics Research A*, 2015.

[21] T. P. A. Ibbotson. Laser-wakefield acceleration of electron beams in a low density plasma channel. *The American Physical Society*, 13 031301, 2010.

[22] D. G. Jang, M. S. Kim, I. H. Nam, H. S. Uhm, , and H. Suk1. Density evolution measurement of hydrogen plasma in capillary discharge by spectroscopy and interferometry methods. *Applied physics letters*, 99, 141502, 2011.

[23] J. Kim, V. L. J. Phung, K. Roh, M. Kim, K. Kang, and H. Suk1. Development of a density-tapered capillary gas cell for laser wakefield acceleration. *Rev. Sci. Instrum*, 92, 023511, 2021.

[24] T. Kurz, T. Heinemann, and e. a. M. F. Gilljohann. Demonstration of a compact plasma accelerator powered by laser-accelerated electron beams. *Nature communications*, 12, 2895, 2021.

[25] L. Liang. *Beam-driven plasma wakefield acceleration in AWAKE*. PhD thesis, University of Manchester, 2022.

[26] I. LNF. Particle-driven wakefield accelerators, 2019. URL `https://sparclab.lnf.infn.it/sparc_lab-home`.

[27] A. Macchi, M. Borghesi, and M. Passoni. Ion acceleration by superintense laser-plasma interaction. *Reviews of modern physics*, 85, 2013.

[28] R. Pompili. *Longitudinal diagnostics for comb-like electron beams by means of Electro-Optic Sampling*. PhD thesis, Universitá degli studi di Roma Tor Vergata, 2013.

[29] J. B. Rosenzweig, N. Barov, M. C. Thompson, and R. B. Yoder. Energy loss of a high charge bunched electron beam in plasma: Simulations, scaling, and accelerating wakefields. *The American Physical Society*, 7 061302, 2004.

[30] TIARA. Accelerators for society, 2013. URL `http://www.accelerators-for-society.org/`.

[31] R. M. G. M. Trines and P. A. Norreys. Wave-breaking limits for relativistic electrostatic waves in a one-dimensional warm plasma. *Physics Of Plasma*, 13, 123102, 2006.

[32] M. G. Umran Inan. *Principles of Plasma Physics for Engineers and Scientists*. Cambridge University Press, 2011.

[33] J. van Tilborg, S. Steinke, and C. G. R. G. et al. Active plasma lensing for relativistic laser-plasma-accelerated electron beams. *Physical Review Letters*, 115, 184802, 2015.

[34] C. H. W. Lu and M. Z. et al. A nonlinear theory for multidimensional relativistic plasma wave wakefields. *Physics of Plasmas*, 13, 056709, 2006.

A | Appendix A

A.1. Data analysis technique and software

To analyse the the spectra obtained with the plasma diagnostic system described in section 3.2.3, and using the acquisition method described in section3.3, a software needs to be implemented.
Starting from the acquisition of the spectrum (fig.3.14), a software called ImageJ permits us to see the Stark broadening at a certain longitudinal position (fig. A.1); as it is shown in the picture, the FWHM corresponds to the broadening of the length, and is called $\lambda_{1/2}$.

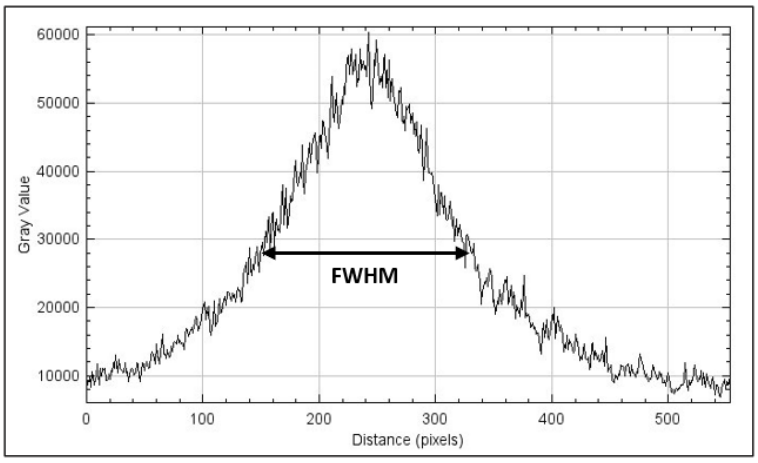

Figure A.1: Example distribution profile for a single longitudinal position acquired with ImageJ

The exact FWHM, shown in fig.A.1, is calculated by fitting a distribution function that describes in a good way the spectrum. The broadening graph in fig.A.2a shows different profiles, depending on the predominant variable; the most important two are the Gaussian (normal bell-curve distribution eq.A.1) caused by natural broadening and Lorentzian (Cauchy-Lorentz distribution eq.A.2)

$$f_{Gaussian}(x,\sigma) = C + A \cdot \exp\left[\frac{-(x-x_0)^2}{2\sigma^2}\right] \tag{A.1}$$

$$f_{Lorentzian}(x, \sigma) = C + \frac{A \cdot \sigma^2}{(x - x_0)^2 + \sigma^2} \tag{A.2}$$

In eq.A.1 and eq.A.2, the parameters C and A are added to shift and widen the profile, to fit better the distribution, while x_0 is the coordinate of the peak.
In spectroscopy, the convolution of these two broadening mechanisms (Cauchy-Lorentz distribution and Gaussian distribution) yield a Voigt line shape and its variants, listed in [13]. Analyzing the different spectral profiles acquired in the laboratory, it has been seen to see which profile fits the best the distributions which come out from the spectra images; the comparison of the different profiles can be seen in fig.A.2a.

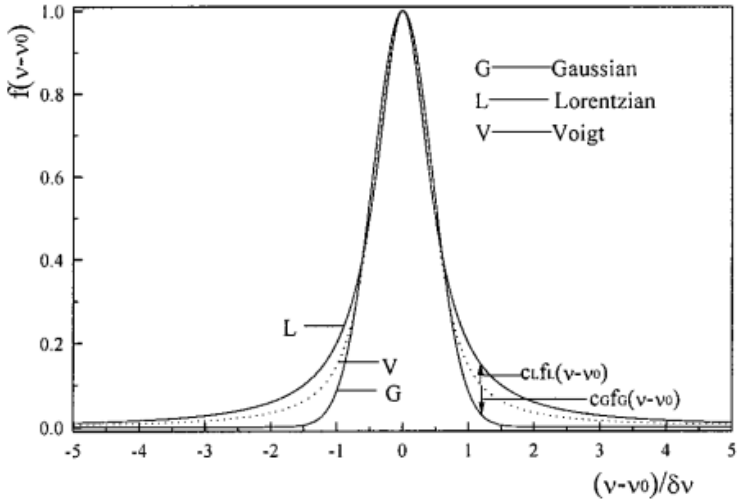

(a) Comparison between Voigt, Lorentzian and Gaussian distribution [13].

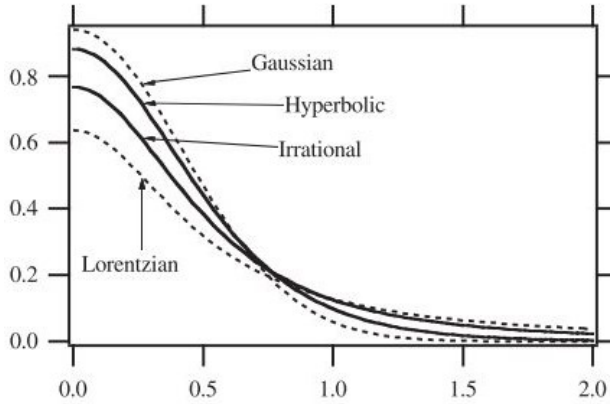

(b) Comparison between variants of Voigt functions and the other profiles [13].

Figure A.2: Different fitting functions for peak profiles.

Looking and comparing fig.A.1 and fig.A.2a, the Voigt distribution is chosen as fitting function. Then, from experimental datas has been seen that, to improve the fitting, the irrational alternative form of the Voigt function is the best choice of function(fig.A.2b):

$$f(x,\gamma) = C + \frac{A}{\gamma}\left[1 + \left(\frac{x - x_0}{\gamma}\right)^2\right]^{-2/3} \qquad FWHM = \gamma(2^{2/3} - 1)^{1/2} \tag{A.3}$$

Finding the three parameters A, C and γ and using the the function for every point along the longitudinal axis of the capillary, we are able to delineate a longitudinal profile of density of the capillary, inside and outside the channel; outside the capillary the so called plumes are present, in which the plasma spread with an isotropic behaviour in the vacuum.
Using python language, I created a software that, when given the images of the spectra, generate the longitudinal profile and time trend of the density.
The first step of the algorithm is to import the image from a folder to the code: to do that, it has been used the PIL library.

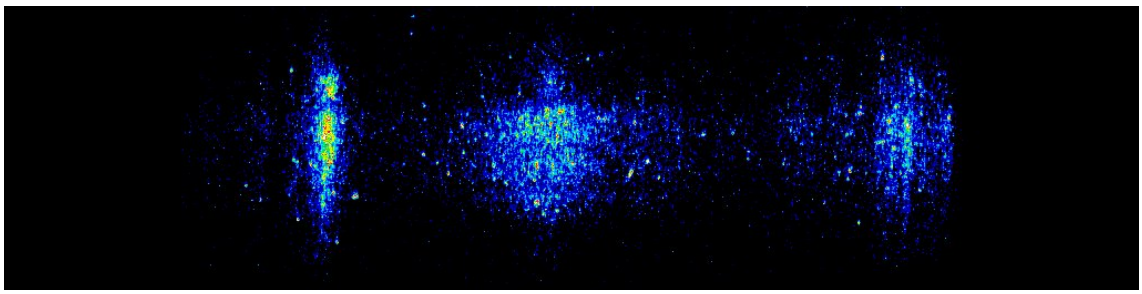

Figure A.3: Capillary n. 1 from table 4.1 at 10kV, 1900 ns of delay.

With this tool, the image with 1024x255 pixel is read as a matrix, which have the same shape, and for every element has a value that depends on how bright the light is.
After importing and creating the matrix, every line of it is analyzed to find the right parameters of the fitting function in eq. A.3.
An example of this step it is shown in picture A.4, where the fitting function for line 138 (almost the central line of the picture) is:

$$f(x) = 4.658 \cdot 10^3 + \frac{2.098 \cdot 10^6}{71.25}\left[1 + \left(\frac{x - 485}{71.25}\right)^2\right]^{-2/3} \tag{A.4}$$

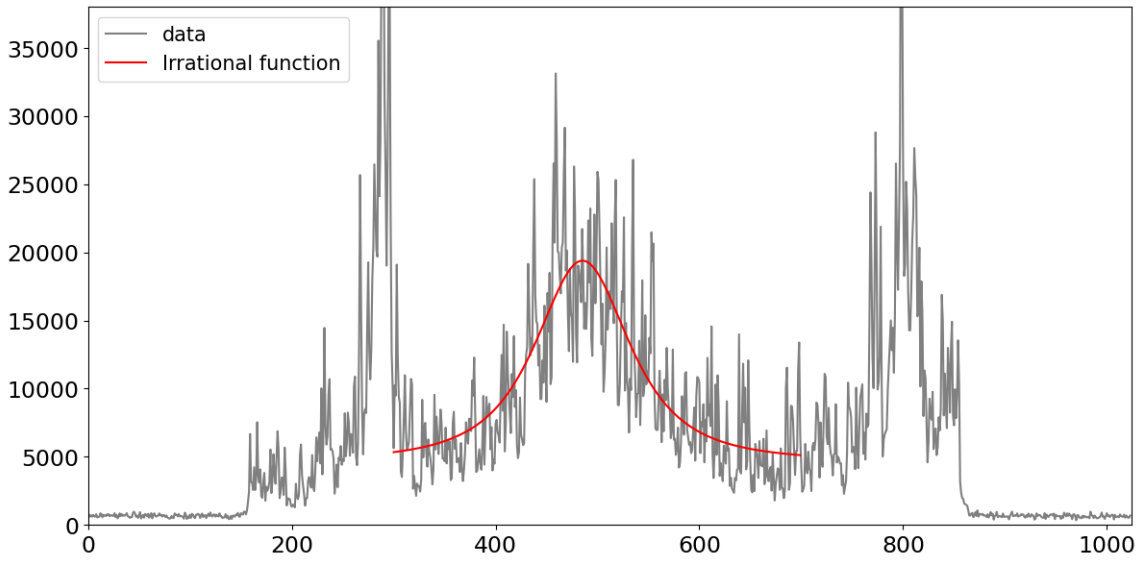

Figure A.4: Fitting function of the Capillary n. 1 from table 4.1.

The two peaks at the sides of the image have been explained in section 3.3.2, and not taken into account when fitting the function. To avoid counting them there are different methods; for example, it is possible to change the x-axis range of datas used to fit the function, not taking into account the intervals in which the peaks are present. Another method is to use just the center peak range of x-coordinates, but in this way it is harder to find the FWHM, since it will be higher than the real one. Another method can be to filter the light before it arrives at the spectrometer, but in this case the acquired light is much less than the actual one. In our case, the first method has been the best one for the fitting procedure.

Implementing this procedure for every line of the matrix created from fig.A.3, and calculating the FWHM from eq. A.3, and then inserting it in eq. 3.7, it's possible to obtain the graph similar to the ones of section 4.1.1.

This process needed to create the actual graphs is the same one described above, but weighted over 50 images taken at the same delay and in the same conditions. Doing this statistical step, better and more realistic results can be found.

Then, to have the time graphs, an average value of the density inside the electrodes and the error is found for every delay acquired, so that it is possible to plot a trend over time of the measurements, as it can be seen in section 4.1.

At the end of the section, the general algorithm is shown.

Starting from the definition of the fitting function and defining the calibration constants in lines 1-2, different *for* cycles are implemented.

The first one in line 3 permits to analyse different delays, to subquentially plot the trend

over time; the one in line 4 is inserted to analise the 50 images acquired for every delay; the one in line 6 in implemented to analise every line of every image.
To plot the results, a simple code is written to show *Ne_i* and *NeMean*.
This kind of software is modified for every type of capillary used; for example, in case of different voltage, the constants are changed. The interval of pixel used to find the fitting function is also tune for every capillary, since the peaks caused by a second species can lower the capability of fitting a function over the datas.

Algorithm A.1 Data Analysis general software

1: Define different constants, as radius, voltage, to find the temperature and so α, needed in equation 3.7.
2: Define the fitting function:
`def` $F_{IRR}(x, x_0, A, \gamma, I)$:
`return` $I + A / (2\gamma)\cdot(1+((x-x_0)/\gamma)^2)^{-3/2}$
3: Define the calibration costants, to pass from pixels to millimiters: Xcalib and Ycalib
4: **for** i in zip(np.arange(1500, 3300, 100)): **do**
5: **for** j in np.arange(1, 51): **do**
6: im1 = Image.open('*name of the image*'.format(j, i))
7: **for** k in np.arange(0, 255): **do**
8: Pguess = [x0, A0, γ0, I0]
popt, pcov =curve_fit(F_{IRR}, x, y, p0=Pguess, maxfev=20000000)
f(y) = IRR(xINT, *popt)
FWHM_i = $(2^{2/3}\text{-}1)^{1/2} \cdot$ popt[2]
FWHM.append(FWHM_i)
9: **end for**
10: FWHM = np.array(FWHM)
FWHM_Ang = FWHM$\cdot$ Xcalib
Ne_i= 8.02$\cdot$ 1e12 $\cdot$ ((FWHM_Ang/alpha)$^{3/2}$)
Ne.append(list(Ne_i))
11: **end for**
12: Ne=np.array(Ne)
Ne_mean=np.nanmean(Ne,axis=0)
Dev_std=np.nanstd(Ne,axis=0)
NeMean.append(list(Ne_mean))
13: **end for**
14: NeMean=np.array(NeMean)

List of Figures

List of Tables

Acknowledgements